Mon. Not. R. Astron. Soc. **000**, 1–29 (201x) Printed 24 April 2018 (MN LATEX style file v2.2)

A catalogue of masses, structural parameters and velocity dispersion profiles of 112 Milky Way globular clusters

H. Baumgardt[1⋆], M. Hilker[2]
[1] *School of Mathematics and Physics, The University of Queensland, St. Lucia, QLD 4072, Australia*
[2] *European Southern Observatory, Karl-Schwarzschild-Str. 2, 85748 Garching, Germany*

Accepted 2017 xx xx. Received 2017 xx xx; in original form 2017 xx xx

ABSTRACT

We have determined masses, stellar mass functions and structural parameters of 112 Milky Way globular clusters by fitting a large set of N-body simulations to their velocity dispersion and surface density profiles. The velocity dispersion profiles were calculated based on a combination of more than 15,000 high-precision radial velocities which we derived from archival ESO/VLT and Keck spectra together with $\sim 20,000$ published radial velocities from the literature. Our fits also include the stellar mass functions of the globular clusters, which are available for 47 clusters in our sample, allowing us to self-consistently take the effects of mass segregation and ongoing cluster dissolution into account. We confirm the strong correlation between the global mass functions of globular clusters and their relaxation times recently found by Sollima & Baumgardt (2017). We also find a correlation of the escape velocity from the centre of a globular cluster and the fraction of first generation stars (FG) in the cluster recently derived for 57 globular clusters by Milone et al. (2017), but no correlation between the FG star fraction and the global mass function of a globular cluster. This could indicate that the ability of a globular cluster to keep the wind ejecta from the polluting star(s) is the crucial parameter determining the presence and fraction of second generation stars and not its later dynamical mass loss.

Key words: globular clusters: general – stars: luminosity function, mass function

1 INTRODUCTION

Globular clusters are excellent laboratories to study star formation and the early evolution of galaxies since they contain large samples of equidistant stars that have coeval ages (at least to within a few tens of Myr) and similar chemical abundance patterns (at least for heavy elements). Measuring the properties of stars in globular clusters therefore allows to accurately determine many of the fundamental parameters of globular clusters like distances, ages, metallicities, sizes and masses. In addition, their high stellar densities make them unique environments for the creation of exotic stars like blue stragglers (Bailyn 1995; Davies, Piotto & de Angeli 2004), low-mass X-ray binaries (Verbunt 1993; Pooley et al. 2003) and millisecond pulsars (Manchester et al. 1991). Globular clusters are also among the prime environments for the creation of black hole binaries that are tight enough so they can merge through the emission of gravitational waves within a Hubble time (Banerjee, Baumgardt & Kroupa 2010; Downing et al. 2011; Rodriguez, Chatterjee & Rasio 2016; Askar et al. 2017). They are also interesting from a theoretical point of view since they allow to study the interplay between stellar evolution, binary evolution and stellar dynamics.

An accurate understanding of the current state and evolutionary history of a globular cluster requires a detailed knowledge of its internal mass distribution as well as the current stellar mass function. In recent years, information on the velocity dispersion profiles has become available through large surveys using either multi-object spectrographs on 4m and 8m class telescopes (e.g. Lane et al. 2011; Kimmig et al. 2015; Lardo et al. 2015; Kamann et al. 2018) or proper motions of stars using HST (Watkins et al. 2015a). In addition, HST photometry has allowed to determine the stellar mass functions of many globular clusters from the tip of the red giant branch down to almost the hydrogen burning limit (e.g. De Marchi, Paresce & Pulone 2007; Paust et al. 2010; Webb & Leigh 2015; Sollima & Baumgardt 2017). At the same time, analytic models like King-Michie models (e.g. Sollima, Bellazzini & Lee 2012) or models based on the solution of lowered isothermal distribution functions like the `LIMEPY` models (Gieles & Zocchi 2015) have become sophis-

⋆ E-mail: h.baumgardt@uq.edu.au

ticated enough to model the internal mass distribution of a globular cluster including mass-segregation. Furthermore, progress in the speed of computers as well as increasing sophistication of the computer codes has allowed to perform simulations of globular clusters with up to 10^6 stars through either direct N-body (Heggie 2014; Wang et al. 2016) or Monte Carlo simulations (e.g. Giersz & Heggie 2011; Askar et al. 2017), meaning that a detailed comparison of observations and simulations for individual globular clusters has become possible (e.g. Zonoozi et al. 2011). While analytic models are flexible and fast, direct simulation methods are naturally self-consistent and offer the opportunity to put constraints on the initial conditions of Milky Way globular clusters.

Baumgardt (2017) have recently derived total masses and mass-to-light ratios of 50 Galactic globular clusters based on a comparison of their velocity dispersion and surface density profiles with the results of a large set of N-body simulations. In the current paper we improve their modeling by including the stellar mass functions of globular clusters in our modeling. We do this by calculating new sets of models that have mass functions that are depleted in low-mass stars compared to a canonical Kroupa (2001) mass function. We also significantly improve the velocity dispersion profiles calculated by Baumgardt (2017) based on individual stellar radial velocities by additional radial velocities from unpublished spectra from the ESO and Keck science archives. Our paper is organized as follows: In section 2 we describe the observational data used in this paper and the reduction of the spectra. In section 3 we present the new grid of N-body simulations that we have calculated and section 4 presents our results. We draw our conclusions in section 5.

2 OBSERVATIONAL DATA

2.1 Radial velocities

The radial velocities used in this work were derived from mainly two sources: We first searched the ESO and Keck Science archives for unpublished spectra of stars in globular clusters. For ESO/VLT spectra, we searched the ESO Science Archive for reduced, high-resolution `FLAMES`, `UVES`, `X-Shooter` and `FEROS` spectra of stars within 15 arcmin around the center of each globular cluster. If the spectra were not already in a heliocentric reference frame, we first applied a heliocentric correction to them using the `bcvcorr` routine from the `RVSAO` software package (Kurtz & Mink 1998). `FLAMES` spectra were then sky subtracted with the help of the `Skycorr` package (Noll et al. 2014). In order to perform the sky subtraction, we used the median of the 8 associated sky fibers as the sky reference spectrum for each stellar spectrum. We then co-added individual spectra taken within 30 days of each other using the IRAF[1] `scombine` task and determined stellar radial velocities with the help of the IRAF `fxcor` task, using as templates the spectra of cool giant stars of a metallicity that is comparable to the cluster metallicity given in Harris (1996). We created the template spectra with the stellar synthesis program `SPECTRUM` (Gray & Corbally 1994) using `ATLAS9` stellar model atmospheres (Castelli & Kurucz 2004). For each cluster we created the template spectrum from the theoretical atmosphere models that were closest in metallicity to the studied clusters and used the same spectral resolution as the observed spectra.

For a few clusters we also determined radial velocities from archival ESO/VLT `FORS2` spectra that include the Calcium triplet lines. In order to derive radial velocities from `FORS2` spectra, we reduced the raw data with the help of the ESO Reflex pipeline (Freudling et al. 2013). We then again ran the IRAF `fxcor` task and applied a telluric correction to the spectra similar to the analysis of the Keck `DEIMOS` spectra described below.

We also derived radial velocities from unpublished Keck `DEIMOS`, `HIRES`, and `NIRSPEC` spectra available from the Keck Observatory archive. The `DEIMOS` spectra were reduced with the `DEEP2` data reduction pipeline developed by the `DEEP2` survey team (Cooper et al. 2012; Newman et al. 2013), while for `HIRES` and `NIRSPEC` data we used the reduced spectra already available in the Keck Observatory archive. We then used `fxcor` to derive the stellar radial velocities from the spectra. `HIRES` and `DEIMOS` spectra were again cross-correlated against synthetic template spectra created with the `SPECTRUM` synthesis program, while the `NIRSPEC` spectra were cross-correlated against the infrared spectrum of the K giant star 10 Leonis available from the `CRIRES` spectral library of Nicholls et al. (2017). In order to correct for residual systematic errors in the absolute wavelength calibration of the `DEIMOS` spectra, we cross-correlated them against a telluric template spectrum that was kindly provided to us by Tony Sohn and Emily Cunningham. Since the telluric lines should be at zero radial velocity, systematic wavelength calibration errors can be corrected from the radial velocity of these lines. Final radial velocities for the `DEIMOS` spectra were then calculated according to $v_r = v_{obs} - v_{tel} - v_{hel}$, where v_{obs} is the radial velocity derived from the stellar template, v_{tel} the radial velocity from the telluric spectrum and v_{hel} the heliocentric correction.

In order to improve the accuracy of the stellar positions for all GCs, we cross-correlated the stellar positions given in the FITS file headers of the individual spectra against the stellar positions in the `2MASS` catalogue (Skrutskie et al. 2006), supplemented in a few cases by HST/ACS data or other catalogues. The stellar positions given in the FITS file headers were replaced whenever a matching position within 2 arcsec was found in `2MASS` or one of the other catalogues.

In total we could derive about 15,000 radial velocities from unpublished ESO/VLT and Keck spectra for stars in about 90 globular clusters. Tables D1 to D53 (made available in their full extend online) list the individual stellar radial velocities that we derived from ESO `FLAMES` and `UVES` observations done before 2014. The membership probabilities P_i in Tables D1 to D53 were calculated according to $P_i = 1.0 - \mathrm{erf}(\sqrt{\chi^2_i}/0.5)$ where erf is the error function and χ^2_i is the error and velocity dispersion weighted difference between the individual stellar radial velocity v_i and the mean cluster velocity $<v>$ calculated according to

[1] IRAF is distributed by the National Optical Astronomy Observatories, which are operated by the Association of Universities for Research in Astronomy, Inc., under cooperative agreement with the National Science Foundation.

$$\chi_i^2 = e^{-\frac{1}{2}\frac{(v_i - <v>)^2}{\epsilon_i^2 + \sigma_r^2}} \quad , \qquad (1)$$

Here ϵ_i is the error of the stellar velocity and σ_r is the expected velocity dispersion at the projected distance of the star calculated from the best-fitting N-body model.

We supplemented the VLT and Keck data by published radial velocities from the literature. Our main source of published literature data is the recent compilation by Baumgardt (2017). Additional literature data used in this work is given in Table B1. We include the velocity dispersion profiles recently published by Kamann et al. (2018) from a MUSE survey of the centers of 25 globular clusters. In order to allow for easy comparison with the other available radial velocity data, which is mainly restricted to giant stars, we restrict ourselves to clusters with a high effective mass in Table 5 of Kamann et al. (2018), i.e. clusters where the MUSE velocity dispersion profiles are dominated by massive turn-off and giant stars. We also replaced the APOGEE DR13 radial velocities used in Baumgardt (2017) with the radial velocities published in the APOGEE DR14 data release (Abolfathi et al. 2017).

Our final sample consists of 42,000 radial velocity measurements of about 35,000 individual stars in 109 globular clusters. The median uncertainty of an individual measurement is about 0.5 km/sec and 90% of our stars have velocity errors of less than 2 km/sec. The errors should therefore be small enough to reliably derive the velocity dispersion profiles of most globular clusters, except for the lowest mass clusters in which the internal velocity dispersion is less than 1 km/sec.

2.2 Radial velocity dispersion profiles

In order to derive velocity dispersion profiles from the individual stellar radial velocities, we cross-correlated the radial velocities from the different data sets against each other to bring them to a common mean radial velocity. The necessary radial velocity shifts were usually less than 1 km/sec. We then merged the individual data sets to create a master catalogue for each globular cluster. Multiple measurements of individual stars were averaged and we performed a χ^2 test to evaluate whether the measured individual radial velocities were compatible with a constant radial velocity. Stars where the individual measurements had a less than 5% probability to be compatible with a constant radial velocity were removed before the velocity dispersion profile was calculated. The velocity dispersion profile of each cluster was then determined using a maximum-likelihood approach. Non-members were removed iteratively during the calculation of the velocity dispersion profiles. More details on the way the velocity dispersion profiles were calculated can be found in Baumgardt (2017). Table C1 presents the velocity dispersion profiles of all clusters calculated from the individual stellar radial velocities.[2] Fig. 1 shows a comparison of the velocity dispersion profiles calculated from literature data alone (blue triangles) vs. the velocity dispersion profiles that we obtain using only radial velocities determined from VLT/Keck spectra for the six globular clusters which have the largest number of stars in both data sets. It can be seen that the profiles are in excellent agreement with each other.

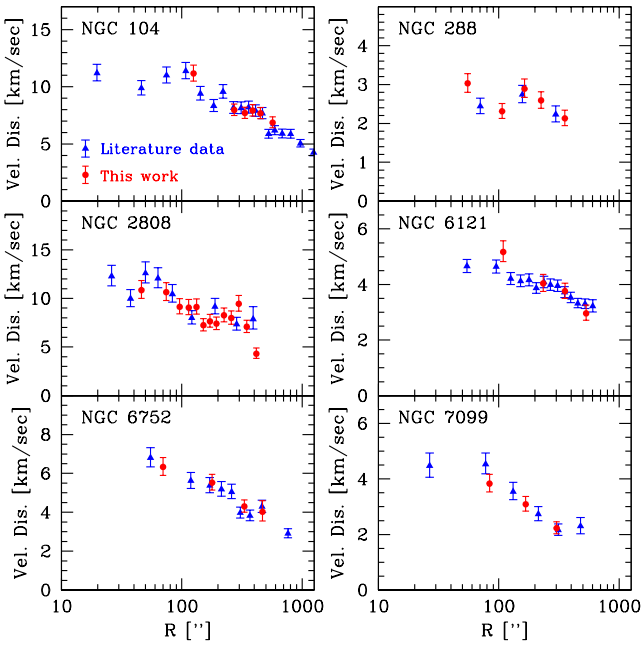

Figure 1. Comparison of the velocity dispersion profile derived from literature radial velocities (blue triangles) vs. the velocity dispersion profile derived from radial velocities determined in this work (red circles) for six clusters which have more than 300 radial velocities in both data sets. It can be seen that the velocity dispersion profile determined from our radial velocities is in excellent agreement with the one based on literature radial velocities.

NGC 2298 and Pal 5 have velocity dispersion profiles which increase towards the outer parts, which could be due to the ongoing tidal disruption of these clusters (Odenkirchen et al. 2002; Balbinot et al. 2011). We therefore neglected the outermost data point of their velocity dispersion profiles in our fits. Blecha et al. (2004) and Bradford et al. (2011) found that the velocity dispersion profile of Pal 13 could be inflated by binaries. In order to reduce the effect of these binaries, we only take stars with more than one radial velocity measurement into account when calculating the velocity dispersion of this cluster. This reduces the velocity dispersion by about 50% compared to the case when we use all stars. However the resulting M/L ratio is still significantly larger than what we find for other globular clusters, indicating that undetected binaries might still be present in the Pal 13 sample. Undetected binaries might also be present in a few other low-mass and low density clusters like Arp 2 or Ter 3 which also have M/L values significantly higher than the rest of the clusters.

2.3 Stellar mass functions and other cluster data

We took most stellar mass functions from Sollima & Baumgardt (2017) who determined stellar mass functions in four annuli inside a projected radius

[2] The radial velocity dispersion profiles including possible updates if new data has become available since the publication of this paper can also be downloaded from https://people.smp.uq.edu.au/HolgerBaumgardt/globular/

of $r < 1.6'$ around the centers of 35 globular clusters using the HST/ACS photometry published by the *Globular Cluster ACS Treasury Project* (Sarajedini et al. 2007). For most clusters these mass functions cover the area inside the half-light radius and the mass range between 0.2 $M_\odot < m < 0.8$ $M_\odot$, although for massive and concentrated clusters, low mass stars are too faint to be observed in the cluster centres. In addition, we also searched the literature for additional deep, completeness corrected HST/ACS and WFPC2 photometry of the luminosity function of main sequence stars in globular clusters. This data often complements the ACS Treasury Project data at larger radii, giving a more complete spatial coverage of the stellar mass function profile for a particular cluster. We determined the stellar mass functions from the luminosity functions by fitting either Dartmouth (Dotter et al. 2008) or PARSEC isochrones (Bressan et al. 2012) to the HST color-magnitude diagrams. The additional photometric data is listed in Table B1. In total we could determine stellar mass functions of 47 globular clusters, i.e. roughly half of all globular clusters in our sample.

Together with the stellar radial velocity dispersion profiles, we also fitted the proper motion dispersion profiles published by Watkins et al. (2015a). We used their combined 1D profiles which are averaged over the radial and tangential component of the proper motions. For clusters with available proper motions, we varied the cluster distances until we obtained the best agreement (lowest combined χ^2) in the simultaneous fit of radial velocity and proper motion dispersion profile. Clusters where distances were fitted are indicated in column 5 of Table 2. The surface density profiles were mostly taken from Trager, King & Djorgovski (1995) and, if available, from Noyola & Gebhardt (2006). Clusters where we used other surface density profiles are listed in Table B1. Apparent V-band magnitudes and their errors were calculated by taking the average of the apparent magnitudes given in Harris (1996), McLaughlin & van der Marel (2005), Dalessandro et al. (2012) and the integrated magnitudes determined in this work from the fit of our models to the surface brightness profiles. For the clusters in common with Baumgardt (2017) we took the ages from their paper. For the other clusters we searched the literature for age determinations. If no age could be found for a particular cluster we assumed an age of 12 Gyr.

3 *N*-BODY MODELS

We determined cluster masses and structural parameters by comparing the observed velocity dispersion, surface density and stellar mass function profiles against a grid of about 1200 N-body simulations. The details of the N-body simulations and the basic strategy to determine the best-fitting model are the same as described in Baumgardt (2017) and we refer the reader to this paper for a detailed description of the modeling. In short, we ran N-body simulations of isolated star clusters, each containing $N = 100,000$ stars initially using the GPU-enabled version of the collisional N-body code NBODY6 (Aarseth 1999; Nitadori & Aarseth 2012). The simulated clusters followed King (1962) density profiles initially. The initial concentrations were varied between $0.2 \leq c \leq 2.5$ and the initial radii were varied between $2 \leq r_h \leq 35$ pc. All simulations were run up to an age of $T = 13.5$ Gyr and final cluster models were calculated by taking 10 snapshots from the simulations centered around the age of each globular cluster. The combined snapshots of the N-body clusters were scaled in mass and radius to match the density and velocity dispersion profiles of the observed globular clusters and the best-fitting model was determined by interpolating in the grid of N-body simulations.

In the simulations done by Baumgardt (2017), cluster stars followed Kroupa (2001) mass functions initially. However, observed present-day mass functions of globular clusters show that many globular clusters have mass functions with significantly fewer low-mass stars than predicted by a Kroupa mass function (e.g. De Marchi, Paresce & Pulone 2007; Paust et al. 2010; Webb & Leigh 2015; Sollima & Baumgardt 2017). This can be understood as a result of ongoing cluster dissolution which preferentially removes low-mass stars from the clusters (Vesperini & Heggie 1997; Baumgardt & Makino 2003). Since the clusters in the simulations of Baumgardt (2017) were isolated, they did not lose stars during their evolution and their mass functions did not become depleted in low-mass stars. These models can therefore not be used to fit the mass functions of most Galactic globular clusters. In this paper we therefore ran a large set of additional simulations with initial mass functions (IMFs) depleted in low-mass stars to be able to match the observed mass functions of globular clusters and derive more accurate estimates of the cluster parameters like the structural parameters and total masses. The initial mass functions were set up as a combination of five connected power-laws $N(m) \sim m^\alpha$ between mass limits of 0.1 and 15 $M_\odot$ and with mass function breaks at 0.2 $M_\odot$, 0.5 $M_\odot$, 0.8 $M_\odot$ and 1.0 $M_\odot$. Table 1 gives an overview of the mass limits of the different power-law segments and the individual mass function slopes. The slopes were derived by fitting power-laws MFs to the stellar mass functions of the N-body simulations from Baumgardt & Sollima (2017), as well as the Monte Carlo simulations of Askar et al. (2017) using the maximum-likelihood approach described in Clauset, Shalizi & Newman (2009) and Khalaj & Baumgardt (2013) to calculate the best-fitting power-law exponents α for the different segments. Baumgardt & Sollima (2017) simulated star clusters in a circular orbit around a central galaxy that was modeled as an isothermal sphere with a circular velocity of $v_c = 220$ km/sec. Their simulations took the full tidal field of the parent galaxy into account. The Monte Carlo simulations of Askar et al. (2017) assumed a point-mass galaxy with the same circular velocity. If fitted by a single power-law in the range $0.2 < m < 0.8$ $M_\odot$, the simulated models have global mass functions slopes of $\alpha = -1.5$ (corresponding to a Kroupa IMF, model 1), $\alpha = -1.0$ (model 2), $\alpha = -0.5$ (model 3), $\alpha = 0.0$ (model 4) and $\alpha = +0.5$ (model 5). Since our clusters are isolated, they undergo only very little mass loss during their evolution. Hence the initial mass functions are more or less equal to the final ones except at the high mass end where stellar evolution turns massive stars into compact remnants.

We linearly interpolated between the simulations, varying initial cluster concentration, initial half-mass radius and cluster mass function to find the cluster model that simultaneously provides the best fit to the surface density profile,

Table 1. Power-law mass function slopes $N(m) \sim m^{\alpha}$ and mass limits used to set-up the N-body models.

Model	m_{Low} [$M_\odot$]	m_{Up} [$M_\odot$]	α	m_{Low} [$M_\odot$]	m_{Up} [$M_\odot$]	α	m_{Low} [$M_\odot$]	m_{Up} [$M_\odot$]	α	m_{Low} [$M_\odot$]	m_{Up} [$M_\odot$]	α	m_{Low} [$M_\odot$]	m_{Up} [$M_\odot$]	α
1	0.10	0.20	-1.35	0.20	0.50	-1.35	0.50	0.80	-2.35	0.80	1.0	-2.35	1.00	15.0	-2.35
2	0.10	0.20	-1.05	0.20	0.50	-0.80	0.50	0.80	-1.70	0.80	1.0	-2.20	1.00	15.0	-2.20
3	0.10	0.20	-0.85	0.20	0.50	-0.30	0.50	0.80	-1.05	0.80	1.0	-2.20	1.00	15.0	-2.00
4	0.10	0.20	-0.60	0.20	0.50	0.15	0.50	0.80	-0.40	0.80	1.0	-1.80	1.00	15.0	-1.80
5	0.10	0.20	-0.40	0.20	0.50	0.55	0.50	0.80	0.30	0.80	1.0	-3.00	1.00	15.0	-1.60

velocity dispersion profile and the mass functions at different radii of each individual globular cluster. In order to compare with the observed mass functions, we determined the sky location and exact boundaries of the HST fields used to derive the stellar mass functions from the `MAST` archive[3], projected the model clusters onto the sky and selected stars in the same area as the observed data.

For clusters which did not have measured mass functions, we estimated the global mass function based on the clusters' relaxation time (see discussion in sec. 4.2). We then performed only a 2D fit in our grid for these clusters, varying only the initial radius and cluster concentration but keeping the mass function fixed. Since the relaxation time is determined from the fit itself, we did the fitting iteratively for clusters without a direct mass function measurement until a stable solution was obtained.

We applied the above procedure to all clusters except NGC 2419, where the radial velocity dispersion profile could not be fitted with isotropic N-body models since it drops too quickly with radius in the outer parts. This is most likely due to a radially anisotropic velocity dispersion profile (Ibata et al. 2011), that could have been created during cluster formation and was not erased by dynamical evolution due to the long relaxation time of NGC 2419. We therefore fitted NGC 2419 using radially anisotropic King (1962) profiles. The profiles were created by the distribution function fitting method described in Hilker et al. (2007) using radially anisotropic Osipkov-Merritt models (Osipkov 1979; Merritt 1985). As Fig. E2 shows, the best-fitting cluster model found this way reproduces the observed velocity dispersion and surface density profile of NGC 2419 very well. Our solution for ω Cen is based on the best-fitting no IMBH model from Baumgardt et al. (2018), who, in addition to the N-body simulations presented in this paper, have run an additional grid of simulations which vary the assumed retention fraction of stellar-mass black holes. Since they lack radial velocity information, masses and structural parameters for NGC 6101 and NGC 6254 were determined by fitting the absolute number of main sequence stars at different radii which Sollima & Baumgardt (2017) derived from the ACS Treasure project data.

4 RESULTS

4.1 47 Tuc and M15

We start the discussion of our results by presenting the solution for the best-fitting models of 47 Tuc and M15, two of the best observed clusters in our sample, in greater detail. Fig. 2 depicts the surface density profile (panel a), velocity dispersion profile (panel b), mass distribution of main-sequence stars at different radii (panel c) and the slope of the best-fitting power-law to the stellar mass function as a function of radius (panel d) of 47 Tuc and our best-fitting N-body model. In all panels, the N-body model is shown by red lines or circles while circles in other colors show the observed cluster data. In panel b), blue circles show the observed radial velocity dispersion profile while orange circles show the proper motion dispersion profile from Watkins et al. (2015a). The number of stars as a function of stellar mass at different radii depicted in panel c) is taken from Sollima & Baumgardt (2017) for radii inside $r = 2.4'$, and de Marchi & Paresce (1995b) and Richer (2017) for larger radii. It can be seen that the best-fitting N-body model reproduces the observed parameters of 47 Tuc very well. The surface density profile of the best-fitting N-body model is within 10% of the observed surface density profile for all radii except near the tidal radius. Similarly the velocity dispersion profiles of the N-body model and 47 Tuc agree to within 0.5 km/sec at all radii between 1" $< r <$ 1000". The reduced χ^2_r value given as the sum of the error weighted velocity differences normalized by the number of data points is almost exactly 1, indicating excellent agreement (see Table 2). The absolute number of stars as a function of mass at different radii in panel c) is also in very good agreement between N-body model and observed cluster. Since the velocity dispersion profile essentially determines the total cluster mass, a good agreement in the absolute number of main sequence stars means that the N-body model must also have the same amount of mass in compact remnants as the real 47 Tuc, i.e. our chosen mass function must be a good description of the mass function of 47 Tuc. The best-fitting N-body model also has about the same amount of mass segregation as 47 Tuc, since at all radii the observed mass function slope is within $\Delta\alpha = 0.3$ of the mass function slope of the best-fitting N-body model.

Fig. 3 shows a comparison of the surface and velocity dispersion profile of M15 with the prediction of our best-fitting N-body model. Shown are the surface density profile (top left), the radial velocity dispersion profile (top right panel), and the proper motion dispersion profiles of giant stars, blue stragglers, upper main sequence stars and lower main sequence stars. The proper motion dispersion profiles were calculated using the data published by Bellini et al. (2014), restricting ourselves to stars outside the central 10" with proper motion errors less than 3 km/sec and absolute velocities within 35 km/sec of the cluster mean. We define upper main sequence stars as stars with magnitudes $19 < F_{814W} < 20$ and $F_{814W} - F_{660W} > 0.4$ and lower main sequence stars as stars with $20 < F_{814W}$ and $F_{814W} - F_{660W} > 0.4$ in the catalogue of Bellini et al.

[3] `https://archive.stsci.edu/`

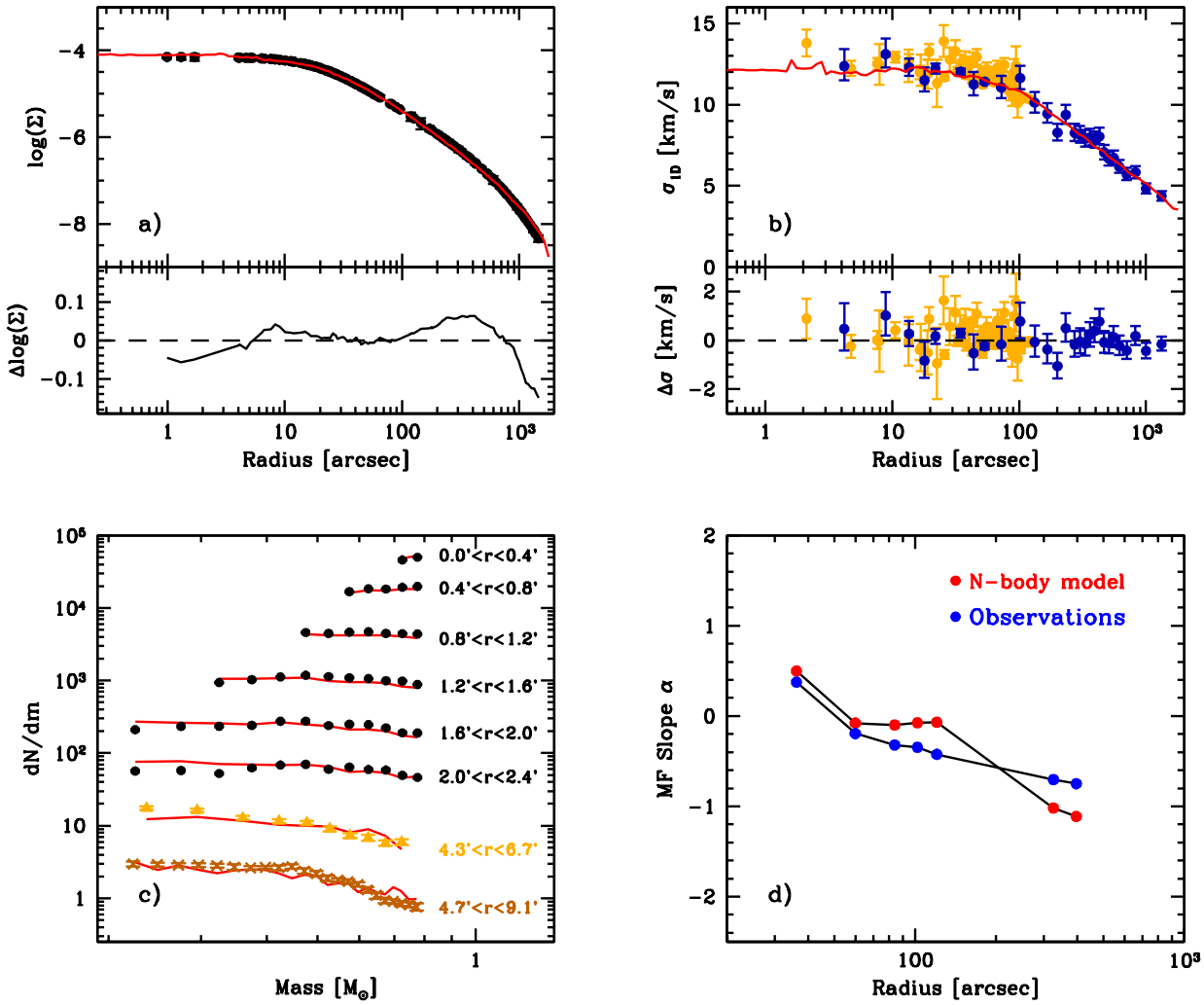

Figure 2. Fit of the surface density profile (panel a), velocity dispersion profile (panel b), number of main-sequence stars as a function of stellar mass at 8 different radii in the cluster (panel c) and mass function slope as a function of radius (panel d) of 47 Tuc. In each panel the best-fitting N-body model is shown by red lines or dots while the observed data is shown in other colors. In panel b), the velocity dispersion profile based on proper motions is shown by orange circles while blue circles show the radial velocity dispersion profile. The best-fitting N-body model is within 10% of the observed surface density profile, within 0.5 km/sec of the observed velocity dispersion profile and within $\Delta\alpha = 0.3$ in mass function slope over the whole range of radii. In addition there is very good agreement in the absolute number of main sequence stars at different radii between N-body model and the observed 47 Tuc.

(2014). These limits translate roughly into mass limits of $0.75 > m > 0.70$ M$_\odot$ and $m < 0.70$ M$_\odot$ for upper and lower main sequence stars respectively. For the comparison with the blue stragglers, which are not present in our N-body models, we use massive white dwarfs with masses $1.0 < m < 1.4$ M$_\odot$.

The observations of Sollima & Baumgardt (2017) show that M15 is strongly mass segregated since the stellar mass function changes from $\alpha = 0.2$ in the centre to $\alpha = -1.2$ outside the clusters' half-mass radius. Furthermore, the surface density of M15 is strongly increasing towards the centre down to the smallest radius for which it can be measured, indicating that M15 is in or past core collapse. The mass segregation of M15 is also evident in the dependency of the velocity dispersion profile with stellar mass, the observed velocity dispersion at a projected radius of $r = 30''$ for example changes from $\sigma \approx 10$ km/sec for blue stragglers to $\sigma = 12$ km/sec for lower main sequence stars. Although small, this change is clearly resolved in the observations. Our best-fitting N-body model is again in excellent agreement with the observed data on M15 since it fits the surface density profile of the cluster and the proper motion dispersion profile of each stellar mass group. In addition the N-body model reproduces the line-of-sight velocity dispersion profile, since the reduced χ^2 values of the fits to the various velocity dispersion profiles all being very close to unity.

4.2 Cluster masses and structural parameters

Table 2 presents the masses and structural parameters of all Galactic globular clusters for which we could derive radial velocity dispersion profiles. For each cluster we deter-

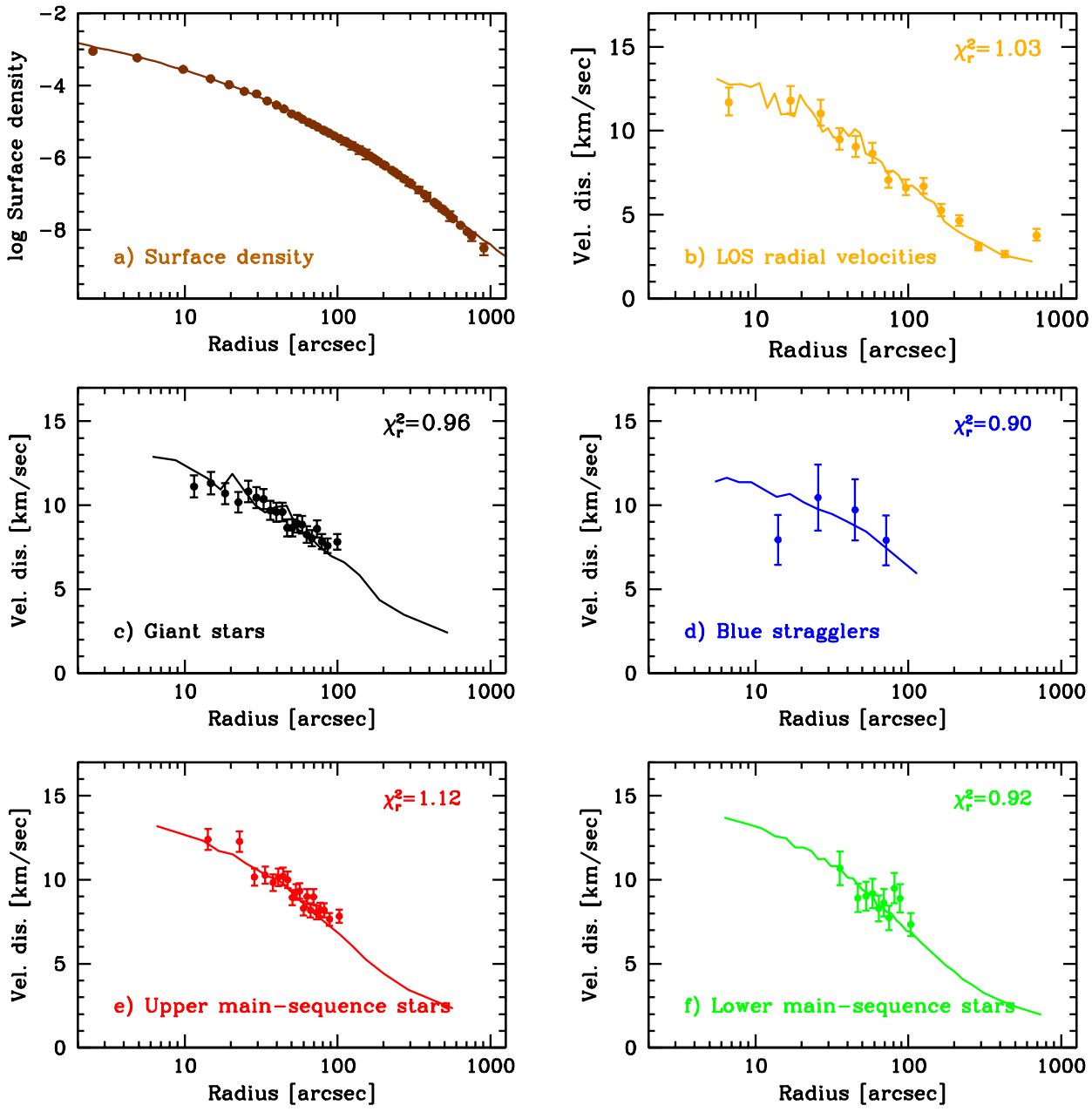

Figure 3. Fit of the surface density profile (panel a), radial velocity dispersion profile (b), and the proper motion dispersion profiles of giant stars (c), blue stragglers (d), upper main sequence stars (e) and lower main sequence stars (f) of M 15. Observed data is shown as solid points with error bars while the prediction of the best-fitting N-body model is shown as solid lines in each panel. The proper motion dispersion profiles were calculated from the HST data published by Bellini et al. (2014). The reduced χ^2_r values from the comparison of the theoretical and observed profiles are given in the upper right corner of each panel. All χ^2_r values are close to unity, indicating excellent agreement between the modeled cluster and the observations.

mined the number of member stars, the mean radial velocity and its error, the total cluster mass and M/L ratio, the core radius, 3D half-mass radius and projected half-light radius, the average density within the core and half-mass radius, the half-mass relaxation time, the global mass function slope between mass limits of 0.2 to 0.8 $M_\odot$, the one-dimensional, mass-weighted, central velocity dispersion, and the central escape velocity. The mass function slopes were either calculated from the N-body model that best reproduces the observed mass functions (for cluster that have measured mass functions) or using the relation between relaxation time and mass function slope that will be discussed in sec. 4.3. We count as radial velocity members all stars with membership probability $P_i > 0.01$ in each cluster. For some bulge clusters with strong field star contamination like Ter 5 these numbers might overestimate the number of true member stars. The mean radial velocities were calculated as the weighted mean of the individual radial velocities

of all cluster members, except for NGC 6101, NGC 6293 and NGC 6584 where we took the mean radial velocity from Kamann et al. (2018) (NGC 6293) or Harris (1996) (NGC 6101 and NGC 6584). Fig. 4 compares the mean radial velocities which we have determined with the radial velocities determined by Kimmig et al. (2015), Lardo et al. (2015) and Ferraro et al. (2018) from resolved spectroscopy of individual member stars (left panel) and the radial velocities given by Harris (1996) (right panel). It can be seen that the mean radial velocities derived here generally agree to within 1 km/sec with the mean radial velocities determined from individual stars. The remaining differences are probably due to uncertainties in the absolute wavelength calibration of the individual spectra, which are difficult to quantify but, judging from Fig. 4, could be around 1 km/sec. For most clusters our radial velocities are also in good agreement with the values given by Harris (1996). Clusters where the radial velocities differ more strongly are usually not very well studied clusters where the mean radial velocities have relative large error bars in the Harris catalogue.

Clusters that have a zero χ^2_r value in column 4 of Table 5 are clusters with few member stars for which we grouped the stars in only one or two velocity bins, which are then reproduced almost exactly by the best-fitting N-body model. Column 5 of Table 5 lists the cluster distances. For clusters for which Watkins et al. (2015a) have determined proper motion dispersion profiles, we vary the cluster distance until we obtain the best fit to the combined proper motion and radial velocity dispersion profile. For all other clusters the cluster distance is taken from the literature. Interestingly our best-fitting distance for 47 Tuc ($d = 4.41$ kpc) is now in much better agreement with other distance methods that generally find a cluster distance around $d = 4.5$ kpc (e.g. Gratton et al. 2003; Bono et al. 2008; Dotter et al. 2010; Woodley et al. 2012) than the kinematic distances derived by Baumgardt (2017) ($d = 3.95 \pm 0.05$ kpc) or Watkins et al. (2015b) ($d = 4.15 \pm 0.08$ kpc). The reason is that the HST proper motion dispersion profile of Watkins et al. (2015a) measures velocities only in the central 100" while radial velocities are available mainly for stars further away from the centre. This together with the fact that the new best-fitting model for 47 Tuc has fewer low-mass stars than the Kroupa mass function used by Baumgardt (2017), which lowers the velocity dispersion in the outer parts compared to the centre, pushes the best-fitting cluster distance to a larger value and brings it into much better agreement with the other methods. This again shows the importance of correctly modeling mass segregation when fitting models to observed clusters.

We calculated the core radius and average density inside the core by applying eq. 149 in Spitzer (1987) iteratively to the N-body data until a stable solution was found, using a correction factor of 0.517 in the conversion of core density to central density as described in Baumgardt et al. (2003). From all stars inside the core radius we then calculated the three-dimensional central velocity dispersion, weighting the individual stellar velocities with the masses of the stars. From the fastest single stars inside the core we also calculated the escape velocities of the clusters given in the final column of Table 2. Figs. E1 to E15 depict our fits to the observed surface density and velocity dispersion profiles for clusters with more than 100 member stars. It can be seen that we generally obtain very good fits to both profiles. The differences in the surface density profiles over most parts of the clusters are usually within 15%. Only in the very centre or near the tidal radius one can sometimes see larger differences. Observational uncertainties might be a reason for the differences since the observed surface density profiles could be affected by low-N noise in the core and uncertainties about the density of background stars near the tidal radius. The velocity dispersion profiles usually also agree to within 1 km/sec. Remaining differences could be due to a variety of reasons like stellar binaries, orbital anisotropy and tidal effects. Stellar binaries in particular could inflate the velocity dispersion profiles of low-mass clusters if present in sufficient numbers (e.g. Blecha et al. 2004; Gieles, Sana & Portegies Zwart 2010). In addition tidal effects (e.g. Küpper et al. 2010) or non-members could be responsible for the higher than predicted velocity dispersion profiles seen in the outer parts of some clusters like NGC 1851. Using proper motions from the `GAIA` satellite will help removing non-members from our data and assess whether the deviations seen are real or due to interlopers.

4.3 Correlations between cluster parameters

We next discuss several univariate correlations that we found among the cluster parameters. Fig. 5 depicts correlations between the cluster mass functions α, galactocentric distances R_{GC}, half-mass relaxation times T_{RH}, half-mass radii $r_{h,m}$, cluster metallicities [Fe/H], cluster masses M_{GC}, and the mass-to-light ratios M/L for all clusters with less than 30% relative mass error. Mass functions are only available for 47 clusters, i.e. about one third of all galactic globular clusters, which could introduce some bias into the cluster distribution since the selection of clusters that have measured mass functions is not random but weighted towards nearby and massive clusters. For all other cluster parameters our sample includes more than 2/3 of all known galactic globular clusters, making a bias much less likely, especially for more massive globular clusters with $M_V < -8.0$ where our sample is almost 100% complete. Each panel also shows the Spearman rank order coefficient ρ and its 1σ error. Our data shows a clear correlation between the galactocentric distance of a globular cluster and its half-mass radius. Part of this correlation could be due to the stronger tidal field in the inner parts of the Milky Way, which limits the size of globular clusters to smaller values. van den Bergh, Morbey & Pazder (1991) found a similar relation between galactocentric distance and the projected half-light radius. We confirm their results for the half-mass radius.

Sollima & Baumgardt (2017) found a correlation between the mass function slope of 35 globular clusters from the *Globular Cluster ACS Treasury Project* and their half-mass relaxation times in the sense that clusters with more positive mass function slopes (fewer low-mass stars) have smaller relaxation times. We confirm this correlation with our larger cluster sample. The reason for the existence of this correlation could be that clusters in stronger tidal fields experience more mass loss while at the same time the stronger tidal field limits them to a smaller volume and therefore radius. In addition clusters with shorter relaxation times develop mass segregation in a shorter amount of time, leading to a stronger depletion of low-mass stars by the tidal field of the Milky Way. Dynamical evolution could also explain

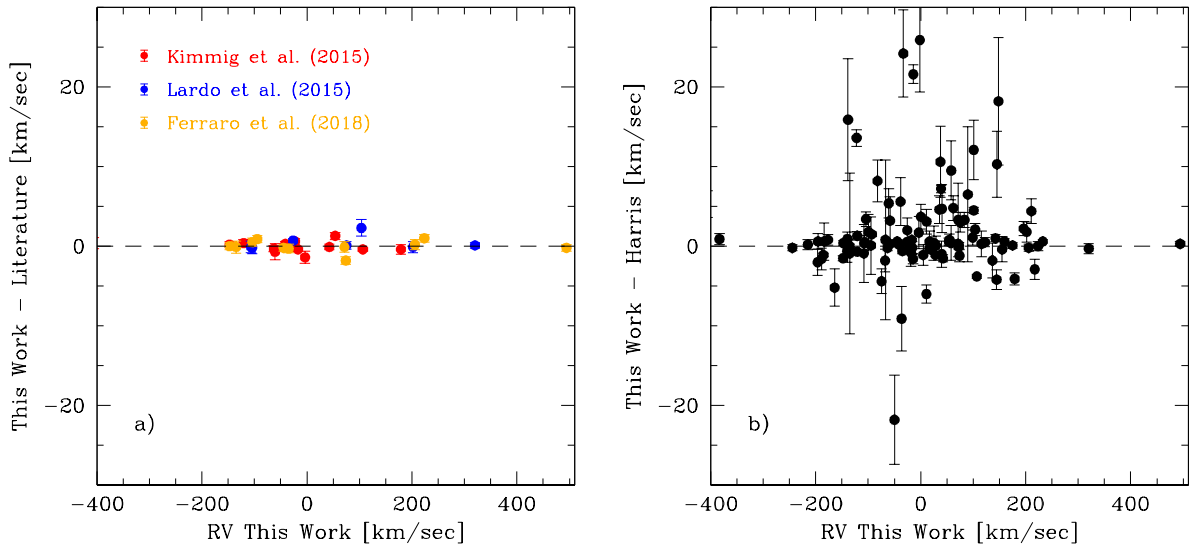

Figure 4. Comparison of the mean cluster velocities derived here with the radial velocities determined by Kimmig et al. (2015), Lardo et al. (2015) and Ferraro et al. (2018) (left panel) and the mean cluster velocities given in the Harris catalogue (right panel). Our data generally agrees to within 1 km/sec with recent literature values. Clusters which show larger differences in the Harris catalogue are mostly clusters where the radial velocities in the Harris catalogue are based on low-resolution spectroscopy and have relatively large error bars.

the correlation of mass function slope with galactocentric distance, although this correlation is weaker then the correlation with the relaxation time. The mass function also correlates with both the half-mass radius and, less strongly, with the mass of a globular cluster.

Most correlations between the cluster metallicity and other cluster parameters can be explained by the fact that high metallicity clusters are related to the Galactic disc and bulge and are therefore on average closer to the Galactic centre than halo clusters (Zinn 1985). They therefore experience a stronger tidal field which makes them more compact and also reduces their relaxation times. The strong correlation between metallicity and mass function slope could therefore be a result of dynamical evolution and might not reflect an initial variation, although we cannot rule out such a variation either. The M/L ratios do not show a significant correlation with any of the other cluster parameters. In particular we do not find a correlation between M/L ratio and either metallicity or mass function slope. Such correlations should in principle exist since for example the loss of low-mass stars decreases the M/L ratio of a globular cluster (Baumgardt & Makino 2003; Kruijssen & Mieske 2009). In addition, the loss of stellar remnants can decrease the M/L ratio of a globular cluster (Bianchini et al. 2017). The reason for the absence of a correlation could be that the resulting change in M/L ratio is too small to cause a noticeable difference or is compensated for by the correlation between mass function slope and cluster metallicity.

The dashed line in the α vs. T_{RH} plot shows the best-fitting linear relation to the observed globular cluster distribution which is given by $\alpha = 8.23 \pm 1.10 - (0.95 \pm 0.11)\ \log T_{RH}$. We use this relation to infer the mass function of globular clusters for which no direct measurement is available (see discussion in sec. 3).

Fig. 6 finally depicts the fraction of first generation (FG) stars in globular clusters found by Milone et al. (2017) through high precision HST photometry of red giant branch stars as a function of the central escape velocity of a cluster (left panel), the cluster mass (middle panel) and the global mass function slope between 0.2 and 0.8 $M_{\odot}$ (right panel). It can be seen that the fraction of first generation stars anti-correlates strongly with either the cluster mass (confirming the results found by Milone et al. 2017) or the central escape velocity. In particular clusters with small central escape velocities consist predominantly of first generation stars while the fraction of these stars drops to about 20% for clusters with escape velocities $v_{esc} > 40$ km/sec. However, as the right panel of Fig. 6 shows, the fraction of FG stars shows no correlation with the global mass function slope of a globular cluster. If clusters formed with a low fraction of second generation (SG) stars which later increases due to the loss of less centrally concentrated first generation stars (e.g. D'Antona & Caloi 2008), one would however expect that such a relation should be established since two-body relaxation will push low-mass stars to the outer cluster parts where they are preferentially lost. Hence clusters that have lost a large fraction of first generation stars should also have lost a higher fraction of their low-mass stars and should therefore have more evolved mass functions. As Fig. 6 shows such a correlation is not observed, calling into question the strong mass-loss scenario. If mass loss of first generation stars has increased the fraction of second generation stars, then this mass loss must have happened very early in the cluster evolution before dynamical mass loss has set in, possible through e.g. gas expulsion (Decressin et al. 2010; Khalaj & Baumgardt 2015) or giant molecular cloud encounters (Kruijssen et al. 2012). Still such a scenario would not be able to explain the strong dependency of the fraction of FG stars on the central escape velocity, which could instead indicate that the formation ef-

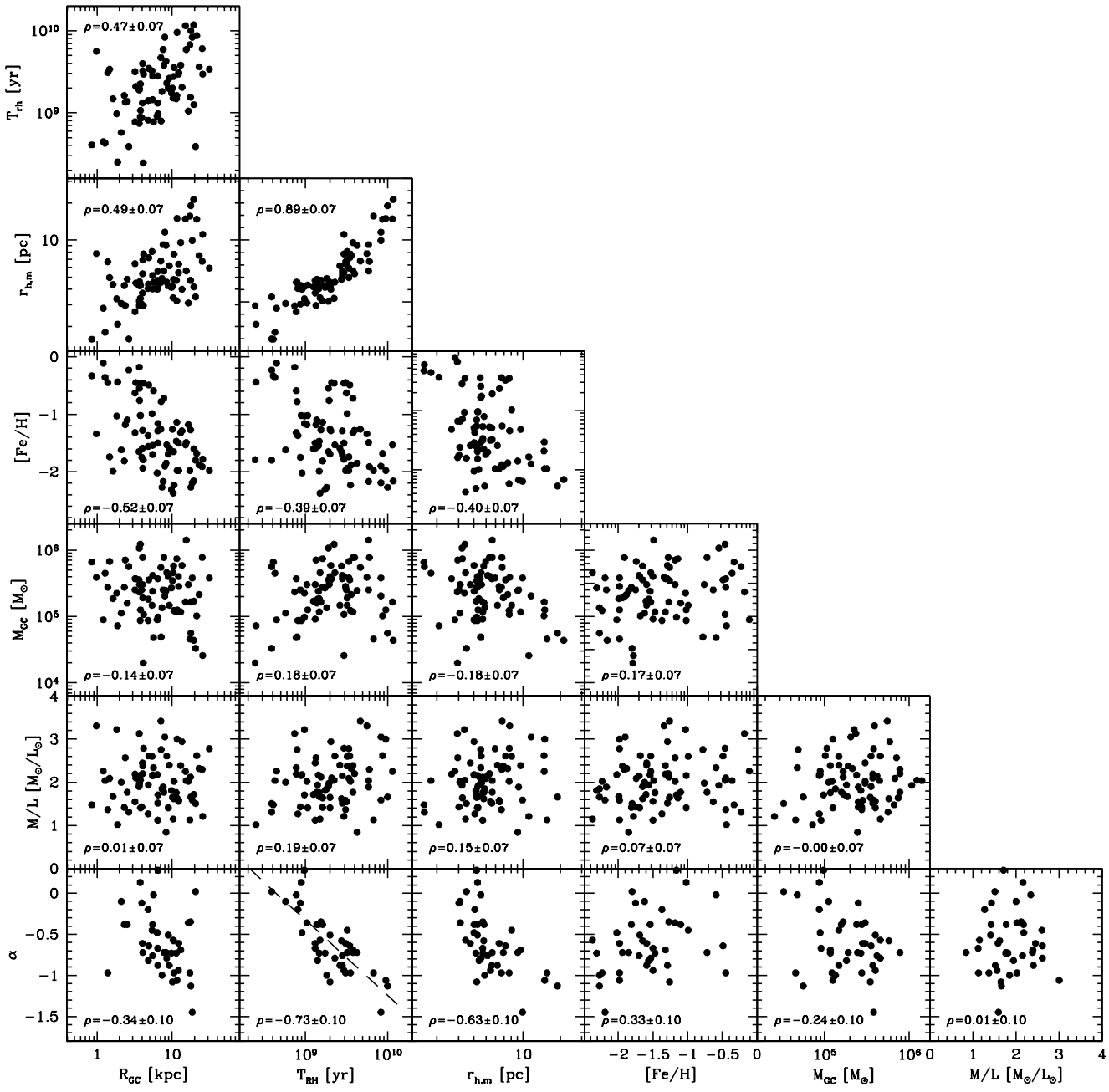

Figure 5. Univariate correlations between the cluster mass functions α, galactocentric distances R_{GC}, half-mass relaxation times T_{RH}, half-mass radii $r_{h,m}$, cluster masses M_{GC} and mass-to-light ratios M/L for all studied clusters. In each panel we also show the Spearman rank order coefficient ρ and its 1σ error. The dashed line in the α vs. T_{RH} plane shows the best-fitting linear relation to the cluster distribution.

ficiency of SG stars depends on the ability of a cluster to retain the stellar wind ejecta from polluting stars: For low escape velocities of $v_{esc} = 10$ km/sec or less nearly all ejecta leave the cluster and only few SG stars are formed, while at escape velocities larger than $v_{esc} = 40$ km/sec all ejecta are kept, meaning that the fraction of SG stars becomes constant.

5 CONCLUSIONS

We have determined individual stellar radial velocities of more than 15,000 stars in 90 globular clusters from archival ESO/VLT and Keck spectra. Combining this data with published literature velocities we then calculated radial velocity dispersion profiles of globular clusters using a maximum-likelihood approach. A comparison of these velocity dispersion profiles together with the surface density profiles of the globular clusters and the stellar mass functions recently determined by Sollima & Baumgardt (2017) with a large set

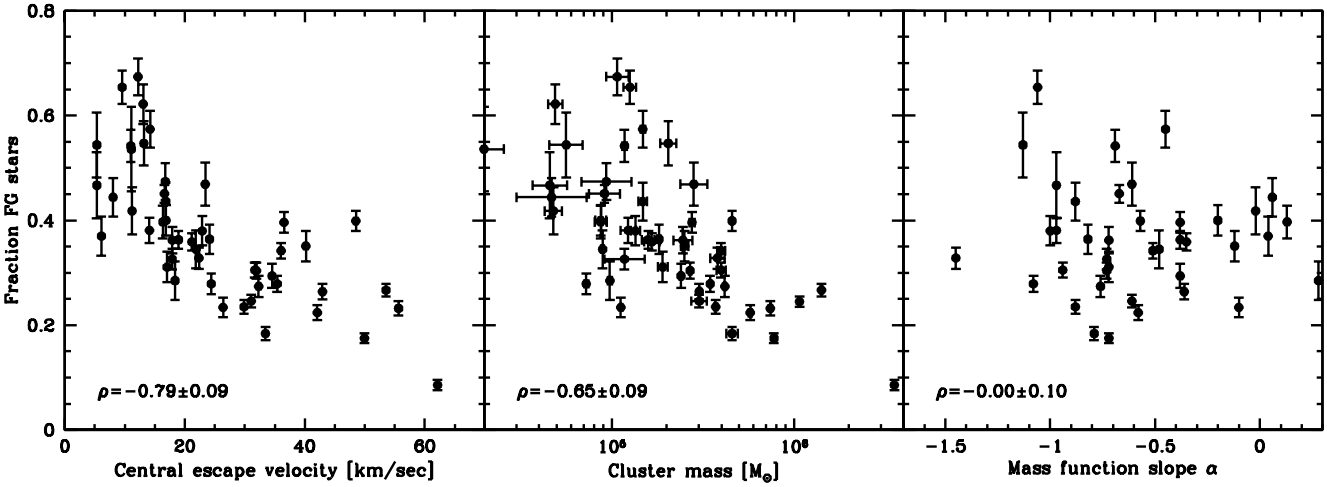

Figure 6. Correlation of the fraction of first generation stars as determined by Milone et al. (2017) with the escape velocity (left panel), the cluster mass (middle) and the mass function slope (right panel). The fraction of first generation stars in a globular cluster shows the strongest dependency on the escape velocity from the center of a globular cluster and shows no dependency on the mass function slope. This could indicate that the ability of a globular cluster to retain stellar ejecta is the most important parameter determining the fraction of second generation stars and not its later mass loss.

of N-body models then allowed us to determine total cluster masses, global mass function slopes and the structural parameters of 112 Galactic globular clusters. Our new cluster sample is more than twice as large as the sample studied by Baumgardt (2017) and includes over 2/3 of all globular clusters in the Milky Way. It is essentially complete for all globular clusters more massive than $2 \cdot 10^5$ M$_\odot$. In addition we are now able to fit the stellar mass functions at different radii in a large sample of globular clusters. Including the stellar mass functions in the fit significantly increases the accuracy of the derived cluster parameters since it allows us to better model the internal mass distribution of a globular cluster. N-body simulations are therefore another way to model globular clusters in addition to fitting them using multi-mass King Michie models (e.g. Sollima, Bellazzini & Lee 2012), `LIMEPY` models (Gieles et al. 2018) or Monte Carlo simulations (e.g. Giersz & Heggie 2009, 2011).

Our data shows several interesting correlations among the globular cluster parameters. We confirm an increase of the cluster sizes with galactocentric distance first found by van den Bergh, Morbey & Pazder (1991) as well as the correlation between mass function slope and cluster relaxation time found by Sollima & Baumgardt (2017). The latter is possibly a result of mass segregation and dynamical mass loss of globular clusters that are evolving in tidal fields of different strengths. We also find a strong correlation between the central escape velocity from a globular cluster and the fraction of second generation stars found by Milone et al. (2017) but no correlation between this fraction and the mass function slope of the clusters. These could indicate that the fraction of second generation stars is determined by conditions prevalent at the formation of globular clusters and not by their later dynamical evolution.

ACKNOWLEDGMENTS

We thank Andreas Koch, Nikolay Kacharov and Sabine Möhler for sharing unpublished radial velocities of stars in NGC 288 and M75 with us and Harvey Richer for sending us unpublished mass function data. We thank Mirek Giersz for useful discussions and his help with the MOCCA simulations which helped improve our fitting method. We also acknowledge the help of Sarah Sweet with the reduction of the `DEIMOS` data and Tony Sohn and Emily Cunningham for providing us with telluric template spectra that were useful in deriving radial velocities from the `DEIMOS` data. We finally thank Ivo Saviane for sharing his `FORS2` spectra of stars in several clusters with us. This paper is based on data obtained from the ESO Science Archive Facility. This research has also made use of the Keck Observatory Archive (KOA), which is operated by the W. M. Keck Observatory and the NASA Exoplanet Science Institute (NExScI), under contract with the National Aeronautics and Space Administration. Some of the data presented in this paper was obtained from the Mikulski Archive for Space Telescopes (MAST). STScI is operated by the Association of Universities for Research in Astronomy, Inc., under NASA contract NAS5-26555. Support for MAST for non-HST data is provided by the NASA Office of Space Science via grant NNX09AF08G and by other grants and contracts. This research has made extensive use of the SIMBAD database, operated at CDS, Strasbourg, France.

REFERENCES

Aarseth S. J., 1999, PASP, 111, 1333
Abolfathi B. et al., 2017, ArXiv e-prints
Albrow M. D., De Marchi G., Sahu K. C., 2002, ApJ, 579, 660
Alves-Brito A. et al., 2006, A&A, 460, 269

Askar A., Szkudlarek M., Gondek-Rosińska D., Giersz M., Bulik T., 2017, MNRAS, 464, L36
Bailyn C. D., 1995, ARA&A, 33, 133
Balbinot E., Santiago B. X., da Costa L. N., Makler M., Maia M. A. G., 2011, MNRAS, 416, 393
Banerjee S., Baumgardt H., Kroupa P., 2010, MNRAS, 402, 371
Barbuy B. et al., 2016, A&A, 591, A53
Baumgardt H., 2017, MNRAS, 464, 2174
Baumgardt H., Heggie D. C., Hut P., Makino J., 2003, MNRAS, 341, 247
Baumgardt H., Makino J., 2003, MNRAS, 340, 227
Baumgardt H., Sollima A., 2017, MNRAS, 472, 744
Baumgardt H., Sweet S., Browne C., Drinkwater M., Sollima A., Hurley J., 2018, MNRAS, in preparation
Bellazzini M., Fusi Pecci F., Montegriffo P., Messineo M., Monaco L., Rood R. T., 2002, AJ, 123, 2541
Bellini A. et al., 2014, ApJ, 797, 115
Bianchini P., Sills A., van de Ven G., Sippel A. C., 2017, MNRAS, 469, 4359
Blecha A., Meylan G., North P., Royer F., 2004, A&A, 419, 533
Boberg O. M., Friel E. D., Vesperini E., 2016, ApJ, 824, 5
Bonatto C., Bica E., 2008, A&A, 479, 741
Bono G. et al., 2008, ApJ, 686, L87
Bradford J. D. et al., 2011, ApJ, 743, 167
Bragaglia A., Carretta E., D'Orazi V., Sollima A., Donati P., Gratton R. G., Lucatello S., 2017, ArXiv e-prints
Bressan A., Marigo P., Girardi L., Salasnich B., Dal Cero C., Rubele S., Nanni A., 2012, MNRAS, 427, 127
Cadelano M., Dalessandro E., Ferraro F. R., Miocchi P., Lanzoni B., Pallanca C., Massari D., 2017, ApJ, 836, 170
Canterna R., Rosino L., 1981, A&A Supl. Ser., 45, 53
Carrera R., Gallart C., Pancino E., Zinn R., 2007, AJ, 134, 1298
Carretta E., Bragaglia A., Lucatello S., D'Orazi V., Gratton R. G., Donati P., Sollima A., Sneden C., 2017, A&A, 600, A118
Carretta E., Cohen J. G., Gratton R. G., Behr B. B., 2001, AJ, 122, 1469
Castelli F., Kurucz R. L., 2004, ArXiv Astrophysics e-prints
Clauset A., Shalizi C. R., Newman M. E. J., 2009, SIAM Review, 51, 661
Cohen J. G., Gratton R. G., Behr B. B., Carretta E., 1999, ApJ, 523, 739
Cohen J. G., Kirby E. N., 2012, ApJ, 760, 86
Cool A. M., Piotto G., King I. R., 1996, ApJ, 468, 655
Cooper M. C., Newman J. A., Davis M., Finkbeiner D. P., Gerke B. F., 2012, spec2d: DEEP2 DEIMOS Spectral Pipeline. Astrophysics Source Code Library
Cordero M. J., Hénault-Brunet V., Pilachowski C. A., Balbinot E., Johnson C. I., Varri A. L., 2017, MNRAS, 465, 3515
Côté P., 1999, AJ, 118, 406
Côté P., Djorgovski S. G., Meylan G., Castro S., McCarthy J. K., 2002, ApJ, 574, 783
Da Costa G. S., 1995, PASP, 107, 937
Da Costa G. S., 2016, MNRAS, 455, 199
Dalessandro E., Ferraro F. R., Massari D., Lanzoni B., Miocchi P., Beccari G., 2015, ApJ, 810, 40
Dalessandro E., Schiavon R. P., Rood R. T., Ferraro F. R., Sohn S. T., Lanzoni B., O'Connell R. W., 2012, AJ, 144, 126
D'Antona F., Caloi V., 2008, MNRAS, 390, 693
Davies M. B., Piotto G., de Angeli F., 2004, MNRAS, 349, 129
de Marchi G., Paresce F., 1995a, A&A, 304, 202
de Marchi G., Paresce F., 1995b, A&A, 304, 211
De Marchi G., Paresce F., Pulone L., 2007, ApJ, 656, L65
de Marchi G., Pulone L., 2007, A&A, 467, 107
Decressin T., Baumgardt H., Charbonnel C., Kroupa P., 2010, A&A, 516, A73
Dotter A., Chaboyer B., Jevremović D., Kostov V., Baron E., Ferguson J. W., 2008, ApJS, 178, 89
Dotter A. et al., 2010, ApJ, 708, 698
Downing J. M. B., Benacquista M. J., Giersz M., Spurzem R., 2011, MNRAS, 416, 133
Feltzing S., Primas F., Johnson R. A., 2009, A&A, 493, 913
Ferraro F. R., Carretta E., Bragaglia A., Renzini A., Ortolani S., 1997, MNRAS, 286, 1012
Ferraro F. R. et al., 2018, ApJ, submitted
Fischer P., Welch D. L., Mateo M., Cote P., 1993, AJ, 106, 1508
Frank M. J., Grebel E. K., Küpper A. H. W., 2014, MNRAS, 443, 815
Frank M. J., Hilker M., Baumgardt H., Côté P., Grebel E. K., Haghi H., Küpper A. H. W., Djorgovski S. G., 2012, MNRAS, 423, 2917
Freudling W., Romaniello M., Bramich D. M., Ballester P., Forchi V., García-Dabló C. E., Moehler S., Neeser M. J., 2013, A&A, 559, A96
Geisler D., Piatti A. E., Claria J. J., Minniti D., 1995, AJ, 109, 605
Gieles M., Balbinot E., Yaaqib R. I. S. M., Hénault-Brunet V., Zocchi A., Peuten M., Jonker P. G., 2018, MNRAS, 473, 4832
Gieles M., Sana H., Portegies Zwart S. F., 2010, MNRAS, 402, 1750
Gieles M., Zocchi A., 2015, MNRAS, 454, 576
Giersz M., Heggie D. C., 2009, MNRAS, 395, 1173
Giersz M., Heggie D. C., 2011, MNRAS, 410, 2698
Gratton R. G., Bragaglia A., Carretta E., Clementini G., Desidera S., Grundahl F., Lucatello S., 2003, A&A, 408, 529
Gratton R. G. et al., 2007, A&A, 464, 953
Gray R. O., Corbally C. J., 1994, AJ, 107, 742
Hankey W. J., Cole A. A., 2011, MNRAS, 411, 1536
Harris W. E., 1996, AJ, 112, 1487
Heggie D. C., 2014, MNRAS, 445, 3435
Hilker M., Baumgardt H., Infante L., Drinkwater M., Evstigneeva E., Gregg M., 2007, A&A, 463, 119
Ibata R., Sollima A., Nipoti C., Bellazzini M., Chapman S. C., Dalessandro E., 2011, ApJ, 738, 186
Ibata R. A., Lewis G. F., Thomas G., Martin N. F., Chapman S., 2017, ApJ, 842, 120
Irwin M. J., Demers S., Kunkel W. E., 1995, ApJ, 453, L21
Johnson C. I., Caldwell N., Rich R. M., Mateo M., Bailey, III J. I., Olszewski E. W., Walker M. G., 2017a, ApJ, 842, 24
Johnson C. I., Caldwell N., Rich R. M., Pilachowski C. A., Hsyu T., 2016, AJ, 152, 21
Johnson C. I., Caldwell N., Rich R. M., Walker M. G., 2017b, AJ, 154, 155

Johnson C. I., Pilachowski C. A., 2006, AJ, 132, 2346
Johnson C. I., Pilachowski C. A., 2012, ApJ, 754, L38
Johnson C. I., Rich R. M., Caldwell N., Mateo M., Bailey, III J. I., Olszewski E. W., Walker M. G., 2018, AJ, 155, 71
Johnson C. I., Rich R. M., Kobayashi C., Kunder A., Koch A., 2014, AJ, 148, 67
Johnson C. I., Rich R. M., Pilachowski C. A., Caldwell N., Mateo M., Bailey, III J. I., Crane J. D., 2015, AJ, 150, 63
Jordi K. et al., 2009, AJ, 137, 4586
Kacharov N., Koch A., McWilliam A., 2013, A&A, 554, A81
Kaisler D., Harris W. E., McLaughlin D. E., 1997, PASP, 109, 920
Kamann S. et al., 2018, MNRAS, 473, 5591
Khalaj P., Baumgardt H., 2013, MNRAS, 434, 3236
Khalaj P., Baumgardt H., 2015, MNRAS, 452, 924
Kimmig B., Seth A., Ivans I. I., Strader J., Caldwell N., Anderton T., Gregersen D., 2015, AJ, 149, 53
King I., 1962, AJ, 67, 471
Koch A., 2017, private communication
Koch A., Côté P., 2017, ArXiv e-prints
Koch A., Hansen C. J., Kunder A., 2017, A&A, 604, A41
Koch A., McWilliam A., 2014, A&A, 565, A23
Kroupa P., 2001, MNRAS, 322, 231
Kruijssen J. M. D., Mieske S., 2009, A&A, 500, 785
Kruijssen J. M. D., Pelupessy F. I., Lamers H. J. G. L. M., Portegies Zwart S. F., Bastian N., Icke V., 2012, MNRAS, 421, 1927
Kunder A. et al., 2017, AJ, 153, 75
Küpper A. H. W., Kroupa P., Baumgardt H., Heggie D. C., 2010, MNRAS, 407, 2241
Kurtz M. J., Mink D. J., 1998, PASP, 110, 934
Kuzma P. B., Da Costa G. S., Keller S. C., Maunder E., 2015, MNRAS, 446, 3297
Lane R. R., Kiss L. L., Lewis G. F., Ibata R. A., Siebert A., Bedding T. R., Székely P., Szabó G. M., 2011, A&A, 530, A31
Lardo C. et al., 2015, A&A, 573, A115
Liu C., Ruchti G., Feltzing S., Primas F., 2017, A&A, 601, A31
Lovisi L., Mucciarelli A., Lanzoni B., Ferraro F. R., Dalessandro E., Monaco L., 2013, ApJ, 772, 148
MacLean B. T., Campbell S. W., De Silva G. M., Lattanzio J., DOrazi V., Cottrell P. L., Momany Y., Casagrande L., 2017, ArXiv e-prints
Majewski S. R. et al., 2015, ArXiv e-prints
Manchester R. N., Lyne A. G., Robinson C., Bailes M., D'Amico N., 1991, Nature, 352, 219
Marconi G. et al., 1998, MNRAS, 293, 479
Marino A. F. et al., 2014, MNRAS, 442, 3044
Marino A. F. et al., 2018, ArXiv e-prints
McDonald I., van Loon J. T., 2007, A&A, 476, 1261
McLaughlin D. E., van der Marel R. P., 2005, ApJS, 161, 304
Merritt D., 1985, AJ, 90, 1027
Milone A. P. et al., 2017, MNRAS, 464, 3636
Muñoz C., Villanova S., Geisler D., Saviane I., Dias B., Cohen R. E., Mauro F., 2017, ArXiv e-prints
Ness M., Asplund M., Casey A. R., 2014, MNRAS, 445, 2994
Newman J. A. et al., 2013, ApJS, 208, 5
Nicholls C. P. et al., 2017, A&A, 598, A79
Nitadori K., Aarseth S. J., 2012, MNRAS, 424, 545
Noll S., Kausch W., Kimeswenger S., Barden M., Jones A. M., Modigliani A., Szyszka C., Taylor J., 2014, A&A, 567, A25
Noyola E., Gebhardt K., 2006, AJ, 132, 447
O'Connell J. E., Johnson C. I., Pilachowski C. A., Burks G., 2011, PASP, 123, 1139
Odenkirchen M., Grebel E. K., Dehnen W., Rix H.-W., Cudworth K. M., 2002, AJ, 124, 1497
Origlia L., Valenti E., Rich R. M., 2008, MNRAS, 388, 1419
Osipkov L. P., 1979, Soviet Astronomy Letters, 5, 42
Paust N. E. Q. et al., 2010, AJ, 139, 476
Piotto G., Cool A. M., King I. R., 1997, AJ, 113, 1345
Piotto G., Zoccali M., 1999, A&A, 345, 485
Pooley D. et al., 2003, ApJ, 591, L131
Pryor C., McClure R. D., Fletcher J. M., Hesser J. E., 1989, AJ, 98, 596
Pryor C., McClure R. D., Fletcher J. M., Hesser J. E., 1991, AJ, 102, 1026
Ramírez S. V., Cohen J. G., 2003, AJ, 125, 224
Rastorguev A. S., Samus N. N., 1991, Soviet Astronomy Letters, 17, 388
Richer H. B., 2017, private communication
Richer H. B. et al., 2004, AJ, 127, 2771
Rodriguez C. L., Chatterjee S., Rasio F. A., 2016, Phys. Rev. D, 93, 084029
Roederer I. U., Sneden C., 2011, AJ, 142, 22
Roederer I. U., Thompson I. B., 2015, MNRAS, 449, 3889
Salinas R., Jílková L., Carraro G., Catelan M., Amigo P., 2012, MNRAS, 421, 960
Sarajedini A. et al., 2007, AJ, 133, 1658
Saviane I., da Costa G. S., Held E. V., Sommariva V., Gullieuszik M., Barbuy B., Ortolani S., 2012, A&A, 540, A27
Schiavon R. P. et al., 2017, MNRAS, 466, 1010
Simpson J. D., De Silva G., Martell S. L., Navin C. A., Zucker D. B., 2017, MNRAS, 472, 2856
Skrutskie M. F. et al., 2006, AJ, 131, 1163
Smolinski J. P. et al., 2011, AJ, 141, 89
Sneden C., Kraft R. P., Guhathakurta P., Peterson R. C., Fulbright J. P., 2004, AJ, 127, 2162
Sollima A., Baumgardt H., 2017, MNRAS, 471, 3668
Sollima A., Bellazzini M., Lee J.-W., 2012, ApJ, 755, 156
Spitzer L., 1987, Dynamical evolution of globular clusters
Tang B. et al., 2017, MNRAS, 465, 19
Trager S. C., King I. R., Djorgovski S., 1995, AJ, 109, 218
Valenti E., Origlia L., Mucciarelli A., Rich R. M., 2015, A&A, 574, A80
van den Bergh S., Demers S., Kunkel W. E., 1980, ApJ, 239, 112
van den Bergh S., Morbey C., Pazder J., 1991, ApJ, 375, 594
Verbunt F., 1993, ARA&A, 31, 93
Vesperini E., Heggie D. C., 1997, MNRAS, 289, 898
Villanova S., Geisler D., Carraro G., Moni Bidin C., Muñoz C., 2013, ApJ, 778, 186
Villanova S., Moni Bidin C., Mauro F., Munoz C., Monaco L., 2017, MNRAS, 464, 2730
Wang L., Spurzem R., Aarseth S., Giersz M., Askar A., Berczik P., Naab T., Kouwenhoven R. S. M. B. N., 2016, MNRAS

Watkins L. L., van der Marel R. P., Bellini A., Anderson J., 2015a, ApJ, 803, 29
Watkins L. L., van der Marel R. P., Bellini A., Anderson J., 2015b, ApJ, 812, 149
Webb J. J., Leigh N. W. C., 2015, MNRAS, 453, 3278
Woodley K. A. et al., 2012, AJ, 143, 50
Yong D. et al., 2014, MNRAS, 441, 3396
Zinn R., 1985, ApJ, 293, 424
Zoccali M. et al., 2004, A&A, 423, 507
Zonoozi A. H., Küpper A. H. W., Baumgardt H., Haghi H., Kroupa P., Hilker M., 2011, MNRAS, 411, 1989

Table 2. Derived parameters of all studied globular clusters. For each cluster, the Table gives the name of the cluster, the number of cluster members with measured radial velocities, the mean radial velocity of the cluster and its error, the reduced χ^2_r value of the velocity dispersion fit, the cluster distance (either from literature data or obtained as part of the fitting process), the total cluster mass and V-band M/L ratio, the core, half-mass and projected half-light radius, the central density and the density inside the half-mass radius,the half-mass relaxation time, the global mass function slope, the mass-weighted central (1D) velocity dispersion, and the central escape velocity.

Name	N_{RV}	$<v_r>$ [km/sec]	χ^2_r	Dist. [kpc]	Mass [$M_\odot$]	M/L_V [$M_\odot/L_\odot$]	r_c [pc]	$r_{h,m}$ [pc]	$r_{h,lp}$ [pc]	$\log \rho_c$ [$M_\odot/pc^3$]	$\log \rho_{hm}$ [$M_\odot/pc^3$]	$\log T_{RH}$ [yr]	MF Slope	σ_0 [km/sec]	v_{esc} [km/sec]
NGC 104	2896	-17.2 ± 0.1	0.98	4.41[b]	$7.79 \pm 0.05 \cdot 10^5$	1.77 ± 0.16	0.49	5.62	3.57	5.31	2.72	9.58	-0.53[c]	12.2	49.9
NGC 288	584	-44.8 ± 0.1	1.34	9.80[b]	$1.16 \pm 0.03 \cdot 10^5$	2.39 ± 0.17	4.77	9.54	6.99	1.62	1.22	9.58	-0.45[c]	3.3	11.0
NGC 362	487	223.5 ± 0.3	0.98	9.40[b]	$3.45 \pm 0.05 \cdot 10^5$	1.65 ± 0.25	0.47	4.21	2.32	4.50	2.75	9.30	-0.89[c]	8.8	35.4
NGC 1261	231	71.5 ± 0.3	2.17	15.49[a]	$1.67 \pm 0.17 \cdot 10^5$	2.12 ± 0.38	1.19	4.72	3.08	3.33	2.33	9.19	-0.53[c]	5.6	21.2
Pal 2	16	-134.9 ± 1.2	0.00	27.20[a]	$3.35 \pm 1.62 \cdot 10^5$	1.66 ± 1.13	2.10	7.78	4.98	2.88	1.95	9.72	-0.98[d]	6.1	22.9
NGC 1851	586	320.2 ± 0.2	2.08	11.40[b]	$3.02 \pm 0.04 \cdot 10^5$	2.02 ± 0.15	0.15	3.09	1.65	6.57	3.32	9.02	-0.54[c]	10.2	42.9
NGC 1904	412	205.6 ± 0.2	2.70	13.27[a]	$1.69 \pm 0.11 \cdot 10^5$	1.72 ± 0.29	0.43	4.18	2.59	4.31	2.45	9.10	-0.40[d]	6.5	26.2
NGC 2298	39	144.7 ± 0.4	0.42	10.80[a]	$1.16 \pm 0.74 \cdot 10^4$	0.46 ± 0.30	0.86	4.03	2.95	2.91	1.76	8.52	0.15[c]	1.6	6.1
NGC 2419	195	-20.6 ± 0.2	0.26	83.20[a]	$9.81 \pm 1.42 \cdot 10^5$	2.23 ± 0.32	8.94	24.20	18.29	3.00	0.92	10.74	-1.50[d]	7.1	22.2
Pyxis	43	40.4 ± 0.2	0.62	39.40[a]	$4.49 \pm 1.29 \cdot 10^4$	2.95 ± 0.93	15.09	25.62	18.09	-0.23	-0.50	10.22	-1.45[d]	1.3	4.1
NGC 2808	2047	103.7 ± 0.3	3.07	9.80[b]	$7.42 \pm 0.05 \cdot 10^5$	1.64 ± 0.12	0.68	3.22	2.06	4.60	3.43	9.21	-0.50[d]	14.4	55.6
E 3	35	4.8 ± 0.5	0.00	8.09[a]	$3.06 \pm 1.69 \cdot 10^4$	8.08 ± 4.70	2.77	8.23	5.45	1.69	0.95	9.26	-0.55[d]	1.8	6.5
Pal 3	14	89.9 ± 1.2	0.00	92.50[a]	$6.15 \pm 3.29 \cdot 10^4$	2.85 ± 1.69	13.55	28.07	19.69	0.01	-0.40	10.32	-1.50[d]	1.4	4.7
NGC 3201	690	494.3 ± 0.1	1.17	4.70[a]	$1.49 \pm 0.09 \cdot 10^5$	2.40 ± 0.42	1.91	6.20	3.77	2.68	1.87	9.42	-0.96[c]	4.5	16.8
Pal 4	23	72.7 ± 0.3	0.00	103.00[a]	$2.98 \pm 1.27 \cdot 10^4$	1.64 ± 0.71	13.61	25.87	17.87	-0.29	-0.63	10.15	-1.52[c]	1.0	3.4
NGC 4147	30	179.1 ± 0.3	2.84	18.20[a]	$3.29 \pm 0.90 \cdot 10^4$	1.51 ± 0.44	0.27	3.47	2.49	4.70	2.63	8.59	0.01[c]	3.1	11.9
NGC 4372	214	75.3 ± 0.3	0.77	6.30[a]	$2.49 \pm 0.25 \cdot 10^5$	1.89 ± 0.19	4.82	9.19	6.34	1.98	1.61	9.77	-1.03[d]	4.9	16.4
Rup 106	38	-38.4 ± 0.3	0.05	24.30[a]	$1.02 \pm 0.28 \cdot 10^5$	2.62 ± 0.86	8.04	14.79	10.47	0.93	0.61	9.94	-1.19[d]	2.5	8.2
NGC 4590	252	-93.2 ± 0.2	0.65	10.59[a]	$1.23 \pm 0.12 \cdot 10^5$	2.02 ± 0.41	1.99	7.71	4.51	2.44	1.44	9.55	-1.04[c]	3.7	14.1
NGC 4833	134	202.0 ± 0.4	0.10	9.00[a]	$2.47 \pm 0.32 \cdot 10^5$	0.84 ± 0.19	2.34	9.04	6.75	2.60	1.65	9.63	-0.10[c]	4.8	17.9
NGC 5024	273	-63.1 ± 0.2	1.46	17.90[a]	$3.80 \pm 0.36 \cdot 10^5$	1.59 ± 0.20	2.16	9.92	6.23	2.81	1.63	9.92	-1.10[c]	5.9	22.4
NGC 5053	56	42.5 ± 0.2	0.08	17.20[a]	$5.66 \pm 1.33 \cdot 10^4$	1.66 ± 0.50	11.00	19.01	13.41	0.32	0.04	10.00	-1.11[c]	1.6	5.3
NGC 5139	5096	232.7 ± 0.2	1.63	5.20[b]	$3.55 \pm 0.03 \cdot 10^6$	2.90 ± 0.27	4.22	10.04	7.04	3.22	2.44	10.39	0.00[d]	17.6	62.1
NGC 5272	731	-147.2 ± 0.2	2.22	10.06[a]	$3.94 \pm 0.23 \cdot 10^5$	1.56 ± 0.22	1.04	5.44	3.36	3.80	2.42	9.47	-0.75[c]	8.1	31.7
NGC 5286	1024	62.2 ± 0.4	0.61	11.70[a]	$4.01 \pm 0.19 \cdot 10^5$	1.41 ± 0.14	0.77	4.26	2.64	4.12	2.79	9.30	-0.67[c]	9.3	36.0
NGC 5466	84	106.9 ± 0.1	0.90	16.90[a]	$4.56 \pm 1.13 \cdot 10^4$	1.13 ± 0.39	8.16	15.68	10.72	0.57	0.20	9.83	-1.04[c]	1.6	5.3
NGC 5634	49	-16.2 ± 0.5	0.97	27.20[a]	$2.13 \pm 0.47 \cdot 10^5$	2.32 ± 0.74	0.88	7.50	4.69	4.22	2.11	9.56	-0.83[d]	5.3	21.7
NGC 5694	89	-139.4 ± 0.4	0.87	37.33[a]	$3.83 \pm 0.38 \cdot 10^5$	2.78 ± 0.32	0.04	5.93	3.31	6.65	2.39	9.53	-0.80[d]	8.9	35.2
IC 4499	37	38.7 ± 0.5	0.55	18.20[a]	$1.67 \pm 0.47 \cdot 10^5$	2.25 ± 0.78	5.30	14.84	9.83	1.47	0.80	10.06	-1.31[d]	3.1	11.2
NGC 5824	191	-25.5 ± 0.5	0.99	31.80[a]	$7.79 \pm 0.42 \cdot 10^5$	2.30 ± 0.34	0.08	6.74	3.74	6.54	2.50	9.78	-1.04[d]	11.9	48.6
Pal 5	37	-58.4 ± 0.3	0.00	23.55[a]	$1.39 \pm 0.65 \cdot 10^4$	1.60 ± 0.80	20.13	35.67	25.10	-1.14	-1.45	10.24	-1.50[d]	0.6	1.9
NGC 5897	241	101.2 ± 0.2	1.33	13.43[a]	$2.03 \pm 0.21 \cdot 10^5$	3.05 ± 0.43	5.85	11.59	8.02	1.59	1.20	9.92	-1.17[d]	3.9	13.2
NGC 5904	889	53.8 ± 0.2	1.13	7.50[b]	$3.72 \pm 0.06 \cdot 10^5$	1.52 ± 0.20	1.20	5.58	3.61	3.66	2.41	9.45	-0.52[c]	7.7	29.9
NGC 5927	386	-104.1 ± 0.3	1.42	8.40[b]	$3.54 \pm 0.03 \cdot 10^5$	2.61 ± 0.36	1.46	7.21	4.98	3.28	2.23	9.54	-0.30[c]	6.5	24.9
NGC 5986	231	101.0 ± 0.4	1.07	9.00[a]	$3.01 \pm 0.31 \cdot 10^5$	2.45 ± 0.38	1.09	3.73	2.44	4.13	3.27	9.12	-0.57[c]	8.3	31.1
Pal 14	17	72.2 ± 0.2	0.00	71.00[a]	$2.27 \pm 1.14 \cdot 10^4$	3.40 ± 1.82	17.10	33.14	23.60	-0.68	-1.06	10.27	-1.52[c]	0.8	2.6
NGC 6093	455	11.2 ± 0.4	1.94	10.50[a]	$2.49 \pm 0.12 \cdot 10^5$	1.43 ± 0.15	0.19	3.02	1.83	5.48	3.15	8.94	-0.31[c]	9.5	40.2
NGC 6121	2981	71.0 ± 0.1	0.85	2.14[a]	$9.69 \pm 0.26 \cdot 10^4$	1.71 ± 0.10	0.66	4.20	2.82	3.63	2.17	8.99	-0.19[c]	4.6	18.4
NGC 6101	0	361.4 ± 1.7	0.00	16.07[a]	$1.27 \pm 0.11 \cdot 10^5$	3.00 ± 1.70	5.45	14.97	10.32	1.32	0.66	9.98	-1.02[c]	2.7	9.6
NGC 6144	19	196.0 ± 0.7	0.08	12.02[a]	$4.63 \pm 2.66 \cdot 10^4$	0.54 ± 0.32	2.72	7.91	5.90	1.77	1.05	9.25	0.12[c]	2.2	8.0
NGC 6139	56	25.0 ± 0.8	0.16	10.40[a]	$3.59 \pm 0.73 \cdot 10^5$	1.90 ± 0.40	0.41	4.29	2.62	4.84	2.71	9.28	-0.57[d]	9.2	37.8
Ter 3	22	-135.7 ± 0.6	0.00	8.10[a]	$5.46 \pm 2.25 \cdot 10^4$	7.70 ± 3.49	2.39	7.92	5.27	1.95	1.12	9.35	-0.63[d]	2.4	9.2
NGC 6171	392	-34.7 ± 0.2	1.53	6.09[a]	$8.70 \pm 0.70 \cdot 10^4$	2.16 ± 0.61	0.88	4.27	3.11	3.31	2.12	8.95	0.08[c]	4.3	16.4

Table 2 – *continued*

Name	N_{RV}	$<v_r>$ [km/sec]	χ^2_r	Dist. [kpc]	Mass [$M_\odot$]	M/L_V [$M_\odot/L_\odot$]	r_c [pc]	$r_{h,m}$ [pc]	$r_{h,lp}$ [pc]	$\log \rho_c$ [$M_\odot/pc^3$]	$\log \rho_{hm}$ [$M_\odot/pc^3$]	$\log T_{RH}$ [yr]	MF Slope	σ_0 [km/sec]	v_{esc} [km/sec]
ESO 452-SC11	13	16.4 ± 0.4	0.00	7.80[a]	$1.06 \pm 0.57 \cdot 10^4$	3.38 ± 1.91	0.16	5.21	3.66	4.06	1.02	8.73	-0.05[d]	1.6	6.3
NGC 6205	386	-244.4 ± 0.3	2.92	6.60[a]	$4.53 \pm 0.34 \cdot 10^5$	2.61 ± 0.26	1.58	4.56	3.08	3.58	2.87	9.36	-0.62[c]	9.2	33.4
NGC 6229	21	-138.3 ± 0.8	0.00	30.62[a]	$2.91 \pm 0.94 \cdot 10^5$	2.42 ± 0.88	1.16	5.01	3.18	3.56	2.46	9.35	-0.63[d]	7.1	27.3
NGC 6218	469	-41.2 ± 0.2	0.99	5.22[a]	$8.65 \pm 0.60 \cdot 10^4$	1.27 ± 0.30	0.71	4.05	2.82	4.05	2.51	8.91	-0.25[c]	4.5	16.9
NGC 6254	400	74.0 ± 0.2	1.07	4.71[a]	$1.84 \pm 0.04 \cdot 10^5$	1.94 ± 0.07	0.81	4.39	2.78	3.78	2.49	9.15	-0.50[c]	6.2	24.1
NGC 6256	15	-99.6 ± 1.1	0.00	6.40[a]	$7.23 \pm 3.32 \cdot 10^4$	2.23 ± 1.43	0.05	4.38	2.93	5.98	1.99	8.96	-0.26[d]	4.5	17.7
NGC 6266	239	-74.5 ± 0.7	1.67	6.47[b]	$7.07 \pm 0.05 \cdot 10^5$	2.57 ± 0.21	0.39	2.95	1.83	5.13	3.52	9.13	-0.43[d]	15.2	60.9
NGC 6273	296	145.3 ± 0.5	0.55	8.24[a]	$6.80 \pm 0.59 \cdot 10^5$	2.09 ± 0.20	1.11	4.97	3.13	4.04	2.82	9.53	-0.81[d]	11.0	42.5
NGC 6284	56	29.0 ± 0.7	0.24	15.30[a]	$5.51 \pm 1.13 \cdot 10^5$	3.42 ± 1.11	0.63	6.77	3.91	4.17	2.38	9.67	-0.94[d]	8.9	36.2
NGC 6293	0	-142.6 ± 0.4	1.06	9.50[a]	$1.88 \pm 0.18 \cdot 10^5$	1.67 ± 0.29	0.11	4.37	2.76	5.55	2.34	9.17	-0.46[d]	7.5	29.9
NGC 6304	193	-108.2 ± 0.4	0.65	9.40[a]	$2.77 \pm 0.29 \cdot 10^5$	1.37 ± 0.26	1.02	6.68	4.45	3.39	2.03	9.49	-0.66[c]	5.7	23.0
NGC 6316	70	99.1 ± 0.8	0.39	11.60[a]	$3.75 \pm 0.69 \cdot 10^5$	2.10 ± 0.75	0.59	4.49	2.72	4.40	2.69	9.32	-0.61[d]	9.0	35.9
NGC 6341	422	-120.7 ± 0.3	0.75	8.10[b]	$2.68 \pm 0.03 \cdot 10^5$	1.81 ± 0.09	0.61	4.14	2.28	4.94	2.67	9.24	-0.82[c]	8.0	31.9
NGC 6342	19	116.0 ± 0.8	0.00	8.43[a]	$4.64 \pm 1.60 \cdot 10^4$	2.82 ± 1.44	0.07	2.88	2.10	6.69	2.96	8.53	0.14[d]	4.5	17.0
NGC 6356	20	37.6 ± 1.2	0.00	15.10[a]	$3.98 \pm 1.54 \cdot 10^5$	1.62 ± 0.65	1.14	5.89	3.71	3.76	2.42	9.54	-0.81[d]	7.8	30.7
NGC 6355	10	-196.4 ± 1.3	0.00	8.70[a]	$1.53 \pm 0.77 \cdot 10^5$	1.22 ± 0.66	0.33	4.22	2.64	4.82	2.41	9.09	-0.39[d]	6.2	24.6
NGC 6352	33	-140.1 ± 0.8	0.02	5.89[a]	$9.38 \pm 3.49 \cdot 10^4$	2.47 ± 0.95	0.57	4.71	3.23	3.64	1.97	9.08	-0.37[d]	4.4	16.8
NGC 6366	220	-120.9 ± 0.2	0.51	3.30[a]	$4.73 \pm 0.56 \cdot 10^4$	2.34 ± 0.73	1.38	4.54	3.31	2.65	1.83	8.89	-0.16[c]	3.0	11.2
HP 1	24	40.1 ± 1.1	0.00	6.80[a]	$1.11 \pm 0.38 \cdot 10^5$	5.04 ± 1.95	0.27	3.86	2.55	5.16	2.41	8.95	-0.26[d]	5.5	21.3
NGC 6362	374	-14.7 ± 0.2	1.11	8.00[b]	$1.47 \pm 0.04 \cdot 10^5$	2.60 ± 0.14	2.85	8.07	5.77	2.22	1.53	9.51	-0.39[c]	3.9	14.2
Lil 1	64	58.2 ± 2.2	0.30	8.10[a]	$6.66 \pm 1.17 \cdot 10^5$	1.48 ± 0.29	0.06	1.57	1.11	7.85	4.91	8.61	0.07[d]	23.2	94.3
Ter 1	27	57.7 ± 1.2	0.00	6.70[a]	$2.23 \pm 0.66 \cdot 10^5$	3.22 ± 1.81	0.61	3.34	2.27	4.18	2.89	8.99	-0.29[d]	7.8	30.2
Ton 2	24	-183.8 ± 0.8	0.00	6.40[a]	$8.01 \pm 4.02 \cdot 10^4$	5.31 ± 3.05	0.95	6.39	4.45	2.67	1.38	9.18	-0.47[d]	2.9	11.8
NGC 6388	481	83.4 ± 0.5	2.89	11.00[b]	$1.06 \pm 0.01 \cdot 10^6$	1.93 ± 0.16	0.35	3.20	1.96	5.55	3.59	9.28	-0.57[d]	18.2	74.2
NGC 6402	333	-60.7 ± 0.4	1.22	9.30[a]	$7.74 \pm 0.61 \cdot 10^5$	2.20 ± 0.23	2.28	5.33	3.57	3.32	2.79	9.60	-0.87[d]	11.1	39.0
NGC 6397	2945	18.4 ± 0.1	1.33	2.48[b]	$8.89 \pm 0.16 \cdot 10^4$	2.18 ± 0.34	0.08	4.00	2.19	5.99	2.67	8.96	-0.75[c]	5.2	21.9
Ter 5	398	-82.3 ± 1.3	0.58	5.90[a]	$5.66 \pm 0.71 \cdot 10^5$	1.31 ± 0.26	0.13	1.58	1.14	6.92	4.77	8.59	0.09[d]	19.0	72.1
NGC 6440	164	-67.8 ± 1.0	1.24	8.24[a]	$4.42 \pm 0.64 \cdot 10^5$	2.04 ± 0.40	0.21	1.79	1.25	6.21	4.48	8.63	0.05[d]	15.8	61.7
NGC 6441	326	17.1 ± 0.8	1.78	12.00[b]	$1.23 \pm 0.01 \cdot 10^6$	2.05 ± 0.13	0.42	3.37	2.03	5.40	3.59	9.35	-0.63[d]	18.8	75.8
Ter 6	15	136.6 ± 1.6	0.00	6.70[a]	$1.17 \pm 0.44 \cdot 10^5$	1.15 ± 0.49	0.04	2.01	1.48	8.37	3.87	8.45	0.22[d]	8.7	32.8
NGC 6496	120	-134.7 ± 0.3	0.65	11.69[a]	$1.06 \pm 0.16 \cdot 10^5$	2.79 ± 1.65	3.07	7.73	5.05	2.06	1.47	9.47	-0.75[d]	3.4	12.2
NGC 6522	158	-14.0 ± 0.6	0.99	7.70[a]	$3.92 \pm 0.54 \cdot 10^5$	3.31 ± 1.03	0.15	7.78	4.34	5.58	2.01	9.75	-1.01[d]	8.2	33.3
NGC 6535	30	-214.9 ± 0.4	0.41	7.28[a]	$2.00 \pm 0.56 \cdot 10^4$	4.80 ± 2.65	0.20	2.94	2.22	5.04	2.37	8.39	0.82[d]	2.8	11.1
NGC 6528	50	211.0 ± 0.7	1.43	7.45[a]	$8.96 \pm 1.85 \cdot 10^4$	2.26 ± 0.75	0.11	2.80	1.97	5.94	3.02	8.65	0.03[d]	6.4	26.3
NGC 6539	139	35.6 ± 0.5	0.81	8.40[a]	$2.50 \pm 0.35 \cdot 10^5$	1.55 ± 0.40	0.91	6.44	4.04	3.75	2.03	9.50	-0.78[d]	5.9	23.9
NGC 6544	10	-36.4 ± 1.0	0.00	2.46[a]	$6.34 \pm 3.12 \cdot 10^4$	1.88 ± 0.94	0.08	1.84	1.37	7.71	3.91	8.25	0.41[d]	6.4	25.1
NGC 6541	148	-163.9 ± 0.4	1.10	8.63[a]	$2.77 \pm 0.09 \cdot 10^5$	1.42 ± 0.50	0.22	4.28	2.61	5.66	2.65	9.21	-0.46[c]	8.7	36.5
NGC 6553	431	0.5 ± 0.4	1.12	4.90[a]	$2.35 \pm 0.19 \cdot 10^5$	3.13 ± 0.45	0.55	2.93	2.02	4.83	3.55	8.87	-0.18[d]	8.5	32.8
NGC 6558	17	-195.6 ± 0.7	0.00	6.30[a]	$2.93 \pm 1.09 \cdot 10^4$	1.05 ± 0.40	0.24	2.33	1.77	5.17	3.30	8.26	0.40[d]	3.5	13.7
IC 1276	16	155.3 ± 0.9	0.00	4.00[a]	$5.46 \pm 2.60 \cdot 10^4$	1.99 ± 1.04	1.05	4.60	3.16	3.38	2.29	8.90	-0.21[d]	3.3	12.3
NGC 6569	223	-49.9 ± 0.4	2.55	12.00[a]	$3.02 \pm 0.36 \cdot 10^5$	1.98 ± 0.44	1.21	4.60	2.94	3.55	2.58	9.29	-0.58[d]	7.5	28.4
NGC 6584	0	222.9 ± 15.0	0.00	13.18[a]	$9.07 \pm 2.00 \cdot 10^4$	1.12 ± 0.37	0.72	4.70	2.98	3.16	1.74	9.12	-0.67[c]	4.2	16.6
NGC 6624	196	54.7 ± 0.4	0.96	7.00[b]	$7.31 \pm 0.20 \cdot 10^4$	1.02 ± 0.13	0.19	2.08	1.49	5.21	3.26	8.40	1.25[c]	6.1	24.4

Table 2 – *continued*

Name	N_{RV}	$<v_r>$ [km/sec]	χ^2_r	Dist. [kpc]	Mass [$M_\odot$]	M/L_V [$M_\odot/L_\odot$]	r_c [pc]	$r_{h,m}$ [pc]	$r_{h,lp}$ [pc]	$\log \rho_c$ [$M_\odot/pc^3$]	$\log \rho_{hm}$ [$M_\odot/pc^3$]	$\log T_{RH}$ [yr]	MF Slope	σ_0 [km/sec]	v_{esc} [km/sec]
NGC 6626	201	11.0 ± 0.6	2.02	5.50[a]	$3.69 \pm 0.38 \cdot 10^5$	2.19 ± 0.35	0.13	2.63	1.76	7.42	3.67	8.89	-0.18[d]	12.6	49.5
NGC 6642	13	-33.0 ± 1.0	0.00	8.05[a]	$8.72 \pm 5.49 \cdot 10^4$	1.77 ± 1.13	0.12	1.99	1.50	6.34	3.89	8.36	0.30[d]	6.9	27.5
NGC 6656	720	-147.8 ± 0.3	1.04	3.10[b]	$4.16 \pm 0.05 \cdot 10^5$	2.15 ± 0.08	1.19	5.16	3.26	3.66	2.56	9.45	-0.68[c]	8.4	32.3
NGC 6681	32	217.4 ± 0.9	1.12	9.20[b]	$1.13 \pm 0.02 \cdot 10^5$	2.00 ± 0.28	0.05	3.07	2.10	7.33	3.07	8.76	-0.00[d]	7.1	26.4
NGC 6712	215	-107.5 ± 0.3	0.44	6.73[a]	$1.27 \pm 0.13 \cdot 10^5$	1.41 ± 0.31	1.22	4.31	2.86	3.57	2.69	9.03	-0.33[c]	5.0	18.7
NGC 6715	548	142.3 ± 0.3	4.77	23.50[b]	$1.41 \pm 0.02 \cdot 10^6$	2.04 ± 0.10	0.54	5.62	3.20	5.35	2.98	9.77	-1.03[d]	16.2	53.5
NGC 6723	360	-94.4 ± 0.2	0.88	8.20[a]	$1.57 \pm 0.13 \cdot 10^5$	1.77 ± 0.28	1.69	4.82	3.50	2.99	2.29	9.14	0.02[c]	5.3	19.0
NGC 6749	15	-58.5 ± 0.9	0.00	7.80[a]	$5.68 \pm 3.57 \cdot 10^4$	1.45 ± 0.95	1.30	4.97	3.37	3.00	2.06	8.98	-0.28[d]	3.2	11.8
NGC 6752	1095	-26.2 ± 0.1	1.20	4.30[b]	$2.39 \pm 0.04 \cdot 10^5$	2.17 ± 0.34	0.19	4.01	2.40	5.38	2.64	9.16	-0.45[c]	8.3	34.5
NGC 6760	23	-1.6 ± 1.7	0.00	7.40[a]	$2.54 \pm 1.08 \cdot 10^5$	2.29 ± 0.98	0.75	4.50	2.82	4.03	2.54	9.24	-0.53[d]	7.2	28.6
NGC 6779	96	-122.0 ± 0.5	0.28	13.49[a]	$2.81 \pm 0.52 \cdot 10^5$	1.58 ± 0.38	1.71	6.40	4.38	3.08	2.14	9.49	-0.59[c]	6.1	23.4
Ter 7	42	159.6 ± 0.1	2.12	26.91[a]	$1.66 \pm 0.51 \cdot 10^4$	1.00 ± 0.57	3.26	21.36	13.07	0.71	-0.67	9.84	-1.10[d]	0.8	3.2
Arp 2	65	122.5 ± 0.3	0.30	32.36[a]	$1.09 \pm 0.31 \cdot 10^5$	10.03 ± 3.47	11.21	23.58	16.74	0.40	-0.04	10.32	-1.50[d]	2.0	6.9
NGC 6809	581	174.8 ± 0.2	2.42	5.75[a]	$1.88 \pm 0.12 \cdot 10^5$	2.38 ± 0.49	2.93	6.92	4.70	2.45	1.91	9.51	-0.82[c]	4.8	17.0
Ter 8	110	148.2 ± 0.2	0.70	26.73[a]	$4.39 \pm 1.21 \cdot 10^4$	4.02 ± 1.53	12.44	21.40	15.26	0.02	-0.26	10.07	-1.32[d]	1.4	4.5
Pal 11	18	-67.2 ± 1.0	0.00	14.30[a]	$1.48 \pm 1.17 \cdot 10^5$	2.26 ± 1.83	5.08	9.33	6.63	2.08	1.75	9.64	-0.91[d]	3.7	12.3
NGC 6838	237	-22.5 ± 0.2	1.17	3.86[a]	$4.91 \pm 0.47 \cdot 10^4$	2.76 ± 1.05	0.52	4.54	2.95	3.67	1.94	8.90	-0.19[c]	3.3	13.1
NGC 6864	59	-188.6 ± 0.9	1.12	20.00[a]	$5.86 \pm 1.24 \cdot 10^5$	2.94 ± 0.68	0.56	4.00	2.46	4.81	3.14	9.31	-0.60[d]	11.8	47.1
NGC 6934	29	-406.1 ± 0.5	0.08	14.00[a]	$1.17 \pm 0.34 \cdot 10^5$	1.76 ± 0.51	1.12	4.72	2.63	3.56	2.50	9.17	-0.97[c]	4.7	17.9
NGC 7006	30	-383.2 ± 0.6	0.02	58.80[a]	$2.29 \pm 0.82 \cdot 10^5$	1.23 ± 0.44	3.23	10.33	6.68	2.04	1.22	9.87	-1.12[d]	4.4	16.1
NGC 7078	1473	-106.5 ± 0.2	1.31	9.90[b]	$4.53 \pm 0.05 \cdot 10^5$	1.15 ± 0.11	0.08	3.41	1.90	6.60	3.23	9.18	-0.75[c]	12.9	48.5
NGC 7089	543	-3.6 ± 0.3	2.44	11.50[a]	$5.82 \pm 0.12 \cdot 10^5$	1.62 ± 0.06	0.77	4.79	3.00	4.31	2.80	9.44	-0.56[c]	10.6	42.1
NGC 7099	762	-185.3 ± 0.1	0.93	8.10[a]	$1.33 \pm 0.08 \cdot 10^5$	1.85 ± 0.39	0.06	4.88	2.44	5.99	2.21	9.26	-1.06[c]	5.5	22.9
Pal 12	26	28.2 ± 0.2	0.00	19.05[a]	$1.19 \pm 0.73 \cdot 10^4$	2.92 ± 2.02	3.69	9.98	6.98	1.16	0.50	9.18	-0.38[d]	1.0	3.6
Pal 13	43	25.7 ± 0.3	0.00	24.80[a]	$2.74 \pm 1.45 \cdot 10^4$	10.74 ± 5.75	3.45	18.13	11.08	1.03	-0.24	9.85	-1.11[d]	1.2	4.6
NGC 7492	29	-176.7 ± 0.2	0.37	26.55[a]	$2.58 \pm 0.77 \cdot 10^4$	1.21 ± 0.56	4.09	11.14	7.51	1.06	0.40	9.47	-0.74[d]	1.4	4.3

Notes: a: Cluster distance from literature, b: Fitted cluster distance, c: Global mass function slope determined from observed mass functions,
d: Global mass function slope estimated from clusters' relaxation time

APPENDIX A: ESO/VLT AND KECK PROGRAM IDS USED TO DERIVE RADIAL VELOCITIES OF INDIVIDUAL STARS IN GLOBULAR CLUSTERS

Table A1. ESO/VLT and Keck program IDs used to derive radial velocities of stars in globular clusters.

Cluster	Program IDs
Arp 2	075.D-0075(A), 075.D-0075(B)
E 3	097.D-0056(A)
HP 1	093.D-0124(A)
IC 4499	097.D-0111(A)
Lil 1	085.D-0377(A), 087.D-0716(A), 089.D-0306(A)
NGC 104	71.B-0414(A), 072.D-0777(A), 073.D-0760(A), 074.B-0415(A), 075.D-0043(A), 081.D-0287(A), 087.D-0716(A), 088.B-0403(A), 088.D-0026(A), 091.D-0329(A), 093.D-0818(A), 188.B-3002(Q), 188.B-3002(R), 188.B-3002(S), 188.B-3002(V), 193.D-0232(D)
NGC 288	072.D-0337(A), 074.A-0508(A), 075.D-0043(A), 075.D-0209(A), 087.D-0276(A), 092.D-0205(A), 193.D-0232(D)
NGC 362	075.D-0209(A), 087.D-0276(A), 088.D-0026(B), 094.D-0363(A), 188.B-3002(W), 188.B-3002(X), 193.D-0232(D)
NGC 1261	096.D-0483(A), 188.B-3002(M), 193.B-0936(N), 193.B-0936(O), 193.D-0232(D)
NGC 1851	080.D-0106(A), 083.D-0208(A), 084.D-0470(A), 084.D-0693(A), 088.B-0403(A), 088.D-0519(A), 090.D-0487(A), 092.D-0171(C), 092.D-0477(A), 188.B-3002(B), 386.D-0086(A)
NGC 1904	080.B-0489(A), 080.B-0784(A), 085.D-0205(A), 094.D-0363(A), 193.B-0936(A), 193.B-0936(E), 193.D-0232(D), C251D
NGC 2298	70.B-0398(B), 71.B-0516(B), 074.B-0417(B), 076.B-0662(B), U48D
NGC 2419	096.D-0297(A), C023Hr, C098Hr, C180Hr, C182Hr, C21H, C231Hb, C237Hr, C239Hr, C251D, C363Hr, U033Hr
NGC 2808	072.D-0742(A), 088.D-0026(C), 088.D-0519(B), 091.D-0329(A), 092.D-0171(C), 093.D-0818(A), 094.D-0024(A), 094.D-0363(A), 094.D-0455(A), 188.B-3002(G), 188.B-3002(M), 386.D-0086(A)
NGC 3201	073.D-0211(A), 087.D-0276(A), 088.B-0403(A), 094.D-0024(A), 095.D-0735(A), 171.B-0520(D), 193.D-0232(D)
NGC 4147	C204Hr
NGC 4372	71.D-0219(A), 088.B-0492(A), 088.D-0026(D), 091.D-0019(A), 188.B-3002(C)
NGC 4590	71.D-0311(A), 073.D-0211(A), 095.D-0735(A), 171.B-0520(D), 197.B-1074(D), 197.B-1074(E), C102D, K185D, U15H
NGC 4833	095.D-0539(A)
NGC 5024	085.D-0536(A), C189Hr, C237Hr, C242Hr
NGC 5139	074.D-0369(A), 078.B-0496(A), 078.D-0825(A), 079.D-0021(A), 095.D-0539(A), 096.D-0728(A), 272.D-5065(A)
NGC 5272	093.D-0536(A), 193.D-0232(D), C05H, C10H, C11H, C222Hb, C52H
NGC 5824	087.D-0465(A), 095.D-0290(A)
NGC 5897	093.D-0628(A), C174D
NGC 5904	073.D-0695(A), 084.D-0479(A), 087.D-0230(A), 087.D-0276(A), 088.B-0403(A), 193.D-0232(D), C10H, C19H, H2aH, U02H, U09H, U100Hb, U27H, U34H, U74H
NGC 5927	69.D-0455(A), 074.B-0446(B), 193.D-0232(D), 197.B-1074(F)

Table A1 – *continued*

Cluster	Program IDs
NGC 5986	083.D-0530(A), 193.D-0232(F)
NGC 6093	65.L-0518(A), 073.D-0695(A), 079.D-0021(A), 083.D-0530(A)
NGC 6121	073.D-0093(A), 081.D-0356(A), 083.B-0083(A), 085.D-0205(A), 085.D-0537(A), 089.D-0062(A), 089.D-0298(A), 093.D-0789(A), 093.D-0818(A), 095.D-0819(A), 193.D-0232(B)
NGC 6171	71.D-0311(A), 075.D-0043(A), 095.D-0834(A), 193.D-0232(F)
NGC 6205	C05H, C21H, C55H, C75H, C88H, H03H, H14H, H4aH, U01H, U058Hr, U11H, U204Hr, U21H, U27H, U47H
NGC 6218	073.D-0211(A), 087.D-0276(A), 095.D-0290(A), 193.B-0936(I), 193.B-0936(K), 193.D-0232(B)
NGC 6229	C034Hr
NGC 6254	073.D-0211(A), 193.D-0232(B)
NGC 6266	193.D-0232(B)
NGC 6284	193.D-0232(B)
NGC 6304	193.D-0232(F)
NGC 6316	193.D-0232(F)
NGC 6341	C02H, C07H, C11H, C147H, C189Hr, C21H, C231Hb, C287Hr, C66H, H03H, Y267Hr
NGC 6342	U57
NGC 6352	074.B-0446(B)
NGC 6355	083.D-0063(A)
NGC 6362	093.D-0618(A), 097.D-0325(A)
NGC 6366	69.B-0467(A), 383.D-0261(A)
NGC 6388	087.D-0230(A), 087.D-0344(A), 095.D-0834(A)
NGC 6397	71.C-0162(A), 71.D-0076(A), 072.B-0198(A), 073.D-0058(A), 073.D-0093(A), 075.D-0125(A), 081.D-0356(A)
NGC 6402	193.D-0232(B)
NGC 6440	091.D-0115(A), 093.D-0286(A), 193.D-0232(B), U051NS, U10NS
NGC 6441	073.D-0211(A), 073.D-0760(A), 083.D-0208(A), 095.D-0834(A), 193.D-0232(B)
NGC 6496	193.D-0232(F)
NGC 6522	71.B-0641(A), 71.D-0576(A), 083.B-0324(A), 088.D-0398(A), 091.D-0383(A), 097.D-0175(A), 188.B-3002(F), 188.B-3002(G), 193.D-0232(F)
NGC 6528	67.B-0382(A), 71.B-0617(A), 083.B-0324(A), 093.D-0286(A), 187.B-0909(A)
NGC 6535	087.B-0086(A), 093.B-0583(A)
NGC 6539	193.D-0232(F), U17NS
NGC 6541	093.D-0628(A)
NGC 6553	073.B-0074(A), 093.D-0286(A), 193.B-0936(E), 193.D-0232(F), C47H, U57H
NGC 6558	71.B-0617(A), 083.B-0324(A), 093.D-0123(A), 188.B-3002(I)
NGC 6569	093.D-0286(A), 193.D-0232(F), U154NS
NGC 6624	083.D-0798(D), U154NS, U17NS, U56NS
NGC 6626	091.D-0535(A), 193.B-0936(C), 193.B-0936(E), 193.D-0232(B)
NGC 6642	081.D-0297(A)
NGC 6656	71.D-0217(A), 083.D-0530(A), 085.D-0698(A), 087.D-0230(A), 095.D-0027(A), 095.D-0735(A), 097.A-9009(A)
NGC 6681	71.B-0516(A)
NGC 6712	095.D-0290(A), 193.D-0232(F)
NGC 6715	71.B-0146(A), 71.B-0641(A), 075.D-0075(A), 075.D-0075(B), 081.D-0286(A), 083.B-0403(A), 095.D-0539(A)
NGC 6723	095.B-0028(A), 193.D-0232(F)

Table A1 – *continued*

Cluster	Program IDs
NGC 6752	073.D-0100(A), 075.D-0492(A), 079.D-0674(A), 079.D-0674(B), 079.D-0674(C), 081.D-0356(A), 083.B-0083(A), 089.D-0298(A), 091.D-0329(A), 095.D-0320(A), 193.D-0232(B)
NGC 6809	073.D-0211(A), 091.D-0329(A), 093.D-0270(A), 093.D-0818(A), 095.D-0735(A)
NGC 6838	072.A-0494(A), 073.D-0211(A), 095.D-0735(A), 189.B-0925(A), 189.B-0925(C), C01H, C03H, C04H, C10ANS, C118NS, C19H, C216Hr, C52H, C53H, H30aH, H5aH, U017Hr, U062NS, U154NS
NGC 6864	69.B-0305(A), C215D
NGC 7006	C034Hr, C204M, U11H, U21H
NGC 7078	073.D-0695(A), 080.B-0489(A), 080.B-0784(A), 095.D-0539(A), C05H, C11H, C147Hr, C14H, C21H, C316Hr, C36H, C53H, C75H, N13H, U09H, U27H, U59H
NGC 7089	084.D-0933(A), 193.B-0936(C), 193.B-0936(F), C171D, C174D
NGC 7099	073.D-0695(A), 085.D-0375(A), 088.B-0403(A), 092.D-0477(A), C363Hr, U11H
NGC 7492	C03H, C21H, C88H
Pal 2	U039D
Pal 5	083.B-0403(A), C50H, U25H
Pal 11	U154NS
Pal 12	097.D-0111(B), C11H, C21H, U09H, U47H
Pyxis	089.D-0722(A)
Ter 1	089.D-0392(A)
Ter 3	60.A-9700(A), 60.A-9700(G)
Ter 5	085.D-0377(A), 087.D-0716(A), 087.D-0716(B), 087.D-0748(A), 091.D-0115(A), 283.D-5027(A), C184D, U060D, U062NS, U074D, U092NS, U097NS, U112NS, U146NS, U57NS
Ter 6	091.D-0115(A)
Ter 7	67.B-0147(A), 075.D-0075(A), 097.D-0111(B)
Ter 8	075.D-0075(A), 087.B-0086(A)
Ton 2	091.D-0389(A)

APPENDIX B: SOURCES OF SURFACE DENSITY PROFILES, STELLAR RADIAL VELOCITIES AND MASS FUNCTIONS OF INDIVIDUAL CLUSTERS

Table B1. Sources of published individual stellar radial velocities (LOS), surface density profiles (SD) and stellar mass functions (MF) used in this work in addition to the data published by Baumgardt (2017) and Sollima & Baumgardt (2017).

Name	Source	Type
E3	van den Bergh, Demers & Kunkel (1980)	SD
ESO 452-SC11	Bonatto & Bica (2008)	SD
	Koch, Hansen & Kunder (2017)	LOS
	Simpson et al. (2017)	SD, LOS
HP 1	Barbuy et al. (2016)	LOS
IC 1276	Côté (1999)	LOS
IC 4499	Hankey & Cole (2011)	LOS
NGC 104	de Marchi & Paresce (1995b)	MF
	Richer (2017)	MF
	Kunder et al. (2017)	LOS
	Kamann et al. (2018)	LOS
NGC 288	Bellazzini et al. (2002)	MF
	Sollima, Bellazzini & Lee (2012)	MF
NGC 362	Fischer et al. (1993)	SD
	McDonald & van Loon (2007)	LOS
	Paust et al. (2010)	MF
	Kamann et al. (2018)	LOS
	Richer (2017)	MF
NGC 1851	Marino et al. (2014)	LOS
	Kamann et al. (2018)	LOS
NGC 2298	Geisler et al. (1995)	LOS
	de Marchi & Pulone (2007)	MF
	Da Costa (2016)	LOS
NGC 2419	Cohen & Kirby (2012)	LOS
NGC 2808	Kamann et al. (2018)	LOS
NGC 3201	Kunder et al. (2017)	LOS
NGC 4833	Roederer & Thompson (2015)	LOS
NGC 5024	Boberg, Friel & Vesperini (2016)	LOS
	Abolfathi et al. (2017)	LOS
NGC 5053	Abolfathi et al. (2017)	LOS
NGC 5139	Kunder et al. (2017)	LOS
	Kamann et al. (2018)	LOS
NGC 5272	Marconi et al. (1998)	MF
	Sneden et al. (2004)	LOS
	Abolfathi et al. (2017)	LOS
NGC 5466	Abolfathi et al. (2017)	LOS
NGC 5634	Carretta et al. (2017)	LOS
	Abolfathi et al. (2017)	LOS
NGC 5824	Saviane et al. (2012)	LOS
NGC 5897	Koch & McWilliam (2014)	LOS
NGC 5904	Ramírez & Cohen (2003)	LOS
	Abolfathi et al. (2017)	LOS
	Kamann et al. (2018)	LOS
NGC 5986	Johnson et al. (2017a)	LOS
NGC 6101	Dalessandro et al. (2015)	SD
NGC 6121	Rastorguev & Samus (1991)	LOS
	Richer et al. (2004)	MF
NGC 6139	Saviane et al. (2012)	LOS
NGC 6144	Geisler et al. (1995)	LOS
	Lane et al. (2011)	LOS
NGC 6171	O'Connell et al. (2011)	LOS
	Abolfathi et al. (2017)	LOS

Table B1 – *continued*

Name	Source	Type
NGC 6205	Johnson & Pilachowski (2012)	LOS
	Cordero et al. (2017)	LOS
	Abolfathi et al. (2017)	LOS
NGC 6218	Rastorguev & Samus (1991)	LOS
	Johnson & Pilachowski (2006)	LOS
	Abolfathi et al. (2017)	LOS
NGC 6229	Johnson et al. (2017b)	LOS
	Abolfathi et al. (2017)	LOS
NGC 6254	Rastorguev & Samus (1991)	LOS
	Piotto & Zoccali (1999)	MF
	Kamann et al. (2018)	LOS
NGC 6256	Côté (1999)	LOS
NGC 6266	Kamann et al. (2018)	LOS
NGC 6273	Johnson et al. (2015)	LOS
NGC 6293	Kamann et al. (2018)	LOS
NGC 6316	Abolfathi et al. (2017)	LOS
NGC 6341	Piotto, Cool & King (1997)	MF
	Roederer & Sneden (2011)	LOS
	Smolinski et al. (2011)	LOS
	Abolfathi et al. (2017)	LOS
NGC 6342	Johnson et al. (2016)	LOS
NGC 6352	Carrera et al. (2007)	LOS
	Feltzing, Primas & Johnson (2009)	LOS
NGC 6356	Saviane et al. (2012)	LOS
NGC 6366	Johnson et al. (2016)	LOS
NGC 6388	McDonald & van Loon (2007)	LOS
	Kamann et al. (2018)	LOS
NGC 6397	Cool, Piotto & King (1996)	MF
	MacLean et al. (2017)	LOS
	Richer (2017)	MF
NGC 6440	Origlia, Valenti & Rich (2008)	LOS
	Muñoz et al. (2017)	LOS
NGC 6441	Gratton et al. (2007)	LOS
	Origlia, Valenti & Rich (2008)	LOS
	Kamann et al. (2018)	LOS
NGC 6522	Ness, Asplund & Casey (2014)	LOS
	Abolfathi et al. (2017)	LOS
NGC 6528	Carretta et al. (2001)	LOS
	Zoccali et al. (2004)	LOS
	Schiavon et al. (2017)	LOS
	Liu et al. (2017)	LOS
NGC 6535	Bragaglia et al. (2017)	LOS
NGC 6544	Abolfathi et al. (2017)	LOS
NGC 6553	Cohen et al. (1999)	LOS
	Alves-Brito et al. (2006)	LOS
	Johnson et al. (2014)	LOS
	Tang et al. (2017)	LOS
	Schiavon et al. (2017)	LOS
	Abolfathi et al. (2017)	LOS
NGC 6569	Johnson et al. (2018)	LOS
NGC 6624	Pryor et al. (1989)	LOS
	Baumgardt et al. (2018)	LOS
NGC 6626	Pryor et al. (1989)	LOS
	Villanova et al. (2017)	LOS
NGC 6656	Piotto & Zoccali (1999)	MF
	Albrow, De Marchi & Sahu (2002)	MF
NGC 6681	Pryor et al. (1989)	LOS
	Kamann et al. (2018)	LOS

Table B1 – *continued*

Name	Source	Type
NGC 6749	Canterna & Rosino (1981)	SD
	Kaisler, Harris & McLaughlin (1997)	SD
	Côté (1999)	LOS
NGC 6752	Ferraro et al. (1997)	MF
	Kunder et al. (2017)	LOS
NGC 6760	Abolfathi et al. (2017)	LOS
NGC 6809	Pryor et al. (1991)	LOS
	Piotto & Zoccali (1999)	MF
NGC 6838	Cadelano et al. (2017)	SD
	Abolfathi et al. (2017)	LOS
NGC 6864	Kacharov, Koch & McWilliam (2013)	LOS
	Koch (2017)	LOS
NGC 6934	Kimmig et al. (2015)	LOS
	Marino et al. (2018)	LOS
NGC 7006	Saviane et al. (2012)	LOS
NGC 7078	de Marchi & Paresce (1995a)	MF
	Abolfathi et al. (2017)	LOS
	Kamann et al. (2018)	LOS
NGC 7089	Smolinski et al. (2011)	LOS
	Yong et al. (2014)	LOS
	Abolfathi et al. (2017)	LOS
	Kamann et al. (2018)	LOS
NGC 7099	Piotto, Cool & King (1997)	MF
	Lovisi et al. (2013)	LOS
HP 1	Saviane et al. (2012)	LOS
Pal 4	Frank et al. (2012)	LOS, SD, MF
Pal 5	Odenkirchen et al. (2002)	LOS
	Kuzma et al. (2015)	LOS
	Majewski et al. (2015)	LOS
	Ibata et al. (2017)	LOS
	Koch & Côté (2017)	LOS
	Abolfathi et al. (2017)	LOS
Pal 12	Salinas et al. (2012)	SD
Pal 13	Côté et al. (2002)	SD,LOS
	Blecha et al. (2004)	LOS
	Bradford et al. (2011)	LOS
Pal 14	Jordi et al. (2009)	LOS
	Frank, Grebel & Küpper (2014)	MF
Pyxis	Irwin, Demers & Kunkel (1995)	SD
	Da Costa (1995)	SD
Rup 106	Villanova et al. (2013)	LOS
Ter 1	Valenti et al. (2015)	LOS
Ter 3	Côté (1999)	LOS
	Saviane et al. (2012)	LOS
Ter 5	Abolfathi et al. (2017)	LOS
Ter 7	Saviane et al. (2012)	LOS

APPENDIX C: VELOCITY DISPERSION PROFILES OF GLOBULAR CLUSTERS CALCULATED FROM INDIVIDUAL STELLAR RADIAL VELOCITIES

Table C1. Velocity dispersion profiles of globular clusters derived from individual stellar radial velocities. For each bin, the table gives the name of the cluster, the number of stars used to calculate the radial velocity dispersion, the average distance of stars from the cluster centre, and the velocity dispersion together with the 1σ upper and lower error bars.

Name	N_{RV}	r [arcsec]	σ [km/sec]	$\Delta\sigma_u$ [km/sec]	$\Delta\sigma_l$ [km/sec]
Arp 2	25	48.40	2.03	0.40	0.32
	24	129.77	1.38	0.37	0.30
E 3	18	124.71	1.56	0.47	0.39
ESO 452-SC11	13	39.47	1.40	0.44	0.31
HP 1	21	31.23	5.08	0.97	0.76
IC 1276	16	73.62	3.07	0.84	0.62
IC 4499	19	82.54	3.12	0.66	0.51
	18	212.94	1.90	0.44	0.35
Lil 1	22	14.09	20.03	3.49	2.71
	22	26.50	17.51	3.04	2.37
	19	58.32	12.63	2.39	1.84
NGC 104	130	18.02	11.50	0.78	0.70
	130	43.85	11.24	0.76	0.68
	130	72.49	11.05	0.73	0.66
	130	101.96	11.62	0.77	0.69
	130	132.70	10.12	0.67	0.60
	130	1322.70	4.37	0.30	0.27
	130	166.74	9.45	0.63	0.57
	33	1782.53	4.62	0.67	0.55
	130	200.68	8.28	0.55	0.50
	130	232.99	9.38	0.62	0.56
	130	274.19	8.26	0.55	0.50
	130	302.46	8.13	0.54	0.49
	130	332.44	7.91	0.53	0.48
	130	361.68	7.98	0.53	0.48
	130	393.64	7.83	0.52	0.47
	130	428.55	8.04	0.53	0.48
	130	466.97	7.06	0.47	0.43
	130	510.22	6.67	0.44	0.41
	130	555.78	6.72	0.46	0.41
	130	617.04	6.17	0.42	0.38
	130	704.08	5.72	0.39	0.35
	130	825.08	5.83	0.40	0.36
	130	998.11	4.83	0.33	0.30
NGC 288	80	46.61	3.02	0.27	0.24
	80	87.76	3.27	0.29	0.25
	80	121.04	2.65	0.24	0.21
	80	163.43	2.63	0.25	0.21
	80	209.64	2.59	0.23	0.21
	80	276.01	2.49	0.25	0.22
	41	411.42	1.62	0.25	0.21
NGC 362	70	28.62	7.37	0.68	0.59
	70	61.51	6.30	0.58	0.51
	70	92.03	6.32	0.58	0.51
	70	128.64	6.09	0.56	0.49
	70	179.20	4.07	0.39	0.33
	70	267.52	4.26	0.41	0.35
	36	402.56	2.98	0.40	0.33
NGC 1261	42	34.73	3.98	0.50	0.41
	42	64.91	3.95	0.50	0.41
	42	94.29	3.43	0.42	0.36
	42	143.57	3.64	0.46	0.38
	37	251.80	2.42	0.32	0.27
NGC 1851	65	53.74	6.13	0.59	0.51
	65	88.84	5.66	0.54	0.47
	65	117.83	5.13	0.49	0.43
	65	154.15	5.00	0.48	0.42

Table C1. (contd.)

Name	N_{RV}	r [arcsec]	σ [km/sec]	$\Delta\sigma_u$ [km/sec]	$\Delta\sigma_l$ [km/sec]
	65	193.22	4.94	0.48	0.42
	65	247.27	3.38	0.33	0.29
	65	324.90	3.92	0.38	0.32
	55	464.73	3.37	0.37	0.31
NGC 1904	62	34.95	3.97	0.40	0.34
	62	66.39	3.86	0.39	0.33
	62	96.01	3.91	0.40	0.34
	62	130.71	3.44	0.34	0.30
	62	189.35	2.77	0.28	0.24
	66	333.52	2.13	0.22	0.19
NGC 2298	20	45.86	1.46	0.42	0.33
	19	165.16	2.64	0.68	0.54
NGC 2419	40	25.81	6.70	0.87	0.72
	40	65.76	2.95	0.47	0.40
	40	109.69	2.41	0.43	0.35
	40	159.66	2.03	0.31	0.26
	23	251.10	1.23	0.37	0.30
NGC 2808	100	40.10	11.00	0.84	0.74
	100	65.98	10.43	0.79	0.70
	100	89.91	10.50	0.80	0.70
	100	113.40	8.94	0.68	0.60
	100	138.03	8.90	0.68	0.60
	100	163.27	7.38	0.56	0.50
	100	191.13	7.77	0.59	0.53
	100	228.39	8.61	0.66	0.58
	100	274.86	7.85	0.60	0.54
	100	336.28	7.00	0.54	0.48
	46	419.74	5.15	0.60	0.51
NGC 3201	80	44.08	3.85	0.34	0.29
	80	75.30	4.17	0.37	0.32
	80	109.48	3.56	0.31	0.27
	80	147.10	3.94	0.34	0.30
	80	190.60	3.68	0.32	0.28
	80	245.37	3.91	0.34	0.30
	80	345.96	3.06	0.27	0.24
	68	659.12	2.58	0.25	0.22
NGC 4147	17	39.38	1.75	0.36	0.28
	15	174.86	1.54	0.36	0.27
NGC 4372	45	77.51	5.00	0.59	0.49
	45	146.34	3.90	0.46	0.39
	45	211.26	3.56	0.42	0.35
	45	319.62	3.71	0.44	0.36
	34	486.61	3.12	0.43	0.35
NGC 4590	45	51.61	3.24	0.39	0.32
	45	105.87	3.25	0.39	0.33
	45	157.41	2.53	0.32	0.27
	45	248.44	2.16	0.27	0.22
	44	427.73	1.91	0.25	0.21
NGC 4833	42	64.12	4.82	0.58	0.49
	42	128.80	4.16	0.51	0.42
	43	244.69	3.48	0.42	0.35
NGC 5024	45	54.91	4.68	0.57	0.48
	45	113.21	4.08	0.50	0.43
	45	188.12	3.48	0.43	0.36
	45	260.37	3.10	0.39	0.33
	45	373.37	2.86	0.38	0.31
	39	696.11	2.22	0.30	0.25
NGC 5053	19	106.17	1.32	0.30	0.23
	19	178.84	1.39	0.30	0.23
	17	374.18	0.92	0.23	0.18
NGC 5139	62	40.89	19.09	1.86	1.60
	47	67.72	20.12	2.27	1.91

Table C1. (contd.)

Name	N_{RV}	r [arcsec]	σ [km/sec]	$\Delta\sigma_u$ [km/sec]	$\Delta\sigma_l$ [km/sec]
	125	90.48	17.05	1.14	1.03
	250	1056.53	8.40	0.39	0.37
	250	121.52	17.87	0.83	0.78
	250	1459.37	7.66	0.36	0.34
	250	154.90	15.69	0.73	0.68
	250	195.05	15.13	0.71	0.66
	80	2322.46	7.54	0.64	0.57
	250	233.38	14.65	0.69	0.64
	250	269.81	13.20	0.62	0.58
	250	311.03	13.01	0.61	0.57
	250	352.25	13.33	0.62	0.58
	250	408.54	11.89	0.56	0.52
	250	477.77	12.34	0.58	0.54
	250	549.70	11.19	0.53	0.49
	250	641.53	10.12	0.48	0.44
	250	810.19	9.98	0.47	0.44
NGC 5272	71	17.19	7.07	0.66	0.57
	71	53.95	6.41	0.59	0.51
	71	92.24	5.94	0.55	0.48
	71	132.85	5.62	0.52	0.45
	71	182.35	4.72	0.44	0.38
	71	258.01	4.28	0.40	0.35
	71	352.38	4.86	0.45	0.40
	71	517.26	2.60	0.24	0.21
	53	844.01	2.21	0.25	0.22
NGC 5286	72	7.91	8.61	0.79	0.69
	72	15.72	8.18	0.76	0.65
	72	24.39	7.66	0.70	0.61
	72	33.16	8.14	0.75	0.65
	72	43.34	7.69	0.71	0.62
	72	60.29	7.54	0.69	0.60
	29	153.95	6.24	0.92	0.74
NGC 5466	25	84.69	1.25	0.28	0.23
	25	190.81	1.15	0.22	0.18
	25	492.76	1.00	0.24	0.20
NGC 5634	25	43.42	3.56	0.63	0.50
	24	112.88	3.44	0.59	0.46
NGC 5694	30	46.47	5.13	0.79	0.64
	30	101.06	3.41	0.53	0.43
	28	216.87	2.38	0.42	0.34
NGC 5824	45	48.05	7.83	0.94	0.79
	45	93.50	5.92	0.72	0.61
	45	168.72	4.44	0.57	0.49
	37	275.97	4.08	0.59	0.49
NGC 5897	50	79.35	3.09	0.36	0.31
	50	139.79	3.38	0.40	0.34
	50	193.98	2.69	0.32	0.28
	50	248.76	2.28	0.31	0.26
	37	361.10	2.68	0.42	0.35
NGC 5904	75	44.37	6.11	0.54	0.48
	75	81.68	6.84	0.61	0.53
	75	111.81	6.74	0.60	0.52
	75	140.65	5.65	0.50	0.44
	75	171.86	5.82	0.52	0.45
	75	200.02	5.71	0.51	0.45
	75	231.65	5.42	0.49	0.43
	75	276.69	4.89	0.44	0.39
	75	325.71	4.20	0.39	0.33
	75	386.41	3.68	0.33	0.29
	75	513.37	3.18	0.29	0.25
	41	761.48	3.11	0.39	0.33
NGC 5927	60	40.00	5.94	0.60	0.52
	60	74.78	4.85	0.49	0.43

Table C1. (contd.)

Name	N_{RV}	r [arcsec]	σ [km/sec]	$\Delta\sigma_u$ [km/sec]	$\Delta\sigma_l$ [km/sec]
	60	111.40	5.46	0.55	0.47
	60	160.62	5.38	0.55	0.47
	60	229.38	4.75	0.49	0.42
	60	330.78	4.19	0.43	0.37
	20	453.04	3.68	0.70	0.55
NGC 5986	52	44.88	7.40	0.80	0.69
	52	82.61	6.09	0.67	0.56
	52	122.97	4.88	0.54	0.46
	53	218.69	4.77	0.52	0.45
NGC 6093	75	7.57	9.92	0.88	0.77
	75	19.78	8.89	0.79	0.70
	75	36.92	7.17	0.65	0.56
	75	57.94	7.09	0.64	0.55
	75	86.15	6.59	0.60	0.52
	71	185.26	5.17	0.48	0.42
NGC 6121	200	50.74	4.65	0.25	0.23
	200	90.09	4.61	0.24	0.23
	200	120.45	4.47	0.24	0.22
	200	144.96	3.99	0.21	0.19
	200	169.89	3.98	0.21	0.20
	200	194.17	3.94	0.21	0.19
	200	221.32	3.86	0.21	0.19
	200	253.32	4.25	0.22	0.21
	200	284.12	3.83	0.20	0.19
	200	321.73	4.03	0.21	0.20
	200	358.35	3.78	0.20	0.19
	200	400.20	3.48	0.19	0.17
	200	453.39	3.20	0.17	0.16
	200	515.57	3.27	0.18	0.16
	181	678.80	3.26	0.19	0.17
NGC 6139	28	64.03	6.73	1.05	0.84
	28	206.42	4.56	0.74	0.60
NGC 6144	19	123.76	1.55	0.83	0.92
NGC 6171	75	38.21	3.61	0.34	0.29
	75	83.90	3.60	0.34	0.30
	75	130.70	3.48	0.33	0.29
	75	195.18	2.88	0.27	0.23
	71	338.51	2.60	0.25	0.22
NGC 6205	70	23.55	8.09	0.75	0.66
	70	94.23	6.49	0.61	0.52
	70	171.63	6.15	0.57	0.49
	70	274.07	5.86	0.55	0.47
	70	449.25	4.82	0.45	0.39
	34	756.11	2.92	0.46	0.38
NGC 6218	70	40.12	4.17	0.39	0.34
	70	80.73	3.88	0.36	0.31
	70	114.78	3.50	0.33	0.28
	70	154.62	3.15	0.29	0.26
	70	200.11	2.98	0.28	0.24
	70	307.65	2.82	0.26	0.23
	20	491.53	2.67	0.51	0.40
NGC 6229	21	82.87	3.48	0.63	0.49
NGC 6254	72	60.72	5.52	0.50	0.44
	72	109.68	4.58	0.42	0.37
	72	163.12	4.71	0.43	0.38
	72	231.41	4.46	0.41	0.35
	76	351.24	4.19	0.38	0.33
NGC 6256	15	40.54	3.96	1.04	0.78
NGC 6266	55	56.46	12.30	1.28	1.09
	55	92.17	10.75	1.12	0.96
	55	135.87	8.12	0.85	0.72
	52	226.05	8.64	0.92	0.79

Table C1. (contd.)

Name	N_{RV}	r [arcsec]	σ [km/sec]	$\Delta\sigma_u$ [km/sec]	$\Delta\sigma_l$ [km/sec]
NGC 6273	65	46.99	10.28	0.98	0.86
	65	84.92	8.94	0.86	0.74
	65	135.85	8.79	0.85	0.73
	65	224.75	6.75	0.65	0.56
	20	372.48	3.84	0.74	0.57
NGC 6284	30	89.04	6.08	0.90	0.73
	23	345.91	3.76	0.67	0.53
NGC 6304	65	35.05	5.52	0.53	0.46
	65	81.69	4.56	0.45	0.39
	63	166.34	4.82	0.48	0.41
NGC 6316	35	44.81	7.06	0.96	0.79
	30	127.15	5.90	0.89	0.71
NGC 6341	47	12.83	7.56	0.87	0.73
	47	56.20	6.22	0.71	0.59
	47	98.41	6.68	0.77	0.65
	47	148.62	4.50	0.51	0.43
	47	211.98	4.40	0.50	0.43
	47	271.00	3.44	0.42	0.35
	47	357.10	3.58	0.42	0.35
	41	553.08	3.21	0.42	0.36
NGC 6342	19	46.56	3.30	0.65	0.49
NGC 6352	20	77.45	3.80	0.93	0.70
	14	187.36	3.39	1.36	1.16
NGC 6355	11	134.53	3.74	1.10	0.79
NGC 6356	20	138.72	4.84	1.04	0.83
NGC 6362	60	40.41	4.04	0.42	0.36
	60	84.19	3.19	0.34	0.29
	60	132.04	3.43	0.36	0.31
	60	213.09	3.09	0.33	0.28
	54	343.98	2.56	0.30	0.26
NGC 6366	45	67.08	3.29	0.41	0.35
	45	128.70	2.55	0.33	0.28
	45	188.71	2.52	0.33	0.28
	47	331.62	2.41	0.30	0.26
NGC 6388	60	27.56	12.66	1.28	1.10
	60	65.95	11.23	1.12	0.96
	60	89.71	12.26	1.21	1.04
	60	117.66	9.39	0.94	0.80
	60	148.87	8.89	0.88	0.76
	60	182.65	8.78	0.88	0.75
	60	243.72	6.78	0.68	0.58
	61	356.01	5.62	0.56	0.48
NGC 6397	200	20.88	4.83	0.28	0.25
	200	43.61	4.27	0.24	0.23
	200	70.50	4.51	0.25	0.23
	200	104.02	4.52	0.24	0.23
	200	135.65	3.93	0.22	0.20
	200	167.48	3.70	0.20	0.19
	200	202.01	4.04	0.22	0.21
	200	239.12	3.61	0.20	0.18
	200	274.63	3.77	0.21	0.19
	200	309.85	3.52	0.19	0.18
	200	347.28	3.45	0.19	0.18
	200	388.53	3.46	0.19	0.17
	200	439.78	3.43	0.19	0.18
	200	498.79	3.05	0.17	0.16
	157	598.56	2.97	0.19	0.17
NGC 6402	55	44.83	9.87	1.03	0.88
	55	77.93	8.14	0.85	0.72
	55	111.58	8.05	0.84	0.72
	55	147.55	7.92	0.83	0.71
	55	195.62	7.17	0.75	0.64

Table C1. (contd.)

Name	N_{RV}	r [arcsec]	σ [km/sec]	$\Delta\sigma_u$ [km/sec]	$\Delta\sigma_l$ [km/sec]
	56	329.81	5.82	0.61	0.53
NGC 6440	35	21.47	11.66	1.56	1.29
	35	66.99	9.62	1.29	1.06
	32	141.17	7.54	1.13	0.92
NGC 6441	45	42.42	13.77	1.60	1.35
	45	86.14	10.83	1.26	1.06
	45	134.02	9.01	1.05	0.88
	31	245.73	6.94	1.00	0.81
NGC 6496	40	56.09	3.32	0.47	0.39
	40	118.32	2.87	0.39	0.33
	40	233.28	1.73	0.27	0.23
NGC 6522	30	30.83	6.09	0.89	0.71
	30	70.90	7.23	1.05	0.85
	30	112.69	6.97	1.02	0.82
	19	185.44	4.66	0.89	0.68
NGC 6528	25	26.00	4.58	0.74	0.59
	25	48.57	5.58	0.91	0.72
NGC 6535	20	50.05	2.02	0.38	0.30
	10	157.66	1.63	0.49	0.34
NGC 6539	39	40.84	6.16	0.81	0.67
	39	89.43	5.29	0.69	0.57
	38	194.76	3.81	0.51	0.43
NGC 6540	10	15.95	2.99	0.95	0.65
NGC 6541	50	74.83	5.71	0.63	0.54
	50	161.83	5.54	0.62	0.52
	48	306.89	3.90	0.45	0.38
NGC 6544	10	301.48	3.09	0.90	0.62
NGC 6553	55	29.41	7.48	0.79	0.67
	55	53.30	7.78	0.82	0.69
	55	83.37	6.53	0.68	0.59
	55	113.49	6.32	0.66	0.57
	55	147.16	7.39	0.78	0.66
	39	183.27	5.78	0.73	0.61
NGC 6558	17	54.92	2.74	0.56	0.43
NGC 6569	50	35.28	5.76	0.65	0.55
	50	86.82	5.45	0.61	0.51
	49	161.38	5.43	0.61	0.52
NGC 6624	40	15.77	6.05	0.77	0.64
	40	40.32	4.61	0.65	0.54
	40	69.46	3.18	0.46	0.39
	36	137.77	3.77	0.55	0.46
NGC 6626	48	43.10	9.14	1.03	0.87
	48	102.68	7.42	0.83	0.71
	48	157.56	7.34	0.83	0.70
	47	243.78	6.67	0.76	0.64
NGC 6642	13	139.85	2.94	1.05	0.80
NGC 6656	80	53.89	8.59	0.73	0.64
	80	97.65	8.19	0.70	0.61
	80	127.70	8.22	0.70	0.61
	80	160.62	7.51	0.64	0.56
	80	196.27	6.84	0.58	0.52
	80	235.14	6.64	0.57	0.50
	80	293.29	6.67	0.58	0.51
	80	362.47	5.77	0.50	0.44
	79	535.74	5.50	0.50	0.44
NGC 6681	15	17.07	5.42	1.21	0.89
	16	63.29	4.13	0.92	0.69
NGC 6712	50	34.87	4.76	0.53	0.45
	50	65.60	4.25	0.48	0.40
	50	105.27	3.92	0.45	0.38
	48	167.20	3.93	0.45	0.38

Table C1. (contd.)

Name	N_{RV}	r [arcsec]	σ [km/sec]	$\Delta\sigma_u$ [km/sec]	$\Delta\sigma_l$ [km/sec]
NGC 6715	65	34.65	8.57	0.82	0.71
	65	61.60	8.51	0.81	0.70
	65	93.75	7.99	0.76	0.66
	65	125.34	8.17	0.78	0.68
	65	163.69	6.33	0.61	0.52
	65	227.99	5.41	0.52	0.46
	65	308.98	7.68	0.73	0.64
	69	427.62	9.21	0.85	0.74
NGC 6723	65	43.58	4.36	0.43	0.37
	65	85.94	4.50	0.44	0.38
	65	128.27	4.65	0.45	0.39
	65	173.89	3.49	0.35	0.30
	67	266.50	2.77	0.27	0.24
NGC 6749	15	98.27	2.64	0.94	0.72
NGC 6752	100	43.45	6.81	0.52	0.46
	100	89.68	5.89	0.46	0.40
	100	134.53	5.83	0.45	0.40
	100	173.54	5.24	0.41	0.35
	100	212.06	5.29	0.41	0.36
	100	252.86	5.03	0.39	0.34
	100	289.63	4.83	0.38	0.33
	100	332.43	3.70	0.29	0.26
	100	395.07	4.05	0.31	0.28
	100	480.33	4.16	0.33	0.29
	94	775.63	2.90	0.25	0.23
NGC 6760	23	122.66	5.55	1.36	0.99
NGC 6779	28	87.38	5.06	0.85	0.69
	28	123.24	4.12	0.75	0.62
	25	189.98	4.32	0.80	0.65
NGC 6809	85	47.34	3.91	0.33	0.30
	85	95.92	3.75	0.32	0.29
	85	142.16	3.95	0.34	0.30
	85	183.98	4.19	0.36	0.31
	85	234.10	4.26	0.36	0.32
	85	317.55	3.98	0.34	0.30
	72	553.86	3.12	0.30	0.27
NGC 6838	50	27.96	3.61	0.41	0.34
	50	64.13	2.83	0.32	0.27
	50	111.03	2.88	0.33	0.28
	50	166.31	2.25	0.26	0.22
	37	342.98	2.42	0.32	0.26
NGC 6864	20	41.92	7.53	1.53	1.18
	20	72.19	6.27	1.34	1.05
	19	148.60	5.91	1.21	0.93
NGC 6934	15	83.49	3.42	0.77	0.56
	14	265.63	1.51	0.38	0.28
NGC 7006	15	32.47	3.34	0.89	0.65
	10	65.45	2.78	0.92	0.64
NGC 7078	110	6.70	11.69	0.87	0.78
	110	16.96	11.80	0.86	0.77
	110	26.78	11.04	0.81	0.72
	110	35.70	9.28	0.68	0.61
	110	45.74	9.06	0.66	0.59
	110	58.80	8.57	0.62	0.56
	110	74.66	7.40	0.55	0.49
	110	97.84	6.66	0.49	0.44
	110	129.35	6.68	0.49	0.44
	110	169.89	4.80	0.35	0.31
	110	224.19	4.78	0.35	0.31
	110	300.90	2.98	0.22	0.20
	110	459.47	2.85	0.22	0.19
	43	725.37	3.45	0.43	0.36

Table C1. (contd.)

Name	N_{RV}	r [arcsec]	σ [km/sec]	$\Delta\sigma_u$ [km/sec]	$\Delta\sigma_l$ [km/sec]
NGC 7089	50	38.48	9.52	1.04	0.89
	50	76.25	8.07	0.89	0.76
	50	115.04	8.15	0.90	0.76
	50	148.38	7.00	0.78	0.66
	50	189.45	6.11	0.69	0.59
	50	240.33	5.16	0.58	0.49
	50	301.41	5.10	0.59	0.50
	50	399.83	4.35	0.51	0.44
	38	656.70	5.00	0.66	0.55
NGC 7099	79	20.73	4.59	0.47	0.41
	79	50.74	4.00	0.37	0.32
	79	83.45	3.99	0.36	0.31
	79	112.65	3.87	0.35	0.31
	79	142.92	3.55	0.32	0.28
	79	183.11	3.12	0.29	0.26
	79	242.92	2.64	0.25	0.22
	79	304.48	2.34	0.24	0.20
	75	442.88	2.25	0.24	0.21
NGC 7492	16	35.21	1.35	0.30	0.23
	13	75.65	1.27	0.32	0.23
Pal 2	16	58.86	4.73	1.10	0.83
Pal 3	19	19.73	1.27	0.39	0.29
Pal 4	24	26.12	0.89	0.21	0.17
Pal 5	15	86.49	0.55	0.15	0.11
	17	205.13	1.66	0.36	0.28
Pal 11	18	71.82	3.21	1.32	1.21
Pal 12	21	74.58	0.86	0.29	0.24
Pal 14	16	70.69	0.39	0.14	0.11
Pyxis	20	64.93	1.25	0.26	0.20
	18	140.44	0.74	0.19	0.15
Rup 106	20	69.90	2.00	0.46	0.36
	20	142.33	1.84	0.37	0.29
Ter 1	15	41.88	7.10	1.57	1.17
	12	134.96	5.31	1.43	1.04
Ter 3	22	72.01	2.25	0.53	0.40
Ter 5	35	6.51	18.00	2.42	1.98
	35	20.50	16.89	2.26	1.86
	35	47.53	13.36	1.82	1.49
	29	109.84	12.01	1.84	1.49
Ter 6	14	49.24	5.87	1.36	1.00
Ter 7	21	35.24	1.01	0.23	0.17
	21	94.35	0.52	0.14	0.11
Ter 8	35	59.33	1.04	0.24	0.20
	36	139.23	1.24	0.25	0.20
Ton 2	22	92.45	2.73	0.77	0.60

APPENDIX D: INDIVIDUAL STELLAR RADIAL VELOCITIES OF STARS IN THE FIELDS OF 53 GLOBULAR CLUSTERS

Table D1. Individual stellar radial velocities for stars in the field of Arp 2. The table gives the cluster name, the 2MASS ID, the right ascension and declination, the average heliocentric radial velocity and its 1σ error, the distance from the cluster centre, the 2MASS J and K_S band magnitudes, the membership probability based on the radial velocity and the number of radial velocity measurements. For stars with multiple radial velocity measurements, the probability that the star has a constant radial velocity is given in the final column. Full versions of Tables D1 to D53 are only available online.

Name	2MASS ID	RA [J2000]	DEC [J2000]	R_V [km/sec]	d ["]	J [mag]	K_S [mag]	Prob. Mem.	N_{RV}	Prob. Single
Arp 2		292.055125	-30.408778	121.22 ± 2.75	443.07			0.704	1	
Arp 2	19281376-3020014	292.057344	-30.333748	153.94 ± 0.88	400.72	14.74 ± 0.04	13.97 ± 0.07	0.000	1	
Arp 2	19281572-3016559	292.065539	-30.282202	-61.18 ± 1.64	452.74	15.25 ± 0.05	14.80 ± 0.12	0.000	1	
Arp 2	19283875-3020200	292.161484	-30.338905	125.30 ± 0.62	91.86	16.69 ± 0.15	17.00	0.129	1	
Arp 2	19284024-3021598	292.167701	-30.366631	123.27 ± 0.42	63.79	15.50 ± 0.07	14.89 ± 0.14	0.669	2	0.893
⋮	⋮	⋮	⋮	⋮	⋮	⋮	⋮	⋮	⋮	

Table D53. Same as Table D1 for stars in the field of Ter 8.

Name	2MASS ID	RA [J2000]	DEC [J2000]	R_V [km/sec]	d ["]	J [mag]	K_S [mag]	Prob. Mem.	N_{RV}	Prob. Single
Ter 8		295.286292	-34.052194	145.71 ± 2.25	482.66			0.261	1	
Ter 8		295.302250	-34.012500	147.82 ± 2.29	399.02			0.779	1	
Ter 8	19411316-3403599	295.304859	-34.066650	-66.97 ± 0.99	457.49	15.65 ± 0.06	15.70 ± 0.23	0.000	1	
Ter 8	19411449-3405234	295.310392	-34.089840	-48.27 ± 2.67	494.02	16.73 ± 0.14	16.00	0.000	1	
Ter 8		295.316917	-33.947944	164.88 ± 2.75	398.44			0.000	1	
⋮	⋮	⋮	⋮	⋮	⋮	⋮	⋮	⋮	⋮	

APPENDIX E: FITS OF THE SURFACE DENSITY AND VELOCITY DISPERSION PROFILES OF INDIVIDUAL CLUSTERS

Figs. E1 to E15 depict our fits to the observed surface density and velocity dispersion profiles for clusters with more than 100 member stars. The surface densities in the left panels are normalized to 1. In the right panels, the proper motion data from Watkins et al. (2015a) are shown by orange circles while the radial velocity dispersion profiles derived in this work are shown by blue circles. The predictions of the best-fitting N-body models are shown as solid, red lines. For clarity we show only the predicted radial velocity dispersion profiles. The proper motion dispersion profiles usually agree with the radial velocity ones to within a few %.

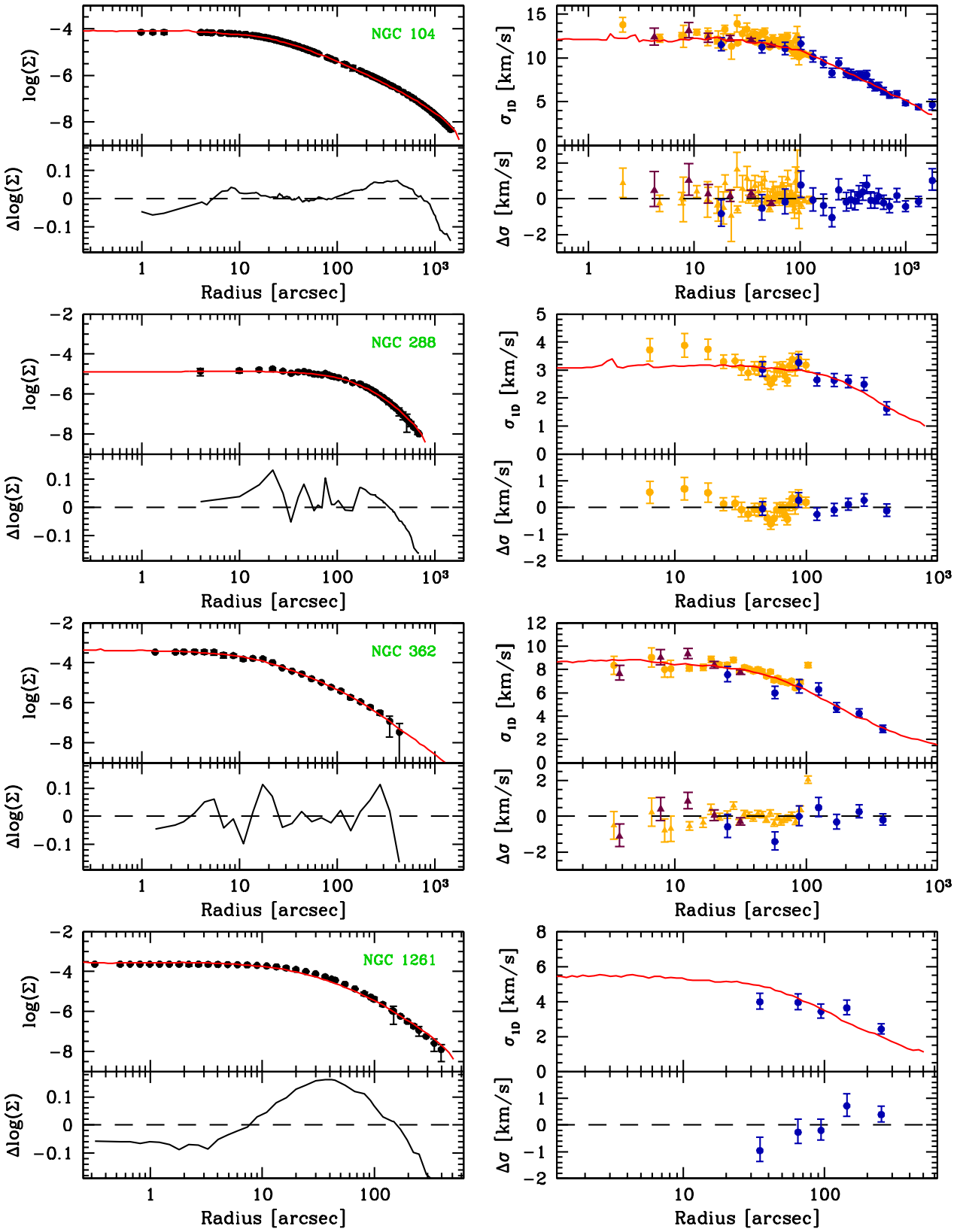

Figure E1. Fit of the surface density profiles (left panels) and velocity dispersion profiles (right panels) for NGC 104, NGC 288, NGC 362 and NGC 1261. In the right panels, the observed proper motion dispersion profile of Watkins et al. (2015a) is shown by orange circles while the radial velocity dispersion profile derived in this work is shown by blue circles. In order to convert proper motions to velocities we use the distances given in Table 2. Triangles mark the radial velocity dispersion profiles from Kamann et al. (2018). Red curves show the surface density (left panel) and line-of-sight velocity dispersion (right panel) of the best-fitting N-body model for each cluster. The lower panels show the differences between the observed data and the N-body models. The N-body data usually provides an excellent fit to the observed data for the depicted clusters.

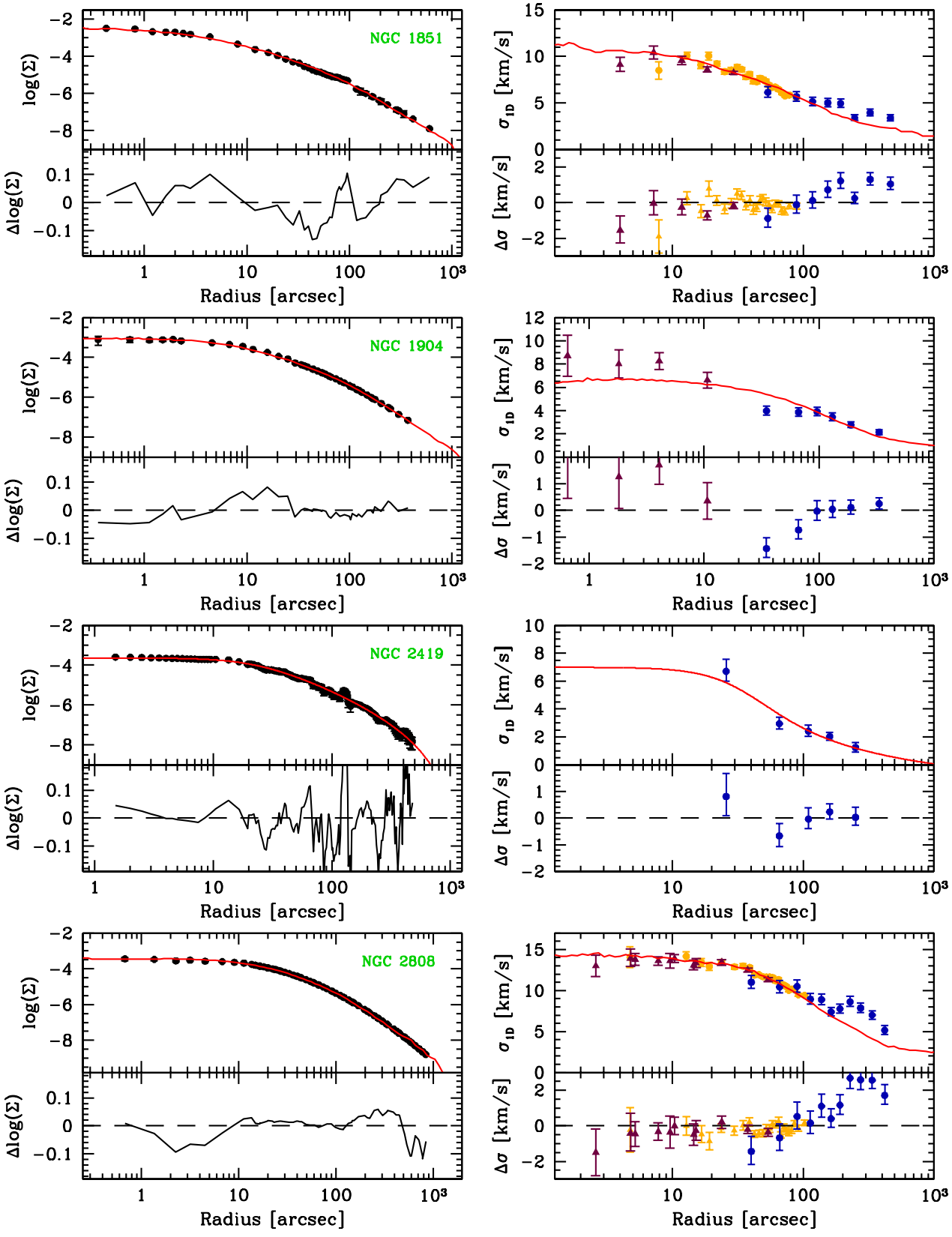

Figure E2. Same as Fig. E1 for NGC 1851, NGC 1904, NGC 2419 and NGC 2808. As discussed in the main text, we use a radially anisotropic King model to fit NGC 2419.

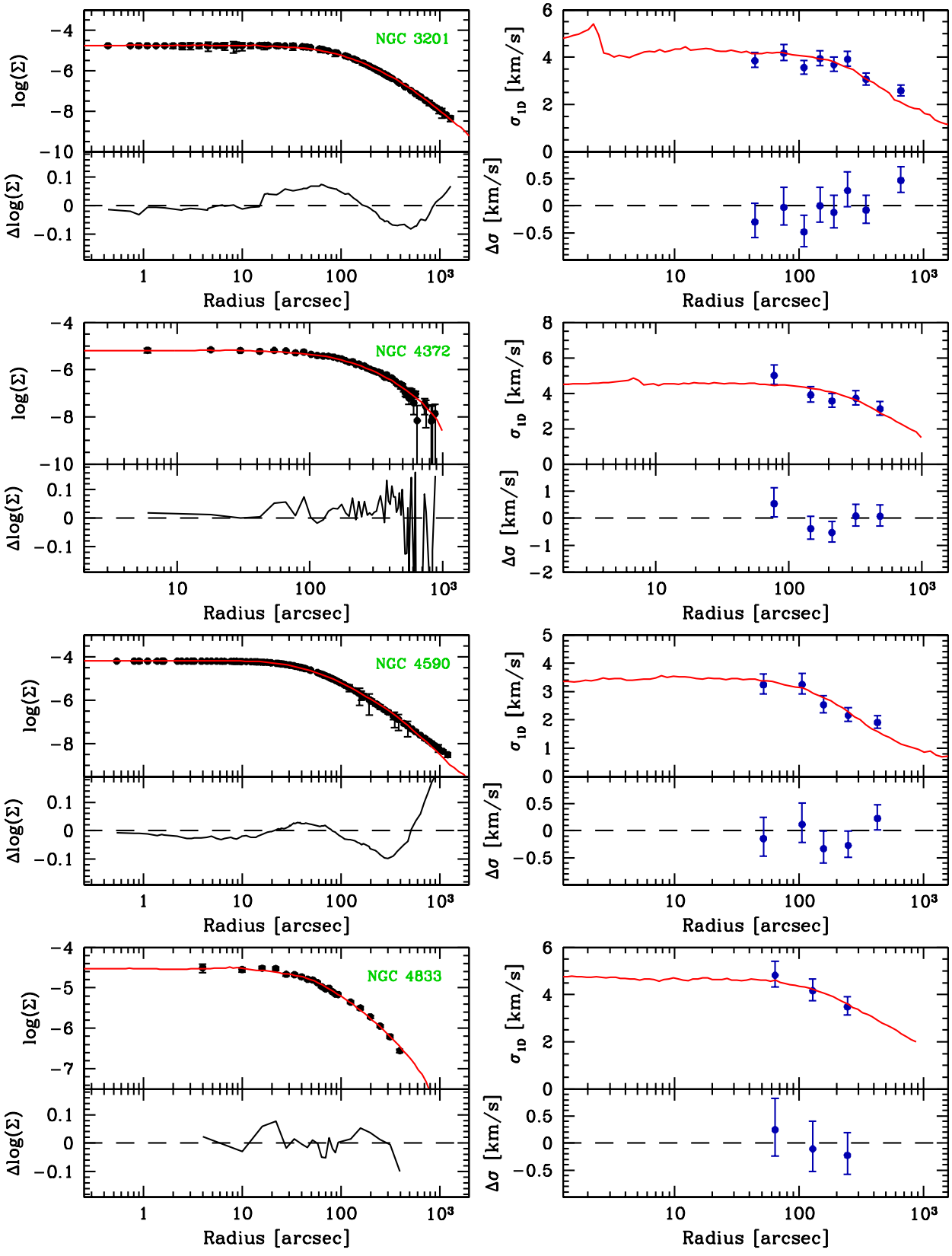

Figure E3. Same as Fig. E1 for NGC 3201, NGC 4372, NGC 4590 and NGC 4833.

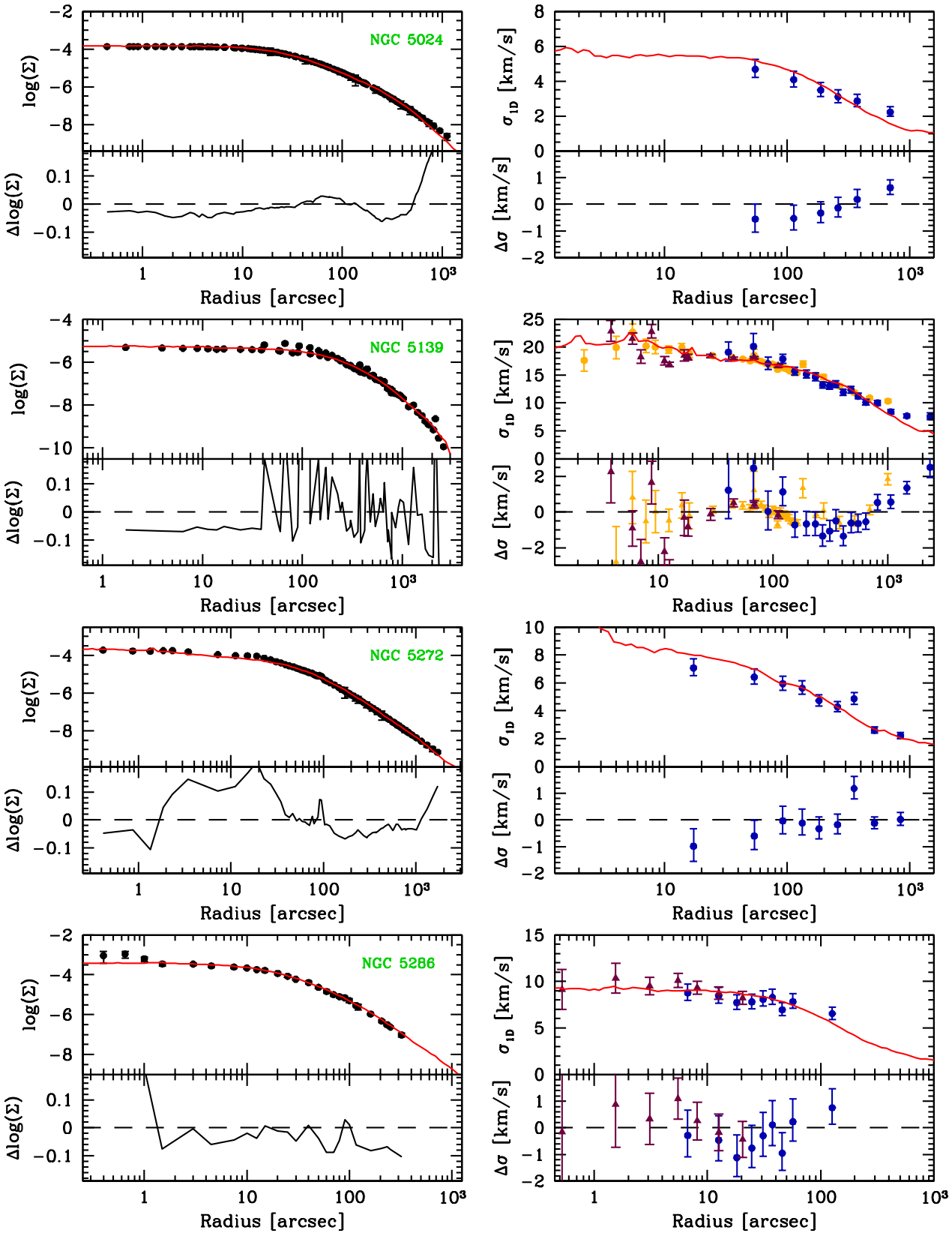

Figure E4. Same as Fig. E1 for NGC 5024, NGC 5139, NGC 5272 and NGC 5286. The red, solid lines for NGC 5139 show the best-fitting no IMBH model from Baumgardt et al. (2018).

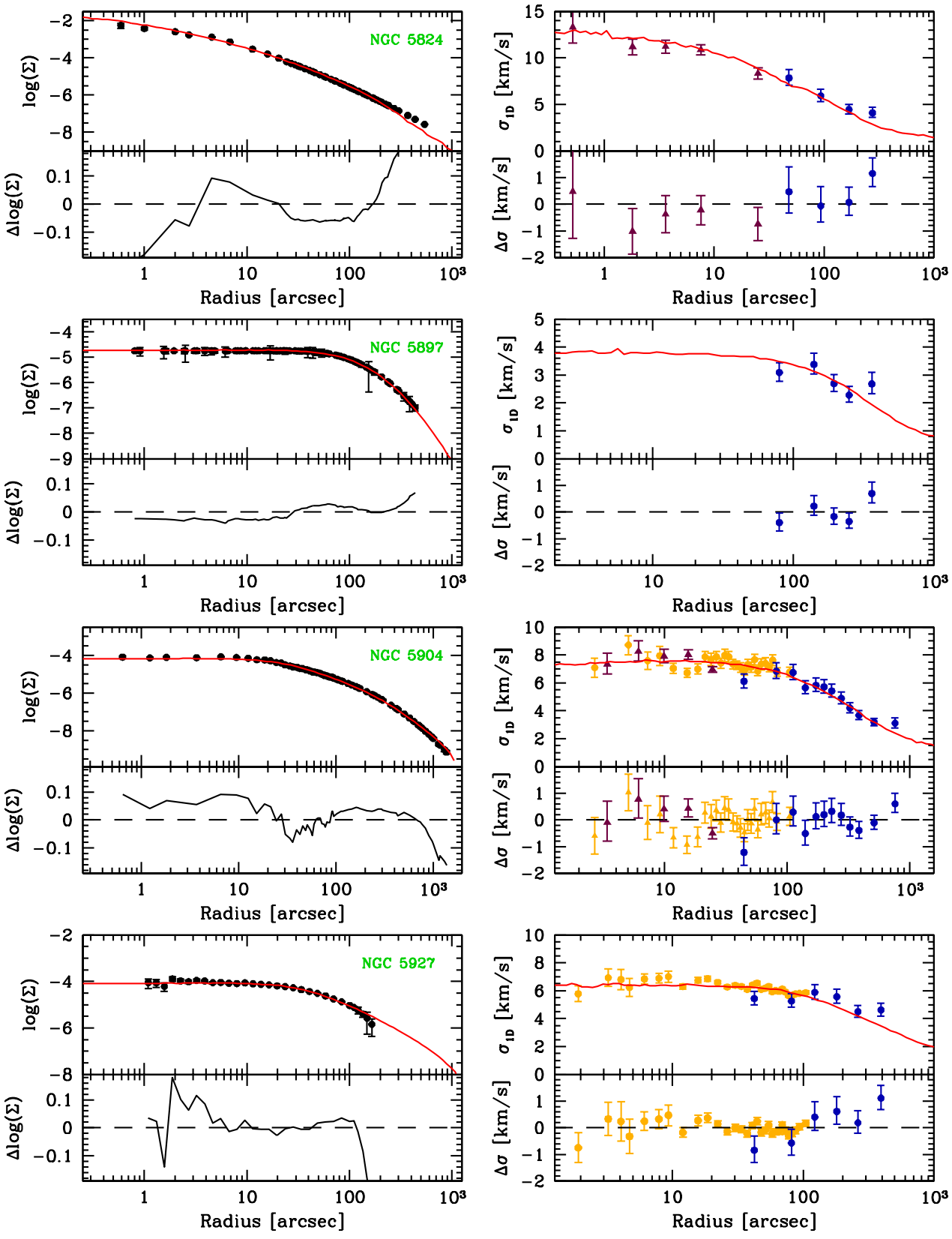

Figure E5. Same as Fig. E1 for NGC 5824, NGC 5897, NGC 5904 and NGC 5927.

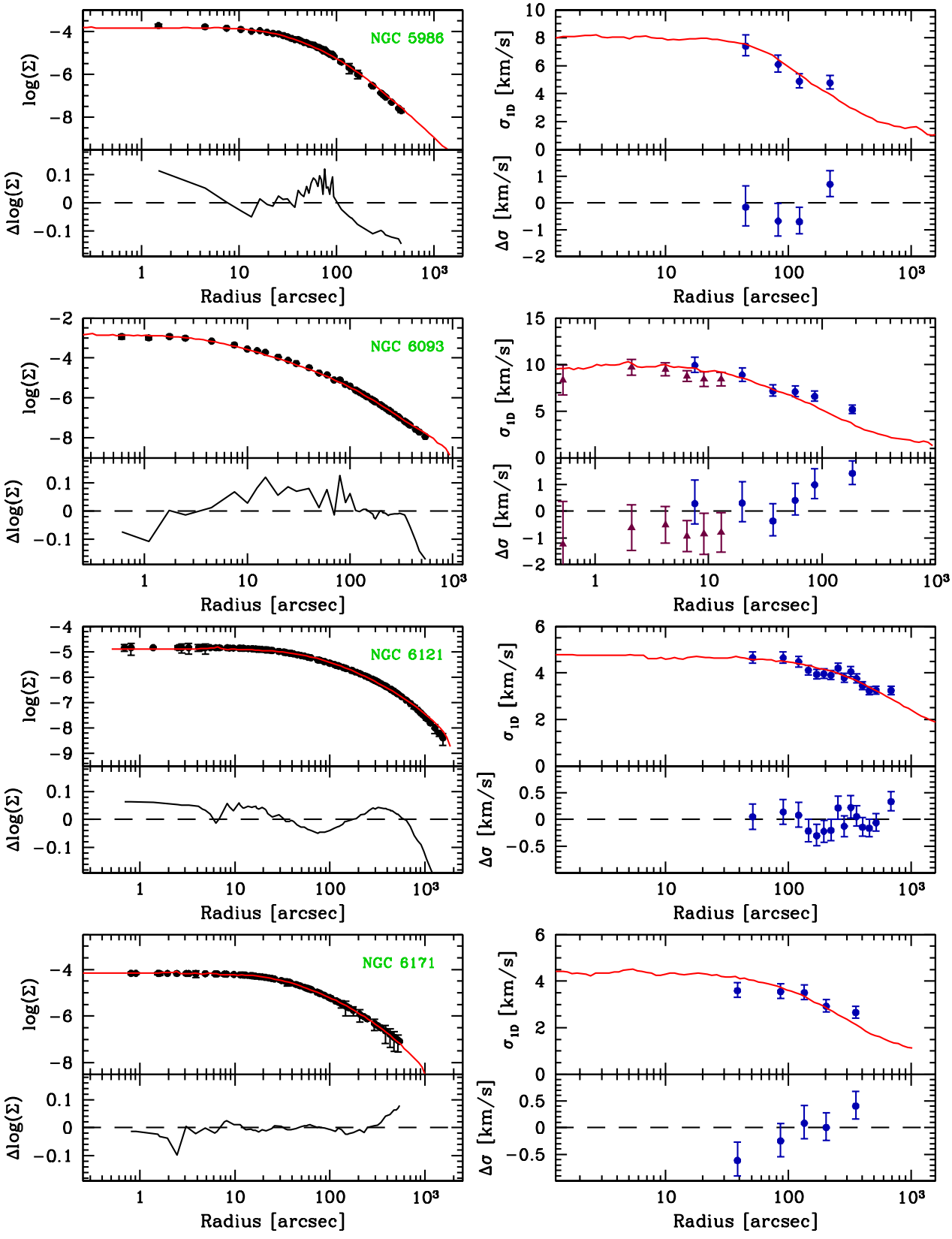

Figure E6. Same as Fig. E1 for NGC 5986, NGC 6093, NGC 6121 and NGC 6171.

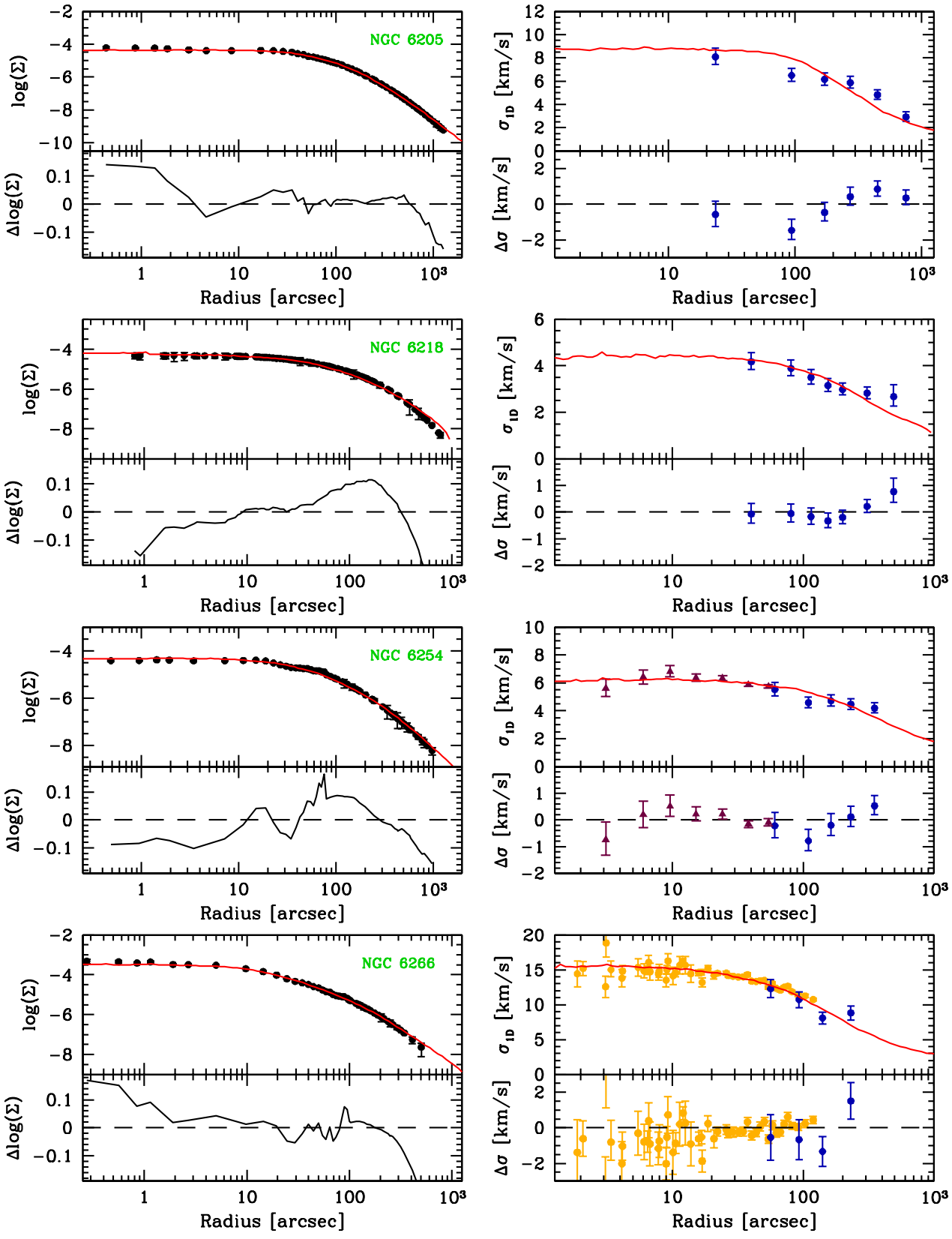

Figure E7. Same as Fig. E1 for NGC 6205, NGC 6218, NGC 6254, and NGC 6266.

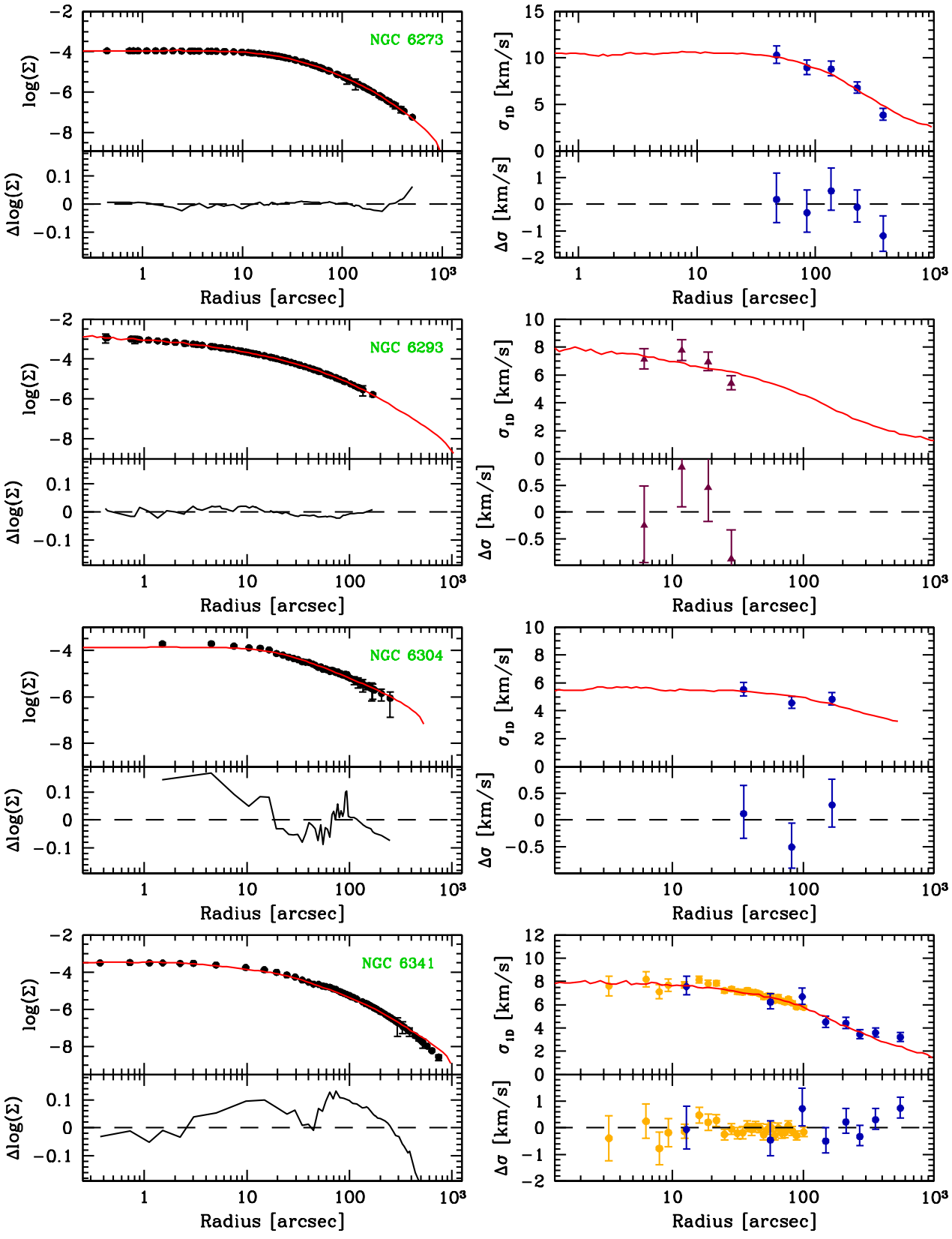

Figure E8. Same as Fig. E1 for NGC 6273, NGC 6293, NGC 6304 and NGC 6341.

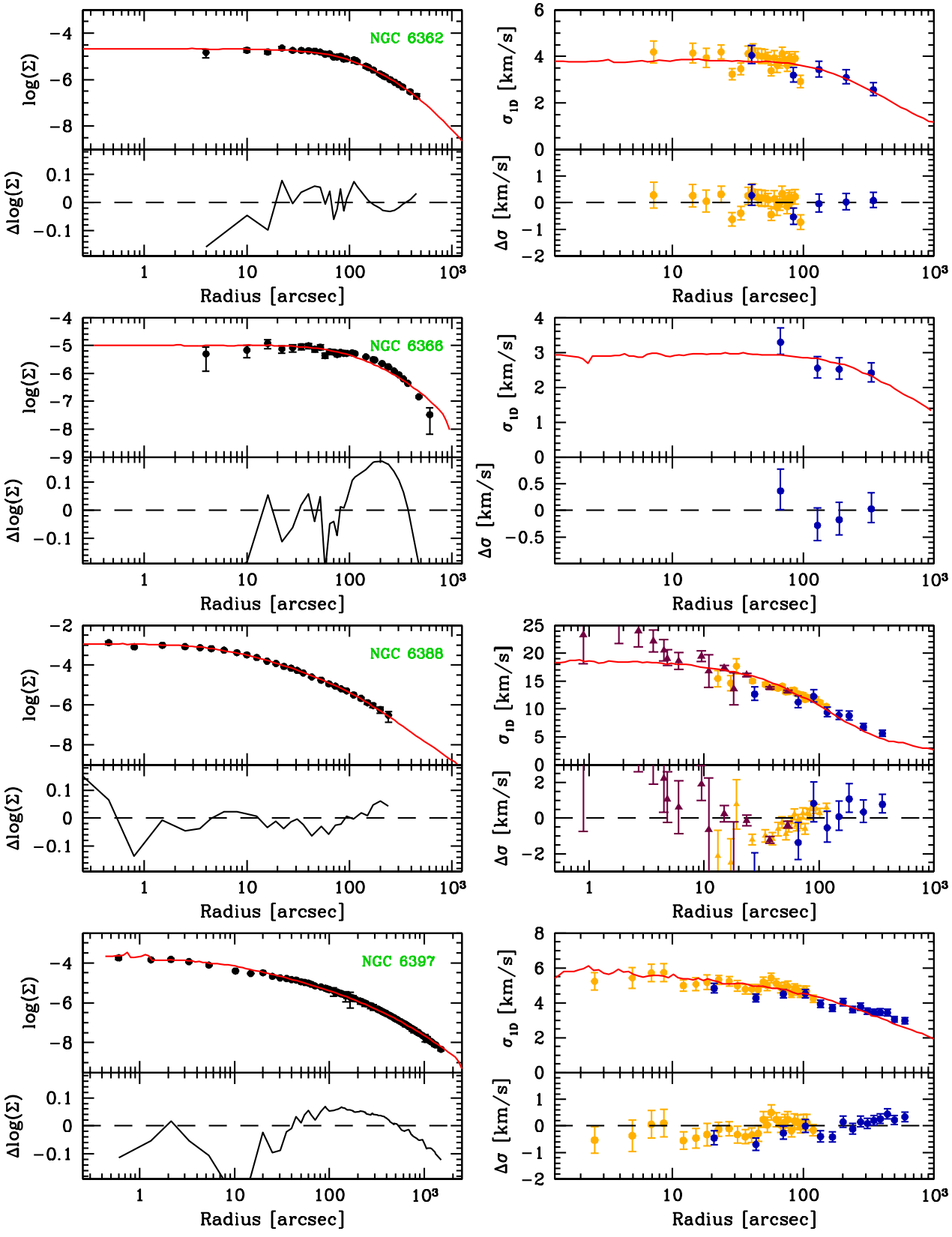

Figure E9. Same as Fig. E1 for NGC 6362, NGC 6366, NGC 6388 and NGC 6397.

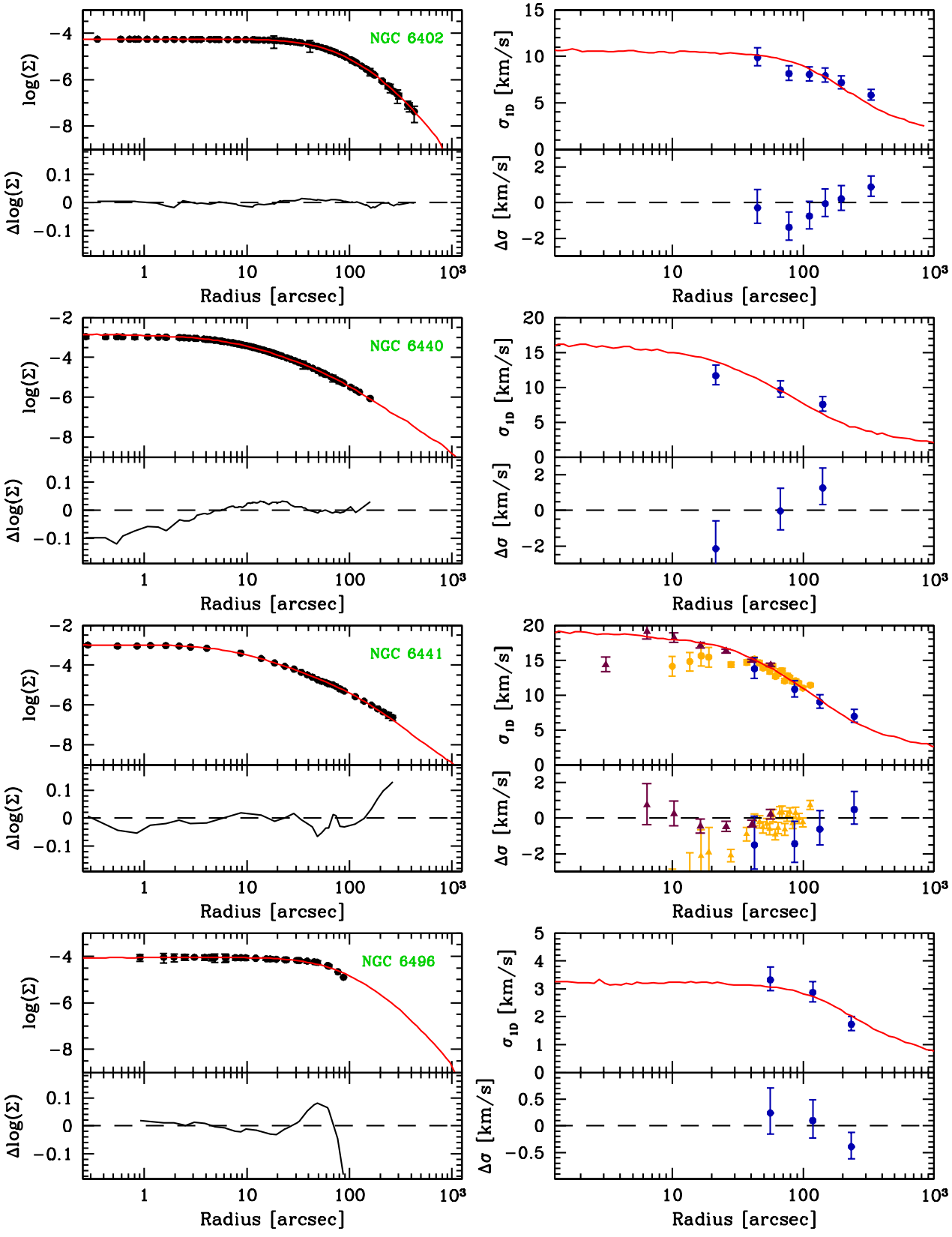

Figure E10. Same as Fig. E1 for NGC 6402, NGC 6440, NGC 6441 and NGC 6496.

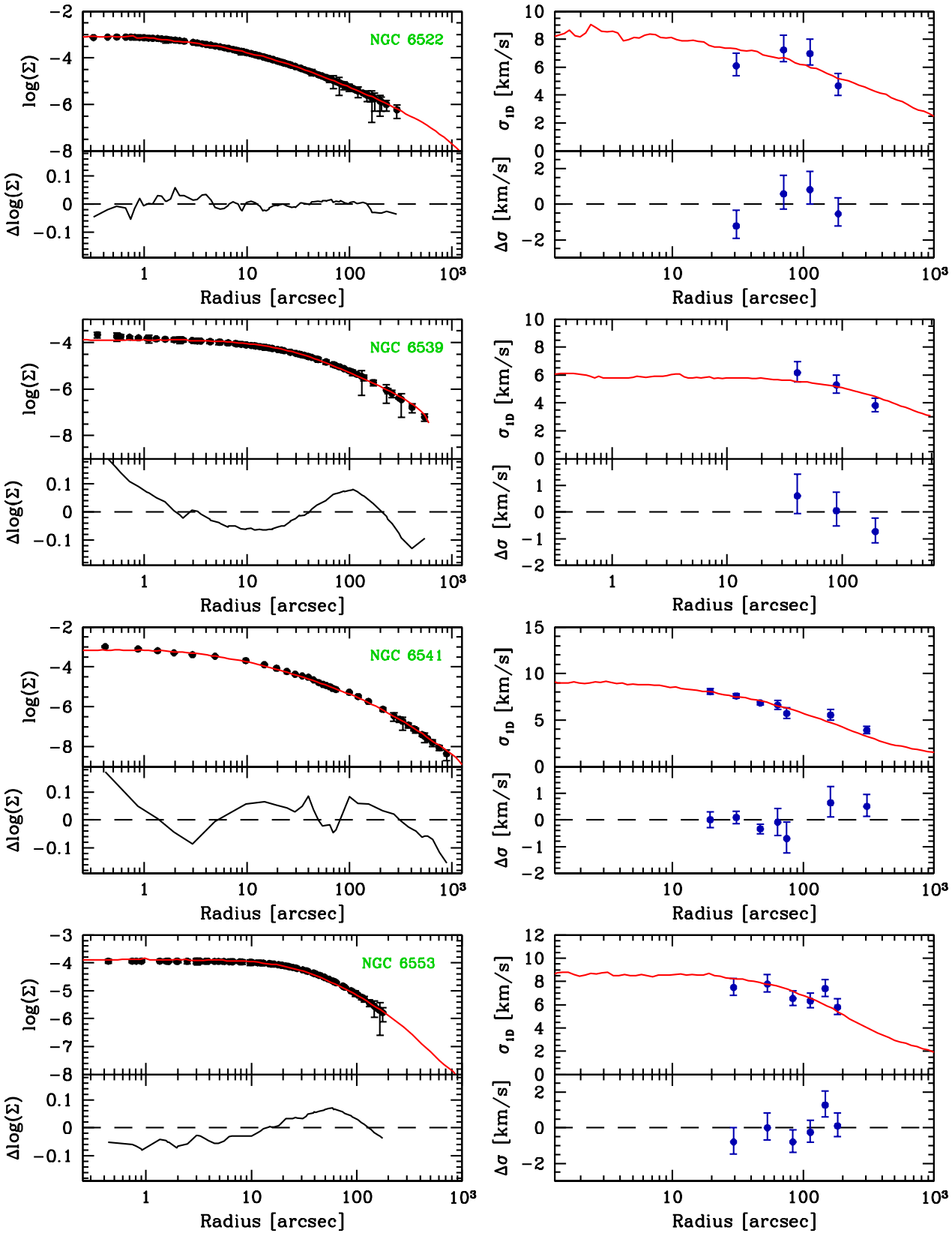

Figure E11. Same as Fig. E1 for NGC 6522, NGC 6539, NGC 6541 and NGC 6553.

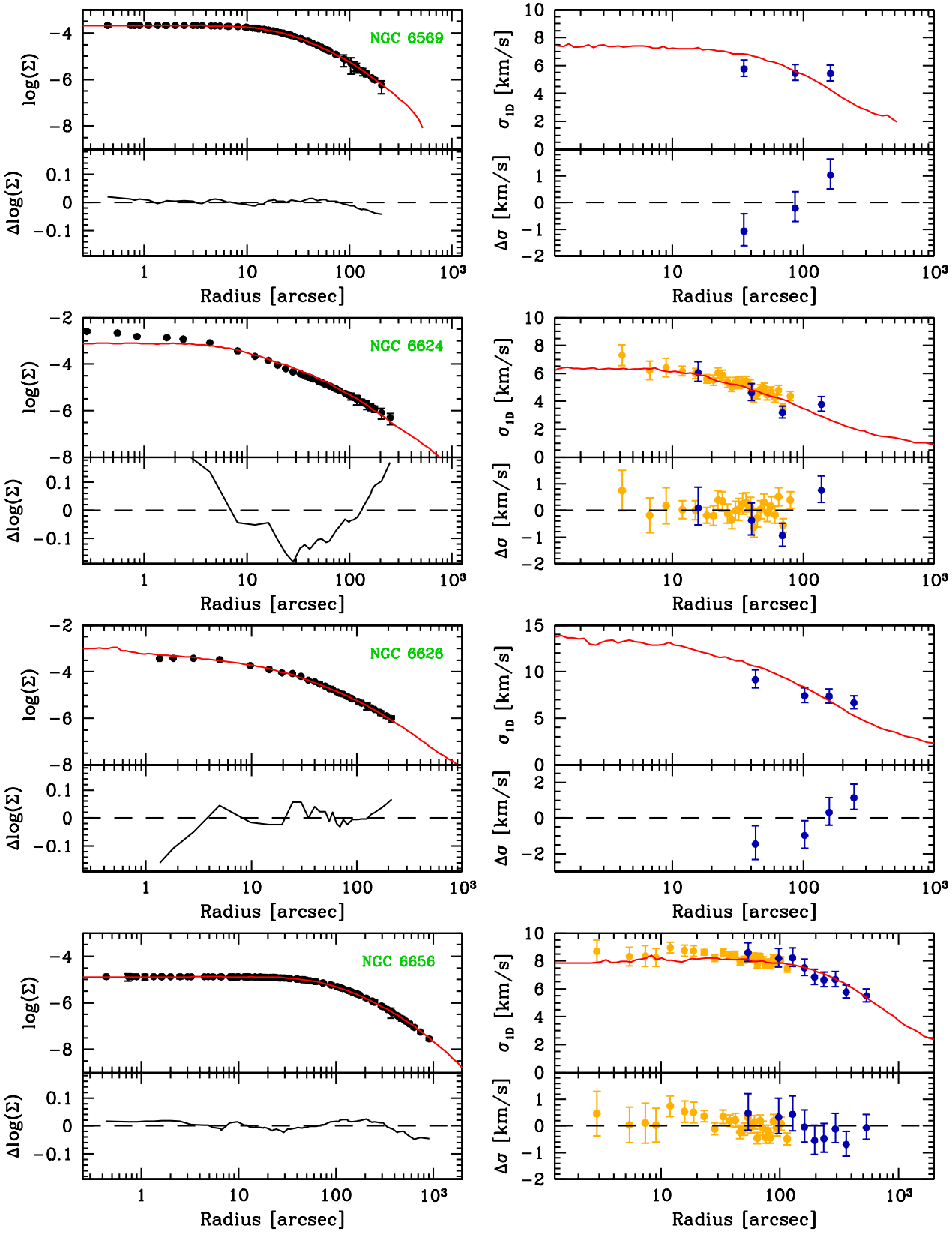

Figure E12. Same as Fig. E1 for NGC 6569, NGC 6624, NGC 6626 and NGC 6656.

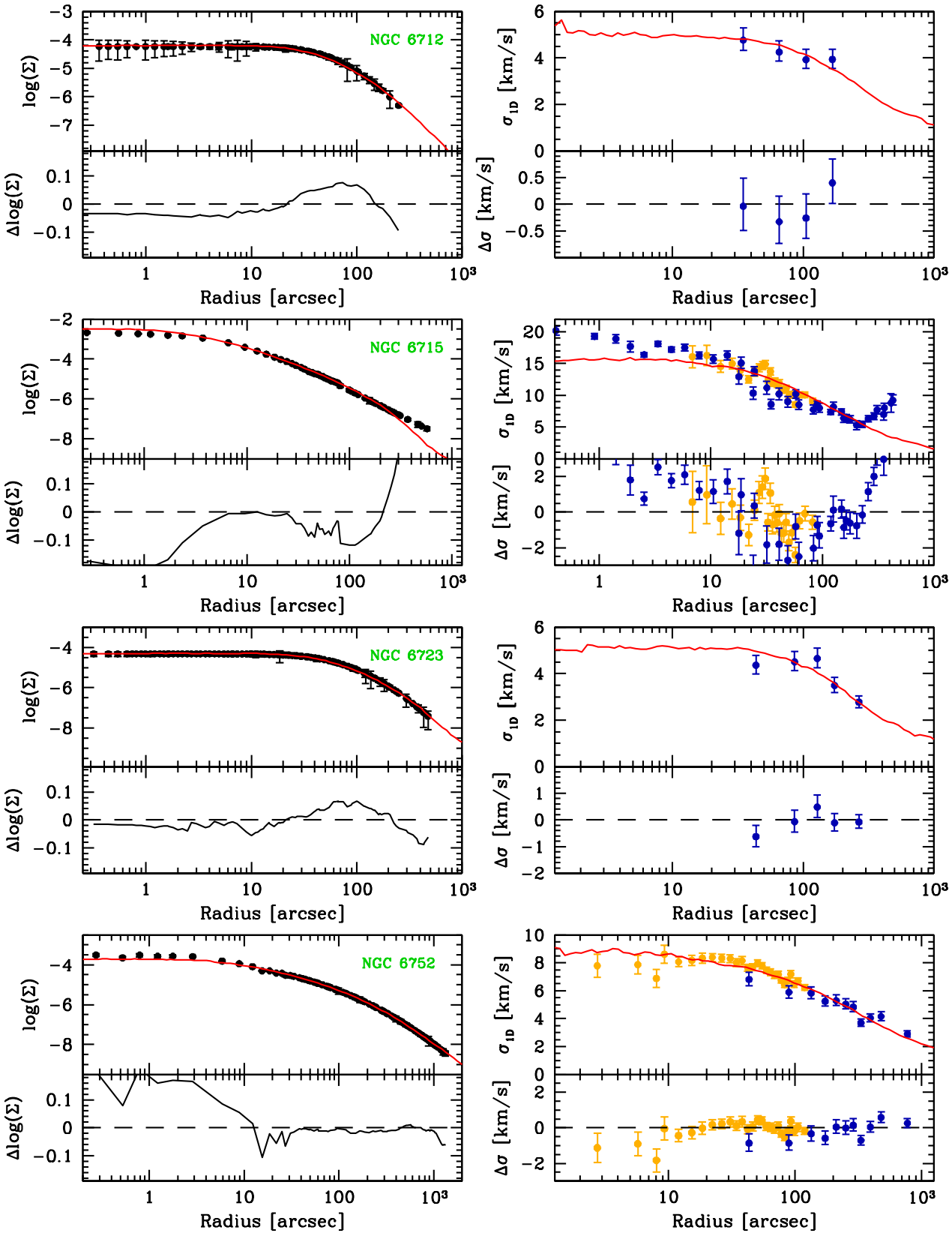

Figure E13. Same as Fig. E1 for NGC 6712, NGC 6715, NGC 6723 and NGC 6752.

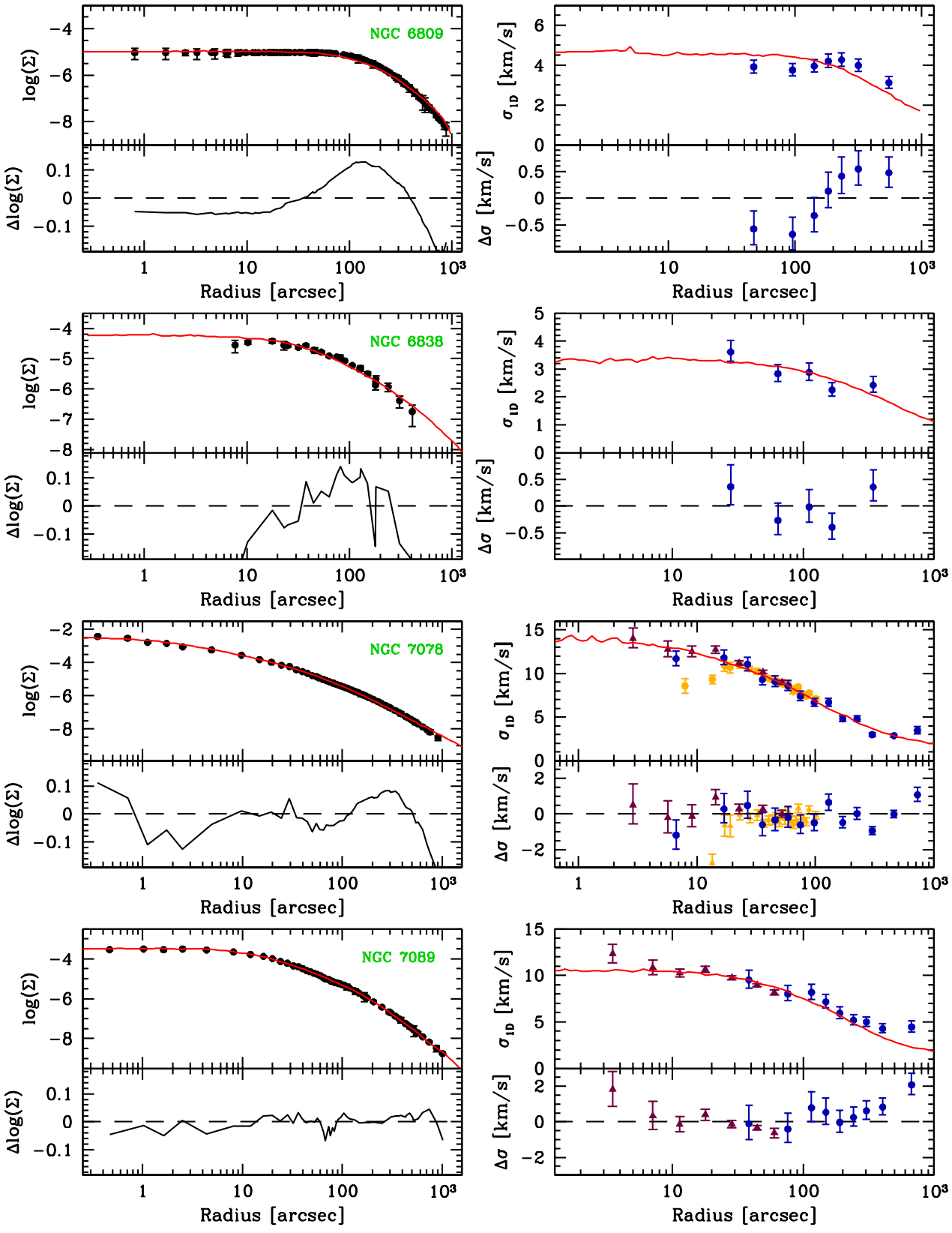

Figure E14. Same as Fig. E1 for NGC 6809, NGC 6838, NGC 7078 and NGC 7089.

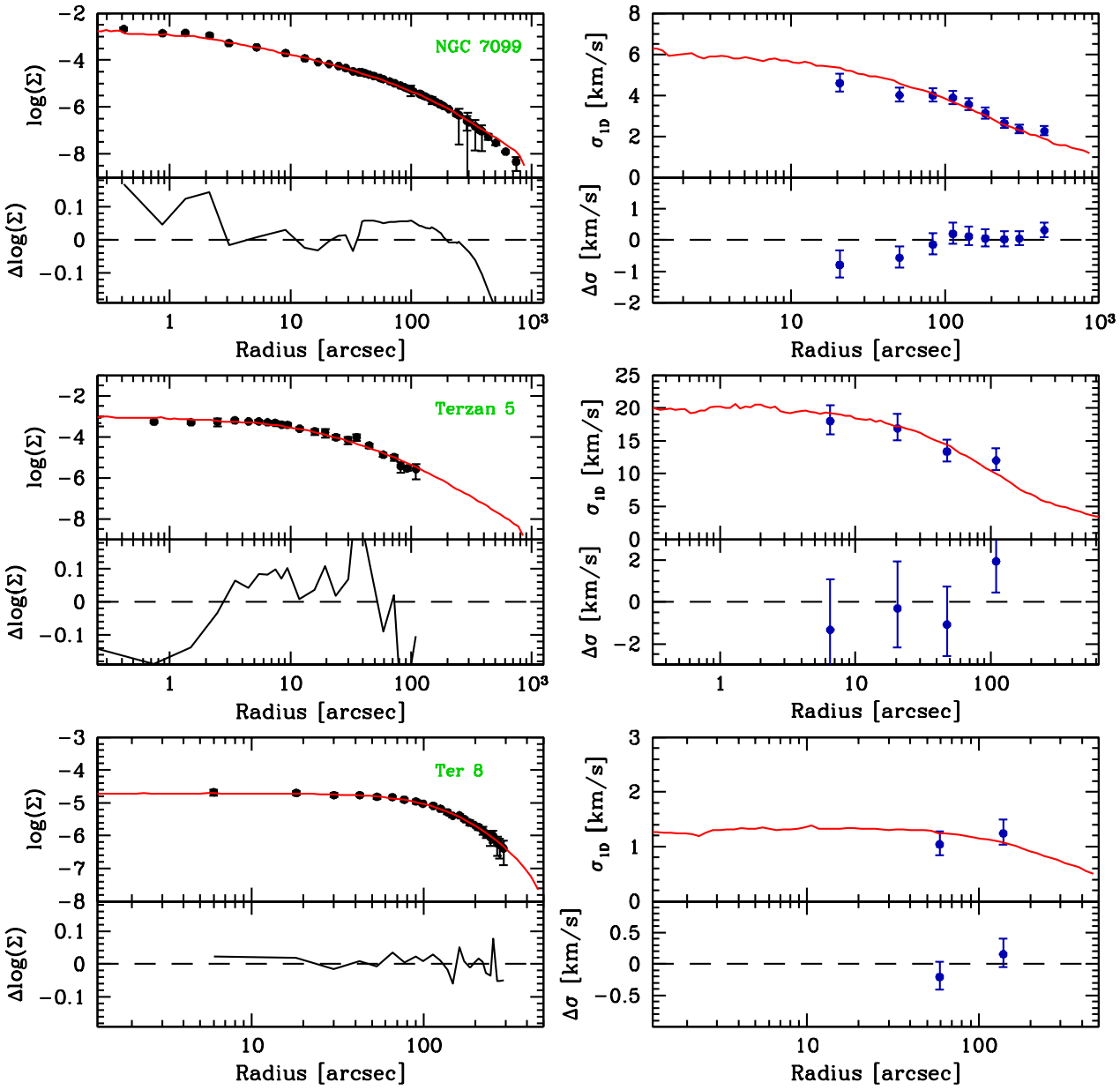

Figure E15. Same as Fig. E1 for NGC 7099, Terzan 5 and Terzan 8.